








EX LIBRIS  
UNIVERSITATIS  
ALBERTENSIS

---

The Bruce Peel  
Special Collections  
Library





Digitized by the Internet Archive  
in 2025 with funding from  
University of Alberta Library

<https://archive.org/details/0162014920563>











**University of Alberta**

**Library Release Form**

**Name of Author:** Colleen Chin Veon Chan

**Title of Thesis:** Investigation of Anomalous Surface Properties of Polyethylene Melt  
Using the Spinning Drop Method, and the Error Analysis of the  
Spinning Drop Tensiometer

**Degree:** Master of Science

**Year this Degree is Granted:** 2001

Permission is hereby granted to the University of Alberta Library to reproduce single copies of this thesis and to lend or sell such copies for private, scholarly or scientific research purposes only.

The author reserves all other publication and other rights in association with the copyright in the thesis, and except as herein before provided, neither the thesis nor any substantial portion thereof may be printed or otherwise reproduced in any material form whatever without the author's prior written permission.







The University of Alberta

**Investigation of Anomalous Surface Properties  
of Polyethylene Melt Using the Spinning Drop  
Method, and the Error Analysis of the Spinning  
Drop Tensiometer**

By

**Colleen Chin Veon Chan**



A Thesis Submitted to the Faculty of Graduate Studies and Research in  
Partial Fulfillment of the Requirements for the Degree of Master of  
Science

In  
Chemical Engineering

Department of Chemical & Materials Engineering

Edmonton, Alberta  
Fall, 2001





University of Alberta

Faculty of Graduate Studies and Research

The undersigned certify that they have read, and recommend to the Faculty of Graduate Studies and Research for acceptance, a thesis entitled *The Investigation of Anomalous Surface Properties of Polyethylene Melt Using the Spinning Drop Tensiometer, and the Error Analysis of the Spinning Drop Tensiometer* submitted by Colleen Chin Veon Chan in partial fulfillment of the requirements for the degree of Master of Science in Chemical Engineering.





*This thesis is dedicated to my parents,  
Na Fok Chan and Seh Lin Loh.  
My gratitude is beyond words;  
And to the Big One and the Middle  
One: Thank you.*





# Abstract

Polyethylene is a widely used product commercially. However, our knowledge is incomplete about the properties of polyethylene (PE) at temperatures above its melting point, where solid crystals disappear. Studies by several authors in the last decade have seen anomalous behavior of the high temperature polymer melt which suggests the possibility of structural order on a long-range level. In this thesis, the interfacial tension of PE melt against silicone oil will be reported in the same temperature range that anomalous phase transitions have been observed in the bulk HDPE (between 200 and 230°C). Phase transitions in the interfacial tension of the HDPE were found. The densities of HDPE in the temperature range of 160 to 250 °C were also measured and small phase transitions were observed between 200 and 230 °C. A spinning drop tensiometer acquired from SDT Ltd. was used for the interfacial tension measurements. A detailed investigation of the precision of the spinning drop apparatus and the errors associated with the system will be given. Preliminary data with water/air and silicone oil/air are described. It was found that the apparent interfacial tension values varied with rotation rate of the samples. Possible causes of this anomaly are discussed in detail. Different experiments were conducted to examine this observation.





## Acknowledgement

I wish to express my endless gratitude to the following individuals, without whom the completion of this thesis is not possible.

To Dr. Janet A.W. Elliott, my supervisor and mentor, and a researcher and teacher whom I hold the utmost respect for. Thank you for showing me what research is about. I am forever grateful for your enthusiasm and encouragement in trying times.

To Dr. Michael C. Williams, my co-supervisor whose knowledge of polymer is unparalleled. Thank you for all the fruitful discussions we have had, and all the encouragements you have given me in the past two years.

To Dr. Anthony Yeung and Dr. Thomas Forest for serving on my exam committee. Your invaluable comments and careful review of this thesis is truly appreciated.

To Dr. Alan Nelson for serving as the chairman for my defense and for your careful review of the thesis.

To Dr. Yadollah Maham and Dr. Xiao Sen Li for your help with the set up of the densitometer, and thank you, Yadi for your energy and encouragement.

To Dr. ZhengGe Xu for your help with the ring tensiometer, and to Dr. Nandakumar for your insight on secondary flows in a spinning drop tensiometer.

To Jiang Bai for your assistance in the polymer lab, and to Bin Lin for your help in using the blender.

To Andree Koenig, Walter Boddez, Richard Cooper and Jack Gibeau for your help with setting up and fixing the lab equipments and computers.

To Ah Cheah for all the “run-around” work you have done for me. The final version of this thesis is not possible without your help.

Last but not least, to my loving parent: Na Fok Chan and Seh Lin Loh, and to my siblings: Tah Yeow and Kimberly. Thank you for your support, patience and encouragement. I am forever in your debt.



# Table of Contents

<b>Chapter 1 – Introduction</b>	<b>1</b>
<b>Chapter 2 – Interfacial Tension Measurements – The Spinning Drop Tensiometer</b>	<b>9</b>
2.1 Methods of Interfacial Tension Measurements of Polymer Melts	9
2.2 The Spinning Drop Tensiometer	14
2.2.1 Theory	15
2.2.2 Description of the Equipment	19
2.2.3 Experimental Methods	25
2.2.3a <i>Cleaning of the Glass Tube, the Sealing End Plugs and the O-rings</i>	25
2.2.3b Loading of Liquid Samples in the Glass Tube	26
2.2.3c Calibrating the Video Measuring System and Measuring the Drop Diameter	27
2.3 Comparison with the duNuoy Ring Tensiometer	29
2.4 Conclusions	30
<b>Chapter 3 – Error Analysis of the Spinning Drop Tensiometer</b>	<b>31</b>
3.1 Materials	32
3.2 Time for the Drop to Reach an Equilibrium Size (Water/Air and Silicone Oil/Air Systems)	33
3.3 Measurement Error of the Spinning Drop Tensiometer- Reading Error	39
3.4 Interfacial Tension as a Function of Rotation Rate	40
3.4.1 <i>Silicone Oil/Air Systems</i>	42
3.4.2 <i>Water/Air Systems</i>	49
3.5 Investigation of the Effect of Rotation Rate on Calculated Interfacial Tension	56
3.5.1 The Possibility of Gyrostatic Disequilibrium Inside the Tube Under Rotation	56





3.5.2 The Possibility of Non-Rigid Body Rotation of the Fluids	60
3.5.3 Possible Calibration Error Due to Parallax Error in the Spinning Drop Tensiometer	64
3.5.4 Possible Error in the Motor Controller or Rotation Rate	69
3.5.5 Possible Pressure Effects on Interfacial Tension for Liquid –Gas Systems	70
3.5.5a The Derivation of the Relationship between Liquid Pressure and Rotation Rate	72
3.5.6 Possible Effects of Heat Generated in the Bearing Housings of the Motor	75
3.5.7 Possible Effect of Different Reticule Placement Methods	79
3.6 Discussion	81
3.7 Conclusions	84
<b>Chapter 4 – Density Measurements of Polyethylene Melts</b>	<b>86</b>
4.1 Introduction	86
4.2 Materials	87
4.3 Experimental Methods	88
4.4 Results	96
4.5 Conclusions	109
<b>Chapter 5 – Interfacial Tension Measurements and the Evidence of Order in Polyethylene Melt</b>	<b>110</b>
5.1 Introduction	110
5.2 Review of Literature	111
5.2.a Evidence of Structural Order in PE Melts	
5.2.b Interfacial Tension of Polyethylene Melts	113
5.3 Materials	116



5.4 Experimental Methods	117
5.4.1 The Measurement of the Interfacial Tension of Silicone Oil and PE Melt	120
5.4.2 Degradation of PE and the Blending of Anti- Oxidants into HDPE	121
5.4.3 The Densities of PE and Silicone Oil for the Calculation of the Interfacial Tension of the Polymer Melts	123
5.5 Results and Discussion	
5.5.1 Interfacial Tensions of HDPE Without Additional Anti-Oxidant	126
5.5.2 Interfacial Tensions of HDPE with Additional Anti-Oxidant	133
5.5.3 Interfacial Tensions of LDPE Without Additional Anti-Oxidant	134
5.5.4 Interfacial Tensions of LLDPE Without Additional Anti-Oxidant	137
5.6 Discussion	141
5.7 Conclusions	143
<b>Chapter 6 – Conclusions and Recommendations for Future Work</b>	143
6.1 Conclusions	143
6.1a The Measurement of the Interfacial Tensions of PE/Silicone Oil and the High Temperature Anomalies	144
6.1b The Measurement of the Density of HDPE and the High Temperature Anomalies	145
6.1c The Error Analysis of the Spinning Drop Tensiometer	146
6.2 Recommendations for Future Work	146
6.2a Examination of the Molecular Order of PE Melts	146
6.2b Examination of the Spinning Drop Method	147
<b>References</b>	147





## LIST OF FIGURES

Figure 1.1 Polyethylene molecules (adapted from Painter and Coleman)	2
Figure 1.2 Hussein and Williams' Torque Melt Experiment of HDPE and PS in the temperature range of 160-260°C. From " <i>Rheological evidence for high-temperature phase transitions in melts of high-density polyethylene</i> ", Hussein, I.A., William, M.C., <u>Macromol. Rapid Commun.</u> <b>19</b> , 323-325 (1998)	6
Figure 2.1 A schematic diagram of the pendant drop.	11
Figure 2.2 A schematic diagram of the sessile drop.	11
Figure 2.3 The schematic of the cylindrical drop under rotation.	16
Figure 2.4 A schematic diagram of the spinning drop tensiometer used in this work (Adapted from the SDT Manual). See also Figure 2.6.	20
Figure 2.5 A schematic diagram of an end plug with multi-step calibration posts.	22
Figure 2.6 A schematic diagram of the glass mount with the glass tube. The retaining ring of the shaft presses the O-ring against the end of the glass tube. The O-ring provides enough friction against the end of the glass tube so that when the motor drives the retaining ring, the glass tube also rotates via the rotation of the O-ring. The glass tube is filled with the denser fluid and a drop of the less dense fluid. When the glass tube rotates, the less dense drop assumes a cylindrical profile with hemispherical ends.	23
Figure 2.7 The image of the drop under rotation as it appears on the monitor screen. The "shadow" region has been exaggerated for emphasis.	28
Figure 3.1 The dynamic interfacial tension of water/air as a function of time over a period of 180 seconds at room temperature (19°C). The rotation rate was kept constant at 4002 rpm after a spin up from 0 rpm at time = 0 s.	34



Figure 3.2 The dynamic interfacial tension of water/air as a function time over a period of 120 minutes at room temperature. The rotation rate was kept constant at 4002 rpm.	35
Figure 3.3 The dynamic interfacial tension of silicone oil and air over a period of two hours at room temperature (19°C). The rotation rate was kept constant at 4002 rpm.	37
Figure 3.4 The interfacial tension of water/air as a function of time during spin-up to a new rotation rate. The initial rotational rate was 4004 rpm, and the experiment was conducted at room temperature (19°C).	38
Figure 3.5 The interfacial tension of silicone oil and air as a function of rotation rate when the measuring system is calibrated with the 2mm calibration post. The experiment was conducted at a room temperature of 19°C.	43
Figure 3.6 The interfacial tension of silicone oil and air as a function of rotation rate when the measuring system is calibrated with the 3mm calibration post. The experiment was conducted at a room temperature of 19°C.	45
Figure 3.7 The interfacial tension of silicone oil and air as a function of rotation rate when the measuring system was calibrated with the 3 mm and the 2 mm calibration post. The experiments were conducted at a room temperature of 19°C.	46
Figure 3.8 The percentage error of SDT interfacial tension value relative to the interfacial tension value obtained from the duNuoy Ring method. This silicone oil/air system was calibrated with the 2 mm calibration post.	47
Figure 3.9 The percentage error of SDT interfacial tension relative to the interfacial tension obtained from the duNuoy Ring method. This silicone oil/air system was calibrated with the 3 mm calibration post. A linear regression line was fitted through the data points for the purpose of illustrating the range of rotation rates at which the error is zero.	48
Figure 3.10 Water/air 1 - The effect of rotation rate on interfacial tension for water/air at 17°C. The measuring system was calibrated with the 2 mm calibration post.	50
Figure 3.11 Water/air 2 - The effect of rotation rate on interfacial tension for water/air at 17°C. The measuring system was calibrated with the 2 mm calibration post.	51





Figure 3.12 Water/air 3 - The effect of rotation rate on interfacial tension for water/air at 17°C. The measuring system was calibrated with the 2 mm calibration post.	52
Figure 3.13 - (Water/air 1,2,3 on the same graph) The interfacial tension of water/air at 17°C.	53
Figure 3.14 Interfacial tension of water/air as a function of rotational rate at 17°C for the experiments calibrated with the 1 mm, 2 mm and 3 mm calibration posts.	55
Figure 3.15 The interfacial tension of silicone oil/air as a function of rotation rate at room temperature (19°C) using the volume/length method by Princen.	66
Figure 3.16 The interfacial tension of silicone oil/air as a function of air drop length using the volume/length method by Princen.	67
Figure 3.17 The interfacial tension of silicone oil/air as a function of rotation rate. Interfacial tension values were calculated by the SDT32 software. The same sample used for the experiment in Figure 3.16 was used for this experiment, and conducted under the same experimental conditions.	68
Figure 3.18 A schematic diagram of the forces acting on the end plug in a glass tube filled with liquid. Note that the liquid pressure acting on the plug is parabolic with radius (r), while the atmospheric pressure is uniform and constant across the surface of the plug. The surface area ( $A_p$ ) of the circular end plug is given by $A_p = \pi R^2$ .	73
Figure 3.19 The interfacial tension of water/air (at room temperature) as a function of arbitrary pressure at the interface.	76
Figure 3.20 The interfacial tension of water/air as a function of rotation rate at a higher temperature of 40°C.	78



Figure 3.21 The measurement of drop diameter by placing the reticules on the *outside* edges of the drop. The width of the unclear region of the drop is the same regardless of the diameter of the drop. The actual diameter of the drop is somewhere between the inner and outer edges of the drop. In (a), the rotation rate  $\omega_1$  is low, hence the drop diameter,  $D_1$  is larger. The percentage error in diameter ( $W_E/D_1$ ), and corresponding interfacial tension is  $E_1$ . In (b), the rotation rate  $\omega_2$  is higher, hence the drop diameter,  $D_2$  is smaller than  $D_1$ . The percentage error in diameter ( $W_E/D_2$ ), and corresponding interfacial tension is  $E_2$ . Since  $W_E$  is constant for both drop diameters,  $E_2$  will be bigger than  $E_1$  in a *positive* direction, i.e.  $E$  increases as  $\omega$  increases. Thus the apparent interfacial tension will increase with increasing rotation rate. 80

Figure 3.22 The measurement of drop diameter by placing the reticules on the *inside* edges of the drop. The width of the unclear region of the drop is the same regardless of the diameter of the drop. The actual diameter of the drop is somewhere between the inner and outer edges of the drop. In (a), the rotational rate  $\omega_1$  is low, hence the drop diameter,  $D_1$  is larger. The percentage error in diameter ( $W_E/D_1$ ), and corresponding interfacial tension is  $E_1$ . In (b), the rotational rate  $\omega_2$  is higher, hence the drop diameter,  $D_2$  is smaller than  $D_1$ . The percentage error in diameter ( $W_E/D_2$ ), and corresponding interfacial tension is  $E_2$ . Since  $W_E$  is constant for both drop diameters,  $|E_1|$  will be smaller than  $|E_2|$ , but the error is negative. Thus, the apparent interfacial tension will decrease with increasing rotational rate. 82

Figure 3.23 The interfacial tension of water/air (at room temperature of 17°C) as a function of rotation rate with the reticules placed on the inside edge of the drop shadow during the measurement of drop diameter. 83

Figure 4.1 A schematic diagram of the densitometer for the measurement of the density of water with a copper ball. 89

Figure 4.2 The measured density of distilled water at different temperatures compared to the literature value reported by Kell, 1975. The magnitude of the error bar on the density is  $\pm 0.4\%$ . 92

Figure 4.3a A paper clip hanging at the end of the PE sample and immersed in silicone oil. 95

Figure 4.3b PE melt deformed and elongated under the weight of the paper clip. The paper clip touches the bottom of the beaker. 95

Figure 4.3c A copper wire wrapped around the PE sample and immersed in silicone oil. 95





Figure 4.4 The density of the silicone oil at various temperatures.	97
Figure 4.5 The PE melt bounded by a copper wire immersed in silicone oil. Although the shape of the PE is deformed, no PE broke away to dissolve in the silicone oil.	100
Figure 4.6a The density measurement of the first Paxon HDPE sample between 145 and 245 °C. A discontinuity or a transition is observed between 185 and 205 °C. The error bar on each data point is 0.4%.	101
Figure 4.6b The density measurement of the second Paxon HDPE sample between 145 and 245 °C. A discontinuity or transition is observed between 208 - 211 °C and 216 - 221 °C. The error bar on each data point is 0.4%.	102
Figure 4.6c The data from Figures 4.6a and 4.6b shown together on the same graph. The open circles indicate data from the first Paxon HDPE experiment while the crosses are data from the second Paxon HDPE experiment.	103
Figure 4.7a The density measurement of the first Solvay HDPE specimen between 130 and 240 °C. The error bar on each data point is 0.4%. The transition arrow identifies where the transition appeared for the Paxon sample (Figure 4.6a)	105
Figure 4.7b The density measurement of the second Solvay HDPE specimen between 150 and 240 °C. The error bar on each data point is 0.4%. The arrow shows the transition for the Solvay sample at approximately 215 °C.	106
Figure 4.7c The density measurement of the third Solvay HDPE specimen between 150 and 240 °C. The error bar on each data point is 0.4%. The arrow shows the transition for the Solvay sample at approximately 228 °C.	107
Figure 4.7d The density measurement of all three Solvay HDPE samples between 130 and 240 °C.	108
Figure 5.1 The interfacial tension of the Exxon 6750 HDPE (no additional anti-oxidant) and silicone oil-A from 150 to 250 °C. A total of six experiments are shown in this graph. The filled data points indicate experiments conducted at a rotation rate of 5000 rpm, while the open data points indicate experiments conducted at 8300 rpm.	125



Figure 5.2 The interfacial tension of the Exxon 6750 HDPE with the addition of 7,000 ppm anti-oxidant and silicone oil - A from 190 to 250 °C. A measurement was made every 10 °C.	128
Figure 5.3 The interfacial tension of the Exxon 6750 HDPE with the addition of 10,000 ppm anti-oxidant and silicone oil - A from 190 to 250 °C. A measurement was made every 10 °C.	129
Figure 5.4a Run 1: The interfacial tension of the Exxon 6750 HDPE with the addition of 20,000 ppm anti-oxidant and silicone oil - B from 190 to 250 °C. A measurement was made every 10 °C.	131
Figure 5.4b Run 2: The interfacial tension of the Exxon 6750 HDPE with the addition of 20,000 ppm anti-oxidant and silicone oil - B from 190 to 250 °C. A measurement was made every 10 °C.	132
Figure 5.5 The interfacial tension of "pure" LDPE and silicone oil-B from 190 to 250 °C. A measurement was made every 10 °C.	135
Figure 5.6 The interfacial tension of "pure" LLDPE and silicone oil-B from 190 to 250 °C. A measurement was made every 10 °C, and note that no transition in the interfacial tension is observed.	136





## LIST OF TABLES

Table 1. A description of LDPE, LLDPE and HDPE	3
Table 3.1. Dimensionless Numbers for the Water and Air System in a Spinning Drop Tensiometer. All data from this table are the same data given in Figure 3.10.	59
Table 3.2. A Comparison Between the Tube Rotation Rate and a 3.5mm OD Plastic Drop Rotation Rate Inside a Tube Filled with Water.	63
Table 3.3. A Comparison Between the Tube Rotation Rate and a 2.6mm OD Plastic Drop Rotation Rate Inside a Tube Filled with Water.	63
Table 3.4. A Comparison between the Rotation Rate of the Glass Tube and the Rotation Rate of the Motor Controller Digital Display.	70
Table 4.1. The properties of the HDPE investigated in this chapter	87
Table 5.1. Data from Pham and Carriere (1997) on the Interfacial Tension of the PC/PE at different temperatures	114
Table 5.2. The properties of the PE investigated in this chapter	116



# Nomenclature

$\gamma$	Interfacial Tension
$\rho$	Density
$\omega$	Angular Velocity
$\nu$	Kinematic Viscosity
B	Numerical Factor for Calculating $\gamma$ in the Sessile Drop Equation
D	Diameter
d	Diameter
E	Energy
F	Numerical Factor for Calculating $\gamma$ in the Sessile Drop Equation
g	Gravitational Acceleration
H	Shape Correction Factor in the Pendant Drop Equation
L	Length of the Cylindrical Drop
M	Molecular Weight
P	Pressure
r	Radius
T	Temperature
V	Volume
w	Weight
y	Vertical Distance from the Center of the Drop

## Suffixes

1	Outer Fluid
2	Inner Fluid
a	In Air
atm	Atmospheric
e	Equatorial
L	Liquid
m	Melt
n	Number Averaged
o	Centreline of the liquid (in the y direction)
P	Piston
R	Rotation
S	Surface Tension
s	Solid
w	Weight Averaged





# CHAPTER 1

## INTRODUCTION

---

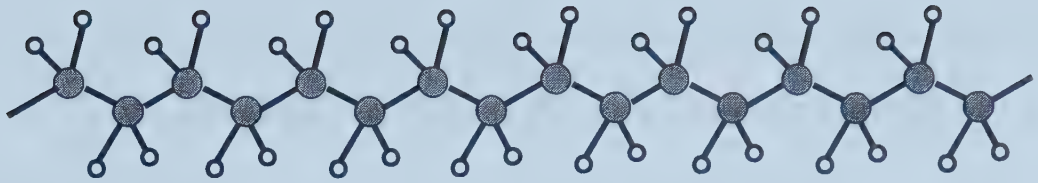
### 1.1 Introduction

Polyethylene (PE) is a widely used product, with both industrial and domestic uses. Some examples of items manufactured using PE are plastic bottles, grocery bags, pipelines, bullet proof vests, toys, coatings, films, etc. Polyethylene was first produced on an industrial scale in the 1930s (Painter and Coleman, p. 4). Since then, the market for PE has increased considerably due to improved technology in the polymer resin processes. Today, over 30 billion pounds of PE are produced annually worldwide (Chemical and Engineering News, p. 47).

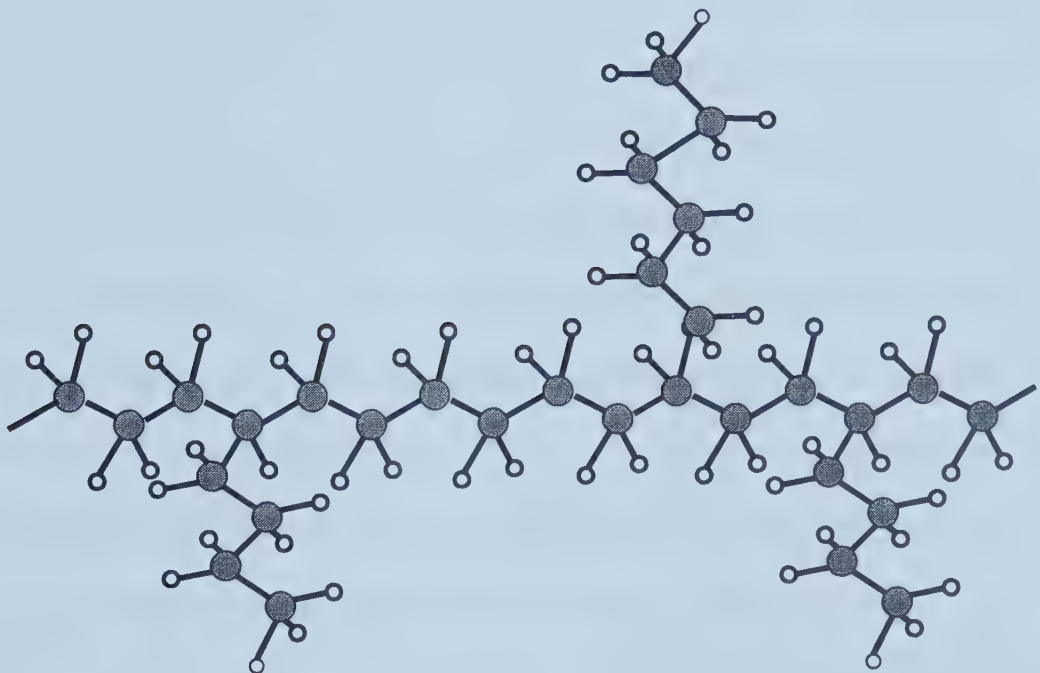
In general, the backbone of a PE molecule consists of many ethylene repeating units  $(\text{CH}_2 - \text{CH}_2)_n$ . The number of repeating units,  $n$ , ranges between 400 and 50,000 for commercial PE (Encyclopedia of Polymer Science and Technology, Vol. 6). A chain of PE polymer may be either *linear* or may have alkyl substituents on its backbone (*branched*). A schematic diagram of the basic PE structure is shown in Figure 1.1 (Painter and Coleman, p. 5).

The long linear portion of a polymer molecule can either be folded, or it can be randomly tangled. The region where three-dimensional folding occurs is called the crystalline phase, in which there is some order in the molecular structure. The region where the molecule chains are randomly tangled with each other is called the





(a) Part of a linear polyethylene molecule (high density polyethylene)



(b) Part of a branched polyethylene molecule (low density polyethylene)

Figure 1.1 Polyethylene molecules (adapted from Painter and Coleman, p. 5).





amorphous phase, in which there is no molecular order. The crystalline phase increases the degree of rigidity of the polymer and also provides a higher melting point, while the amorphous phase provides flexibility and high impact strength of the PE (Encyclopedia of Polymer Science and Technology, Vol. 6, p. 385).

Polyethylene molecules are semi-crystalline, i.e. there is a fraction of crystalline phase embedded in a matrix of amorphous phase. Depending on the thermodynamics and kinetics of the crystallization process of the polymer, the crystalline phases exist in varying sizes and degrees of perfection. The degree of crystallinity affects the density of the bulk PE. As such, PE is generally divided into three main categories based on its density: low density polyethylene (LDPE), linear low density polyethylene (LLDPE) and high density polyethylene (HDPE). Each of these types of PE is synthesized differently with different chemical structures (alkyl substituents or copolymers), which has a direct impact on the degree of crystallinity, and hence on the bulk density of the polymer. The approximate density ranges, synthesis method and types of chemical structures are shown in Table 1.1 (as summarized from Encyclopedia of Polymer Science and Technology, Vol. 6).

Table 1. A description of LDPE, LLDPE and HDPE

<b>PE category</b>	<b>Density (g/cm<sup>3</sup>)</b>	<b>Polymer Synthesis</b>	<b>Common Comonomers</b>	<b>Branching on backbone</b>
LDPE	0.915-0.930	Free radical polymerization at high pressure	Polar groups, such as vinyl acetate, ethyl acrylate etc.	Long branches
LLDPE	0.915-0.940	Most commonly Ziegler type catalysts	$\alpha$ -olefins such as 1-butene, 1-hexene, 1-octene	Short branches, depend on comonomer
HDPE	0.940-0.970	Phillips or Ziegler type catalysts	$\alpha$ -olefins such as 1-butene, 1-hexene	Minimal



Another category of PE which has been gaining popularity is the ultrahigh molecular weight PE. This type of PE consists of unbranched homopolymers with molecular weights as high as three to six million (e.g. Ramex®). Special polymerization techniques are required for the synthesis of these PEs.

High density polyethylene, with an annual production of 15 billion pounds worldwide (Chemical and Engineering News, p. 47), is one of the most plentiful petrochemical commodities produced in the world. The common processing of HDPE includes injection molding, blow molding and extrusion techniques, with processing temperatures commonly in the range of 200-260 °C (Encyclopedia of Polymer Science and Technology, Vol. 6, p.477). Despite its widespread uses and large market, there have been several anomalies reported in the past decade pertaining to the behavior of HDPE in the liquid state, in the range of the processing temperature. It is conventionally believed that above the melting temperature ( $T_m$ ) of 135-140 °C, HDPE undergoes a change from the semi-crystalline to an amorphous melt phase with no long range molecular order i.e. a classical random coil (Flory, 1953). (If so, this would permit only local ordering of the liquid state, meaning there is a well defined average number of neighboring molecules.) However, studies by several authors in the last decade have seen anomalous behavior of the polymer melt which suggests the possibility of structural order on a long-range level (some examples include Bremner and Rudin, 1992, Wang and Drda, 1997, Hussein and Williams, 1998).

The motivation for this thesis project is suggested by a recent finding by Hussein and Williams (1998) that the torque registered in a blender for a sample of molten



HDPE ( $M_w = 78,030$ ,  $M_n = 16,540$ ) contains evidence of transitions in the temperature range of 160 to 260 °C. A figure from their paper is shown in Figure 1.2. As the figure shows, one or more thermal transitions occur in the torque in the temperature range of 200 to 230 °C. The same discontinuity is not observed for the polystyrene (PS) sample, which is normally believed to be amorphous (PS was used as a reference or comparison to the behavior of PE to rule out the possibility of artifacts in the experimental apparatus.) The same group also conducted density measurements of the HDPE and a discontinuity in the volume expansion coefficient curve was also found in the same temperature range of 200-230 °C (Hussein, PhD thesis.)

The observation of a discontinuity in the rheological properties of the HDPE responsible for torque in a temperature range much higher than the HDPE melting temperature suggests the possibility of molecular ordering of some sort in the HDPE liquid state, a behavior similar to the liquid crystalline polymers normally used for optical applications (i.e. poly (n-acrylate), poly( $\alpha$ -styrene) etc.). A liquid crystal, unlike amorphous polymer melts, contains an isotropic phase and maintains some degree of order or an alignment of its molecules in a specific direction. The possibility of ordering of the HDPE melt in this temperature range is intriguing, as most industrial molding and extrusion processes of HDPE occur in the temperature range of 200-260 °C. Analyses of these industrial HDPE processes are based on the conventional belief that the HDPE melts are amorphous without molecular order. Based on Hussein and Williams' observation of anomalous behavior of HDPE melt in the temperature range of specific interest to industry, there may be other methods which may optimize the processing of the HDPE once the properties of its melt are better understood.





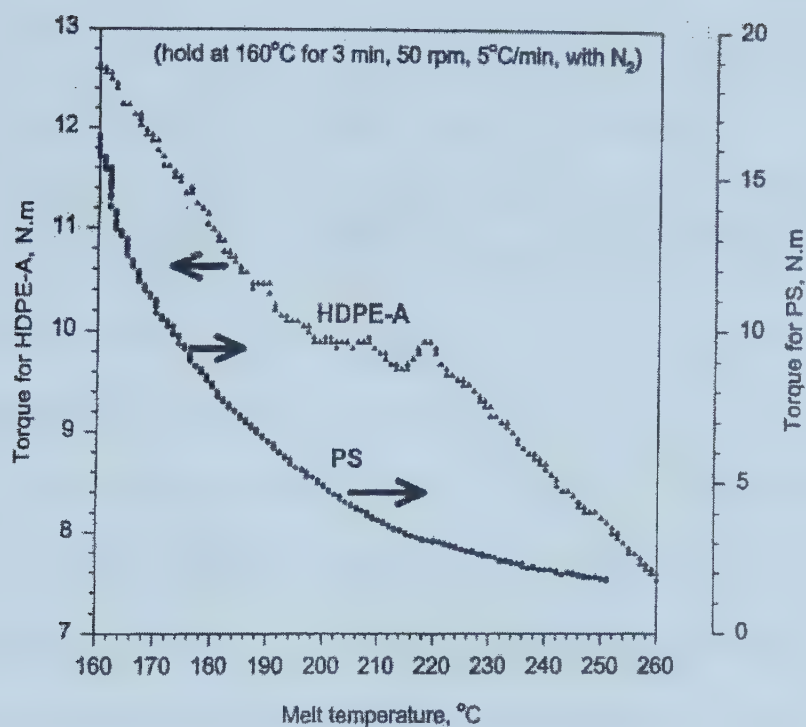


Figure 1.2 Hussein and Williams' Torque Melt Experiment of HDPE and PS in the temperature range of 160-260°C. From *"Rheological evidence for high-temperature phase transitions in melts of high-density polyethylene"*, Hussein, I.A., William, M.C., Macromol. Rapid Commun. **19**, 323-325 (1998).



The objective of this thesis is to further investigate the thermal transition of the HDPE in the temperature range of 200-230 °C. Hussein and Williams conducted different sets of experiments involving bulk HDPE. It is of interest to investigate the possibility of the same transition at the surface of the polymer. This perhaps may provide some insight into the types of transitions similar to the behavior of liquid crystals, and hence help us gain some more understanding of the ordering of the HDPE melt. As such, interfacial measurements of HDPE will be investigated in the temperature range of 180-250 °C to check for the transition at the surface of the HDPE similar to the findings of Hussein and Williams.

There are many different interfacial tension measurement methods available (Wu, 1982). However, the spinning drop method was chosen for all of the polymer interfacial tension measurements to be presented in this thesis because of the flexibility and ease with which the experiments can be conducted in a continuous manner at high temperatures. The spinning drop tensiometer has been gaining popularity for polymer interfacial tension measurements. However, there have also been several reported limitations with the spinning drop tensiometer (Manning and Scriven, 1975, Capelle, 1981, Isaacs et al., 1988), and it has been reported by the afore-mentioned authors that gyrostatic disequilibrium under the experimental conditions affects measured interfacial tension values. In this project, a detailed investigation of the limitations of the spinning drop tensiometer in measuring interfacial tensions was conducted, and an understanding of these limitations was incorporated into the HDPE interfacial tension experiments. In the development of the experiments, a novel technique of loading solid HDPE to measure the interfacial





tension of polymer melts was also developed. This method is easy and minimizes contamination in the polymer systems.

## **1.2 Scope**

- In Chapter 2, the theory of operation and a detailed description of the spinning drop tensiometer will be provided.
- In Chapter 3, the error analysis of the spinning drop tensiometer will be provided. Simple systems such as water/air and silicone oil/air were used for the experiments described in this chapter.
- In Chapter 4, the results of the density experiments for high density polyethylene between 160 and 250 °C will be provided.
- In Chapter 5, the results for the investigation of the surface tensions of HDPE, LDPE and LLDPE melts will be provided. The anomalies observed by other investigators will also be presented as well.



## CHAPTER 2

# INTERFACIAL TENSION MEASUREMENT – THE SPINNING DROP TENSIOMETER

---

### 2.1 Introduction – Methods of Interfacial Tension Measurement for Polymer Melts

Most methods of interfacial tension measurement require a balance between a known force imposed on a surface and the interfacial force created due to a changed surface area. In theory, almost all methods of interfacial tension measurement are suitable to measure the interfacial tension of polymer melts (Wu, 1982, Elmerdorf, 1986). However, data on the interfacial tension of polymer melts are very limited due to the experimental difficulties associated with the measurements. Polymer melts are highly viscous and require high temperatures to remain in the liquid state. Due to their high viscosity, long times are needed before equilibrium can be reached, and the polymers generally degrade before equilibrium is reached (Kamal et al., 1994, Arashiro et al., 1999, Vinagre et al., 1998). Currently, the most common methods of interfacial tension measurement of polymer melts are the pendant drop method, the contact angle method, the sessile drop method, the breaking thread method and the spinning drop method. These methods are described extensively in *Polymer Interface and Adhesion* by Wu, 1982.

The pendant drop method is based on the drop profile of the polymer melt under gravity, where a less dense polymer drop is immersed into a melt of denser



fluid in a controlled and closed environment. A diagram of the pendant drop is shown in Figure 2.1. The interfacial tension can be obtained based on the following expression (Wu, 1982):

$$\gamma = \frac{\Delta\rho g d_e^2}{H} \quad (2.11)$$

where  $\Delta\rho$  is the density difference of the two fluids,  $g$  is the gravitational acceleration,  $d_e$  is the equatorial diameter, and  $H$  is a correction factor based on the shape of the drop. The pendant drop method has been used by Escudie et al. (1986) to measure the interfacial tensions between polypropylene and polystyrene (PP/PS) melt between 220 °C and 270 °C. Kamal et al. (1994) used the pendant drop method to measure the effects of temperature and molecular weight on the interfacial tension of polystyrene and polypropylene pairs, and Arashiro et al. (1999) investigated the same effects with polyethylene and polystyrene pairs. A disadvantage with the pendant drop method is that the drop may detach from the orifice if the interfacial tension is decreased during the experiment, i.e. during an increase in temperature (Wu, 1982). Also, because this method depends on the gravitational pull during the experiment, the equilibration time may be long. In fact, Escudie et al. (1986) observed that in some cases (for PP/PS), at temperatures below 220 °C, the time for the drop to reach equilibrium can be *several days*.

The sessile drop method is also a drop profile method similar to the pendant drop method, as shown in Figure 2.2. The interfacial tension of the polymer system can be found from the following expression:





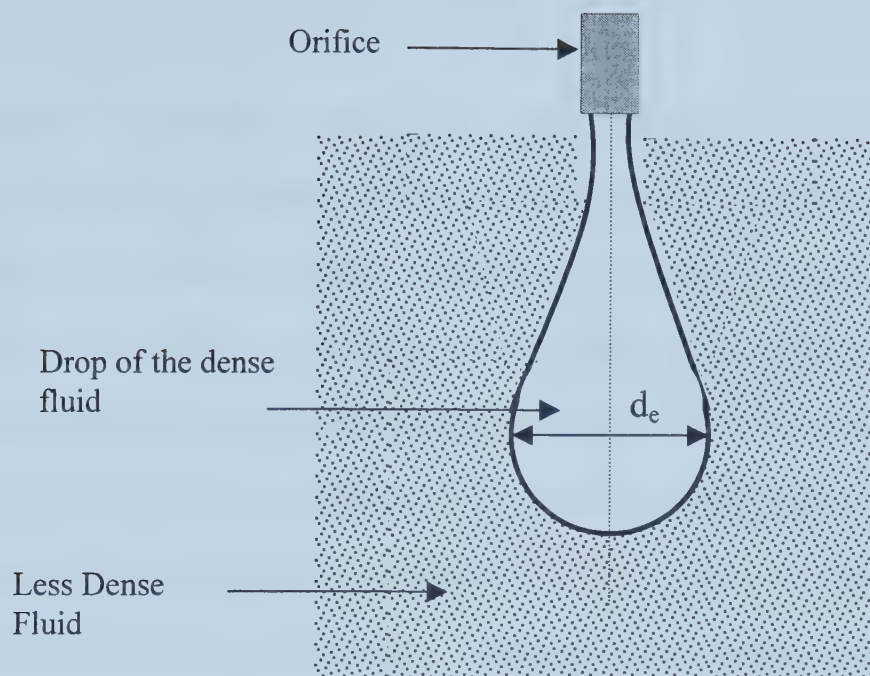


Figure 2.1 A schematic diagram of the pendant drop.

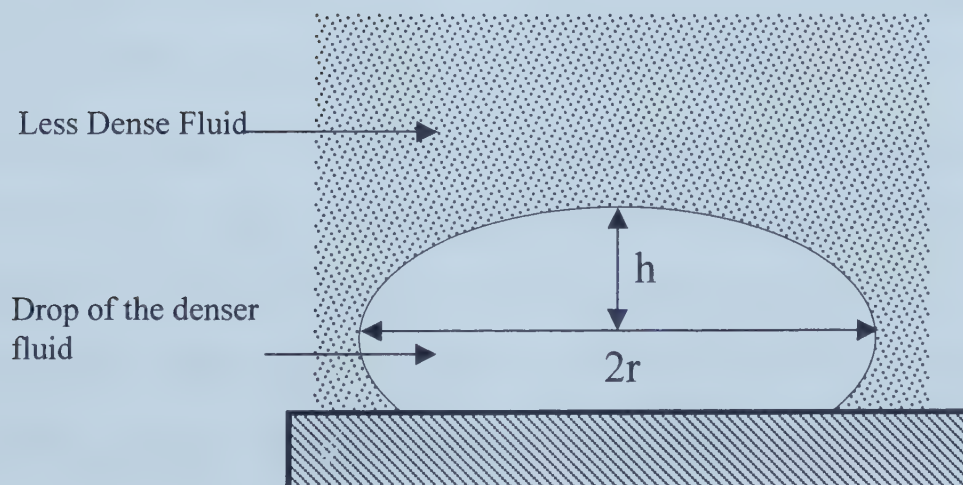


Figure 2.2 A schematic diagram of the sessile drop.



$$\gamma = \frac{\Delta\rho g r^2}{BF^2} \quad (2.12)$$

where  $r$  is the equatorial radius, and  $B$  and  $F$  are functions of the apex height  $h$ , and  $r$ . An advantage of the sessile drop method is that unlike the pendant drop method, there will be no detachment problems since the drop is resting on a solid surface. However, the equilibration time is much longer than for the pendant drop. This is a major disadvantage in measuring the interfacial tensions of highly viscous polymer melts.

The breaking thread method (Tomotika, 1935), unlike all of the above mentioned methods, does not require density data. It is based on a thread of fluid embedded in another fluid matrix. A small perturbation induced on the thread causes instability in the thread. When the wavelength of this perturbation is greater than the diameter of the thread, the instability in the thread will eventually grow and cause the breakup of the thread. Interfacial tension of the fluids can be obtained from the rate of growth of the instability. The details of the breaking thread method can be found elsewhere (Chappelear, 1964, Elemans et al., 1990, Mikhilef et al., 2000). One of the biggest advantages of the breaking thread method is the short experimental times required. This reduces the possibility of degradation of the polymer during the experiments at high temperatures (Chappelear, 1964, Rao, 1999). However, Rao (1999) in his experiments with polystyrene and polypropylene pairs, observed non-uniform diameters of the thread due to uneven tension used to pull the thread. Moreover, since the threads were drawn in the air, the polymer samples were subjected to possible absorption of moisture from the air, and also subjected to contamination from the open environment. Another disadvantage of the breaking



thread method is that the experiments are non-continuous; a new sample was required for each new temperature of the experiment.

Among other methods of interfacial tension measurement are the shear flow deformation method and the imbedded fiber retraction method. In the shear flow deformation method, a polymer drop is placed between two parallel plates, and subjected to a flow of lighter fluid. Interfacial tension can be obtained by analyzing the deformation of the drop under the shear flow of the less dense fluid. Guido et al., (1999) used this method to investigate the diffusion of polyisobutylene into polydimethylsiloxane and its effects on the interfacial tension between the polymers. The imbedded fiber retraction method, first used by Carriere et al. (2000) is similar to the breaking thread method. A thread of polymer melt is placed in the matrix of the other polymer melt, and the rate at which this thread breaks and retracts into a sphere provides information about the interfacial tension between the two polymers. Ellingston et al. (1994) have used this method to examine the effects of molecular weight on interfacial tension between polystyrene/poly(methylmethacrylate). The disadvantage of this method is similar to that of the breaking thread method.

Another method of polymer interfacial tension measurement has been gaining popularity because of the ease of measurement – the spinning drop method (Vonnegut, 1942, Patterson et al., 1971, Elmendorp et al., 1986, Quiron et al., 1995, Stammer et al., 1998, Visscher et al., 1999, Verdier et al., 2000.) A less dense drop of fluid is placed inside a matrix of denser fluid, and both fluids are rotated at high speeds. Under the pull of the centrifugal forces, the less dense fluid assumes a cylindrical shape along the axis of rotation, and the interfacial tension of the system can be





obtained based on the geometry of the drop, density difference and rotational rate of the samples. Unlike the pendant and sessile drop methods, which depend on gravitational forces for the drop profiles, the centrifugal forces upon which the spinning drop method relies can be controlled and changed to higher levels, which allows for faster equilibration times (Verdier et al., 2000). Also, unlike the breaking thread and imbedded fiber retraction method, the spinning drop method allows for a continuous measurement of the polymer interfacial tensions at different temperatures without having to load a new set of samples for each measurement. Also contamination of the samples is minimized. For these reasons, in this thesis, the spinning drop method was chosen to measure all interfacial tensions of the high density polyethylene in the temperature range of 160-250 °C.

## **2.2 The Spinning Drop Tensiometer**

The spinning drop tensiometer, based on the spinning drop method, is a widely used apparatus for interfacial tension measurements in both the petroleum industry (Cappelle, 1981, Neale et al., 1987, Isaacs et al., 1989, Taylor et al., 1990, Touhami et al., 1994, Verma, 1998) and the petrochemical industry (Elmendorp et al., 1986, Quiron et al., 1995, Stammer et al., 1998, Visscher et al., 1999, Verdier et al., 2000.) Part of the reason for the popularity of the spinning drop method is the ease of measurement and its capability of measuring systems with small density differences and very low interfacial tension values (Verdier et al., 2000).

The spinning drop method was first developed by Vonnegut in 1942. Since then, many different modified versions of the spinning drop tensiometer have



surfaced (Princen et al., 1971, Slattery et al., 1980, Joseph et al., 1992, Borchart et al., 1993, Contreras et al., 2000, Levy et al., 2001). The spinning drop tensiometer used in all of the experiments in this thesis is a version purchased from SDT Ltd. (University of Minnesota, Minneapolis). This spinning drop tensiometer can measure interfacial tensions at temperatures up to 280°C with a motor rotational range of 1 to 15,000 rpm, and is capable of measuring interfacial tension as low as  $3.0 \times 10^{-3}$  mN/m (Vinagre 1998 SDT Manual).

### **2.2.1 Theory**

The operation of the spinning drop tensiometer is based on the theory first derived by Vonnegut in 1942. When a drop of fluid is enclosed in a container filled with a denser fluid and subjected to high rotational rates with respect to a horizontal axis, the less dense fluid will migrate to the axis of rotation and assume a cylindrical shape with hemispherical ends (Vonnegut, 1942). The measurement of the cylinder radius  $R$  yields the value of interfacial tension. This theory holds true only if the fluids are in gyrostatic equilibrium (or rigid body rotation), i.e. every element of the fluid inside the rotating tube is stationary relative to the wall of the tube (Manning and Scriven, 1975). Gyrostatic equilibrium is only attained at high enough rotation rates that gravitational forces perpendicular to the axis of rotation are negligible compared with centrifugal forces. A schematic of the drop under rotation is shown in Figure 2.3. The density of the denser outer fluid is designated  $\rho_1$  and the density of the less-dense droplet is  $\rho_2$ .



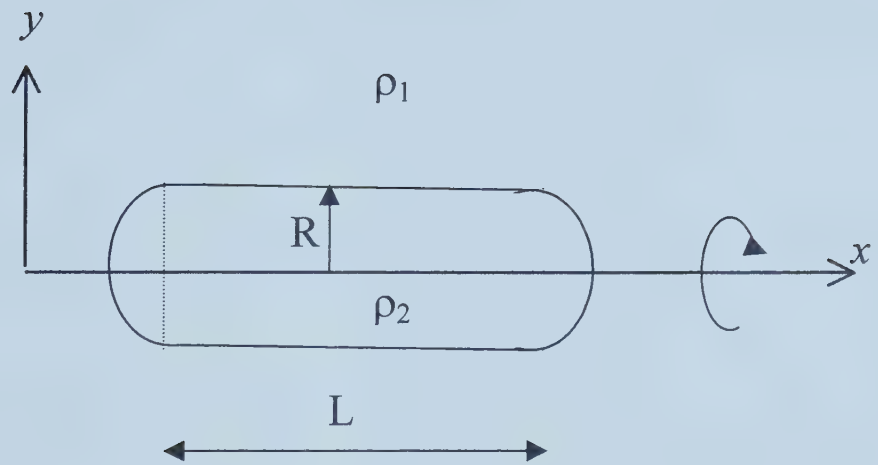


Figure 2.3 A schematic of the cylindrical drop under rotation.





A summary of Vonnegut's derivation is presented here. At high enough rotation rates it is assumed that the drop forms a cylinder with hemispherical ends. Two types of energy vary with the drop radius when the drop is subjected to rotation: the "energy due to rotation of the drop ( $E_R$ )" (Vonnegut, 1942) and the energy due to the surface tension of the drop ( $E_S$ ). The rotation energy of the drop equals the integral of the product of the pressure difference,  $\Delta P$ , at the interface of the drop and the elemental volume,  $dV$ , of the drop.

$$E_R = \int \Delta P dV \quad (2.13)$$

The pressure difference at the interface of the drop is

$$\Delta P = \frac{\omega^2 y^2 (\rho_1 - \rho_2)}{2} \quad (2.14)$$

where  $\omega$  is the rotation rate of the drop,  $y$  is vertical distance from the center of the drop ( $R > y > 0$ ), and  $\rho_1$  and  $\rho_2$  are the densities of the denser and less dense fluids, respectively. By substituting equation 2.14 into equation 2.13 and integrating,  $E_R$  can be expressed as

$$E_R = \frac{1}{4} \pi (\rho_1 - \rho_2) \omega^2 L R^4 + \frac{4}{15} \pi (\rho_1 - \rho_2) \omega^2 R^5 \quad (2.15)$$

The energy due to the surface tension of the drop,  $E_S$ , is expressed as



$$E_s = \gamma(2\pi RL + 4\pi R^2) \quad (2.16)$$

where  $\gamma$  is the surface tension of the drop and  $2\pi RL + 4\pi R^2$  is the total area of the drop.

The total energy of the drop ( $E$ ) is the sum of  $E_R$  and  $E_s$ ,

$$E = \frac{1}{4}\pi(\rho_1 - \rho_2)\omega^2 LR^4 + \frac{4}{15}\pi(\rho_1 - \rho_2)\omega^2 R^5 + \gamma(2\pi RL + 4\pi R^2) \quad (2.17)$$

When the system is in equilibrium, the total energy of the drop is at a minimum.

Taking the derivative of equation 2.17 with respect to radius  $R$  and setting it equal to zero yields the interfacial tension ( $\gamma$ ) as a function drop radius  $R$

$$\gamma = \frac{(\rho_1 - \rho_2)\omega^2 R^3}{4} \left(1 + \frac{2R}{3L}\right) \quad (2.18)$$

At high rotation rates, the length of the bubble is much larger than the radius,

and hence the  $\frac{2R}{3L}$  term can be neglected, and Equation 2.18 may be simplified to

$$\gamma = \frac{(\rho_1 - \rho_2)\omega^2 R^3}{4} = \frac{(\rho_1 - \rho_2)\omega^2 D^3}{32} \quad (2.19)$$

When the ratio of the drop length to diameter ( $L/D$ ) is greater than 4, neglecting of  $D/3L$  in Equation 2.18 is justified. Manning and Scriven (1975) reported that Equation 2.19 is in error by less than 0.4%. This equation is used to calculate the



interfacial tension in all of the spinning drop experiments in this thesis, unless otherwise stated.

### **2.2.2 Description of Equipment**

A schematic diagram of the spinning drop tensiometer used in this work is shown in Figure 2.4. The immiscible fluids (for which the interfacial tension values are to be measured) are placed inside a glass tube, which is held horizontally between two shafts connected to the motor. Two oven heater blocks are placed on top and below the glass tubes to provide temperature control of the samples during measurements. The motor and the oven are both connected to controllers which control the rotation rate and temperature of the sample in the glass tube. A stroboscope light is placed behind the samples and a video camera is placed directly in front of the glass tube. The video camera has a zoom function which allows for different magnification and focus of the drop diameter inside the glass tube. The video camera is connected to a computer with a frame grabber and the SDT32 software. When the fluids are subjected to rotation, the lighter fluid drop will tend to assume a cylindrical shape. The frame grabber and the SDT32 software allow the operator to capture the live image of the cylindrical drop on the monitor and measure its diameter inside the glass tube as the sample is subjected to rotation.

#### ***a. The Glass Tube and the End Plugs***

The glass tube is made of Pyrex glass. It has an inner diameter of  $12.70 \pm 0.015\text{mm}$ , and a wall thickness of  $2.50 \pm 0.01\text{mm}$ . The length of the tube is  $222 \pm 2\text{mm}$ . The glass tube





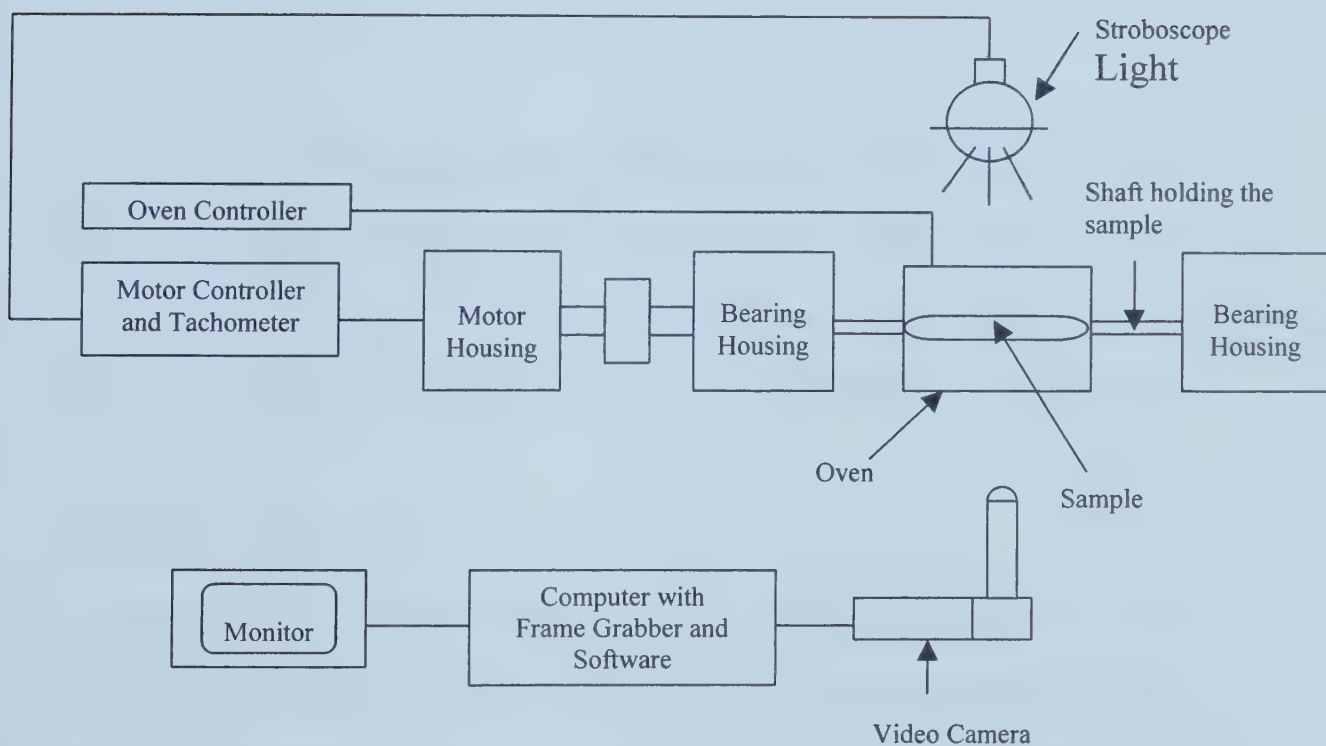


Figure 2.4 A schematic diagram of the spinning drop tensiometer used in this work (Adapted from the SDT Manual). See also Figure 2.6.



can hold liquid sample volumes up to approximately 17 cm<sup>3</sup>. The typical volume of the drop in the glass tube is approximately 0.1 to 0.5 cm<sup>3</sup>. Both ends of the glass tube are sealed with stainless steel plugs. One of the plugs has a multi-step calibration post with known diameters of 1, 2 and 3mm, which can be used to calibrate the reticule distances for the measurement of the drop diameter. A schematic diagram of the end plug with the multi-step calibration post is shown in Figure 2.5.

### ***b. The Oven***

The oven consists of two steel heating blocks (upper and lower) which enclose the glass tube. A J-type thermocouple is placed on the lower heating block. The total oven power is 2000 watts, and the maximum operating temperature of the oven is 290°C. The controller controls the temperature to  $\pm 1^\circ\text{C}$  (Vinagre 1998 SDT Manual).

### ***c. The Motor and the Glass Tube Mount***

A detailed diagram of the glass mount is shown in Figure 2.6. The glass mount consists of two aluminum shafts and retaining rings which hold the weight of the glass tube horizontally. Each shaft is connected to a piston which is inserted in both ends of the glass tube and just touches the sealing plugs. The pistons are spring loaded to allow for expansion of the liquid in the glass upon heating. The retaining ring of the shaft presses the O-ring against the end of the glass tube. The O-ring provides enough friction against the end of the glass tube so that when the motor drives the retaining ring, the glass tube also rotates via the rotation of the O-ring. The motor drives only the left retaining ring,



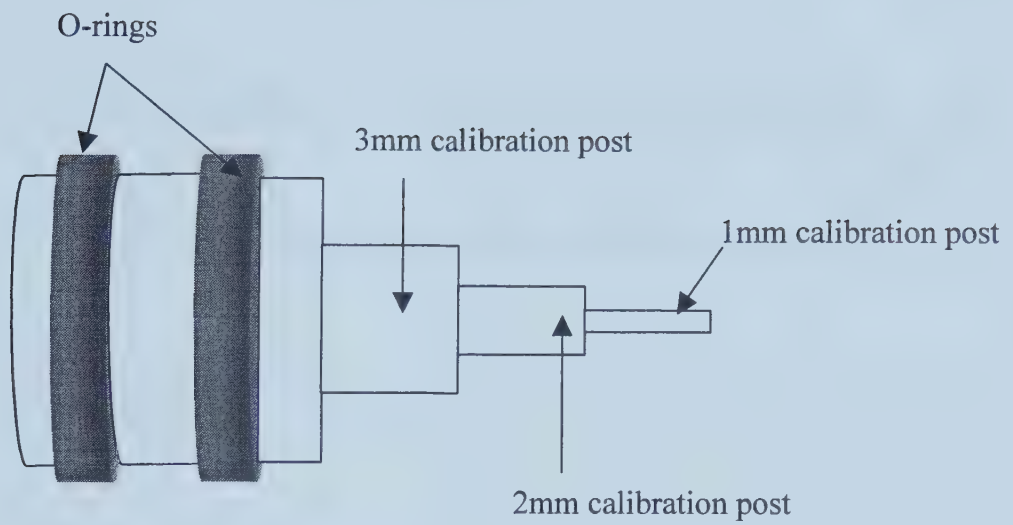


Figure 2.5 A schematic diagram of an end plug with multi-step calibration posts.



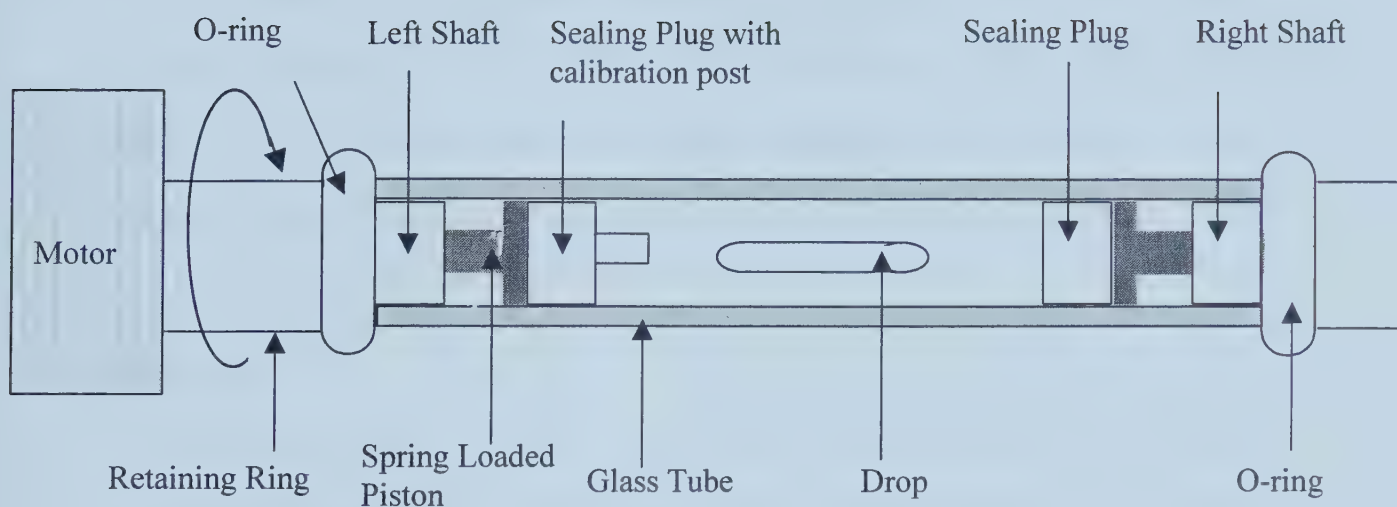


Figure 2.6 A schematic diagram of the glass mount with the glass tube. The retaining ring of the shaft presses the O-ring against the end of the glass tube. The O-ring provides enough friction against the end of the glass tube so that when the motor drives the retaining ring, the glass tube also rotates via the rotation of the O-ring. The glass tube is filled with the denser fluid and a drop of the less dense fluid. When the glass tube rotates, the less dense drop assumes a cylindrical profile with hemispherical ends.





which turns the glass tube. The right retaining ring and the right shaft are driven by the glass tube via the right O-ring. The shafts are connected to special high precision ball bearings which reduce vibration in the system. Exxon Beacon grease is used to lubricate the bearings to reduce vibration in the system.

The motor has an operating range of 1,500 rpm to 15,000 rpm, and it can maintain constant rotation rate within  $\pm 1$  rpm. An internal tachometer is built into the motor and the rotation rate of the motor is displayed on the controller. The accuracy of this rotation rate is 0.2% (Vinagre 1998 SDT Manual).

#### ***d. O-rings***

The O-rings provided by SDT. Ltd. are made from heat resistant teflon with an upper temperature limit of 200 °C. For temperatures higher than 200 °C, Kalrez O-rings by Dupont are used. These Kalrez O-rings have an upper temperature limit of 260 °C.

#### ***e. Video Camera and Measuring System***

A Hitachi black and white camera is used to capture the image of the drop inside the rotating glass tube. Navitar zoom lenses are connected to the camera. The zoom lenses consist of a 12mm internal zoom lens with magnification range of 0.7x to 4.5x, and a right angle mirror. On the computer screen the image of the drop is a mirror image, which has no effect on the magnification or the focus of the image. The field of view of this optical system is 9.4 x 12.5mm to 1.4 x 1.9mm. A stroboscope light is placed behind the glass tube and it is automatically synchronized with the rotation rate of the motor. The SDT32 software is used for the measurement of drop size from



the image of the drop on the computer monitor. Two red movable reticules are visible on the screen, and they can be moved to the outer edges of the drop on both sides to determine the diameter of the drop in millimeters<sup>1</sup>. The measurement system needs to be first calibrated against a known diameter. One of the end-sealing plugs has attached to it three posts with diameters of 1, 2 and 3 mm. Once the reticules are calibrated with the known diameter calibration post, SDT32 applies a multiplication factor which converts the number of grid lines between the edges of the drop to actual distance in millimeters. The maximum resolution of the image on the monitor is 3  $\mu\text{m}$  with precision of up to 0.02 mm (Vinagre 1998 SDT Manual).

### **2.2.3 Experimental Methods**

#### ***2.2.3a. Cleaning of the Glass Tube, the Sealing End Plugs and the O-rings***

The glass tube, O-ring and sealing end plug must be cleaned thoroughly before being used for measurements as any contamination in the system will have a significant effect on the measured interfacial tension value of the system. The following is the cleaning procedure used for *all* spinning drop experiments in this thesis.

##### ***a. Glass Tube***

- Rinse the tube with water thoroughly
- Soak the tube in Chromic Acid (10% Wt) overnight
- Rinse the tube with room temperature distilled water (Millipore) thoroughly (approximately 5 minutes)

---

<sup>1</sup> The SDT32 software places invisible gridlines on the monitor screen, and the diameter of the drop is obtained by counting the number of grids between the visible reticules.



- Rinse with hot distilled water again (place water bottle in hot boiling water for 5 minutes and use this water to rinse the tube)
- Let tube dry in air

#### ***b. End Plugs***

- Remove O-rings from end plugs
- Rinse end plugs with distilled water
- Subject end plug to burning flame (bunsen burner) for 10 seconds
- Let end plug cool in air before putting the O-rings on

#### ***c. O-rings***

- Wash O-rings with Sparkleen (a lab detergent by Fisher Scientific)
- Rinse thoroughly with distilled water

#### ***d. Syringes***

- Subject the metal needle of the syringe to burning flame for 10 seconds
- Rinse the inside of the syringe with distilled water at least 10 times

### ***2.2.3b Loading of Liquid Samples into the Glass Tube<sup>2</sup>***

After the glass tube is cleaned thoroughly, the end plug with the calibration post is inserted into one end of the tube. For the two fluids whose interfacial tension is to be determined, the denser fluid is poured into the tube first. The other sealing plug is

---

<sup>2</sup> This section describes the loading of simple systems such as water/air or silicone oil/air. The loading of polymer samples will be described in Chapter 5.





then inserted into the other end of the glass tube. This sealing plug has a hole in the center to allow air bubbles to escape from the glass tube. A small volume of the less dense fluid (liquid or gas), which is approximately  $0.1\text{ cm}^3 \sim 0.5\text{ cm}^3$ , is then added into the tube with a cleaned syringe. The whole system is then closed off with a small tapered plug inserted in the hole of the sealing end plug. The glass tube with the fluid can now be mounted horizontally and rotated at a specified rotation rate.

### ***2.2.3c Calibrating the Video Measuring System and Measuring the Drop Diameter***

When the drop is subjected to a high rotation rate in the glass tube, it will assume a cylindrical shape with hemispherical ends. The camera is placed 90 degrees to the horizontal axis of the drop so that the cylindrical drop appears vertically on the monitor.

Two red reticules appear on the screen and they can be moved by the mouse to be positioned on the edges of the drop. The SDT32 software counts the number of grid lines between the reticules and converts the grid lines to an actual distance in millimeters once the measurement system has been calibrated with either the 1 mm, 2 mm or 3 mm calibration post. The image of the drop on the black and white screen of the computer monitor has a region of "shadow" around the boundaries of the drop. The width of this shadow region can contribute to a reading error associated with the system (see Chapter 3 for analysis). In all of the measurements discussed, (unless otherwise stated) the diameter of the drop was measured by placing the reticules on the outside boundary of the drop. The image of the drop as it appears on the monitor is shown in Figure 2.7.



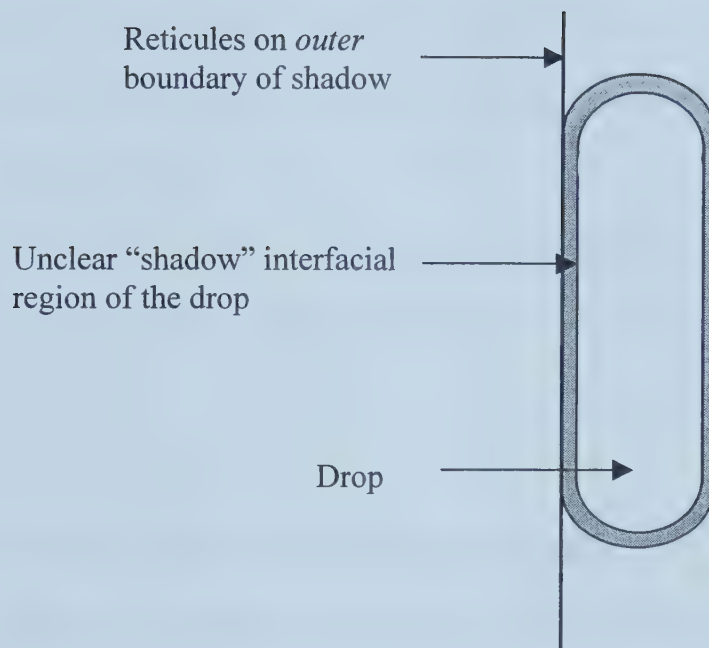


Figure 2.7 The image of the drop under rotation as it appears on the monitor screen. The "shadow" region has been exaggerated for emphasis.



Since the glass tubes are cylindrical, parallax error will occur if the drop diameter is different from the calibration post diameter. In order to reduce the error, the drop diameter must be as close to the diameter of the calibration post chosen as possible. For low viscosity systems e.g. water and air, this can be achieved in a short time by adjusting the rotation rate of the system until the drop has approximately the same diameter as the calibration post. A more detailed investigation of the parallax errors associated with the measurement of the drops will be discussed in Chapter 3.

The refractive index of the liquid changes significantly at higher temperature. As such, it is necessary to calibrate the system before the measurement at each new temperature setting.

### **2.3 Comparison with the duNuoy Ring Tensiometer**

First we need to be confident that the spinning drop tensiometer acquired from SDT Ltd. is set up properly and accurate values can be obtained from the experiments. Therefore, another established method of interfacial tension measurement, a duNuoy Ring tensiometer was used to compare with the interfacial tension values obtained using the spinning drop method. Distilled Millipore water in contact with air at room temperature (22°C) was chosen as the system, and its interfacial tension values were measured by both methods. The water was doubly distilled, degassed, de-ionized and ultrafiltered. Three measurements were taken for the duNuoy Ring and spinning drop experiments and their average values were calculated. The same water, cleaning procedure and room temperature were ensured for both experiments. For the



spinning drop experiment, a rotation rate of 5000 rpm was chosen and the diameter of the air drop was calibrated against the 2 mm calibration post<sup>3</sup>. The average value of the interfacial tension for the water/air system was found to be  $70.8 \pm 2.6$  mN/m. The average value for the duNuoy Ring experiment was  $71.5 \pm 0.5$  mN/m. The values obtained from the spinning drop tensiometer and the duNuoy Ring method are within less than 1% of each other. The interfacial tension of water/air as reported from the CRC Handbook of Chemistry and Physics (p. 6-3) at 22°C is 72.4 mN/m, which is about 2% higher than the values obtained using the spinning drop method. It is possible that the water used in the experiments as reported in the CRC handbook was different than the Millipore water used in this work, causing a small discrepancy between the values. Another possibility for this discrepancy is that there be some contamination in the air (such as dust) during the experiment. Nonetheless, it was concluded that the spinning drop tensiometer in the lab is capable of obtaining reasonable interfacial tension values.

## 2.4 Conclusions

- A spinning drop tensiometer was chosen to study the interfacial tension of the PE system in this thesis due to the ease of experimental methods associated with the spinning drop tensiometer.
- The spinning drop tensiometer in the lab is capable of obtaining reasonably accurate interfacial tension values.

---

<sup>3</sup> A rotation rate of 5000rpm was chosen so that the diameter of the air drop is approximately 2mm, which is the diameter of the calibration post.





## CHAPTER 3

### ERROR ANALYSIS OF THE SPINNING DROP Tensiometer

---

The spinning drop tensiometer is widely used to study the surface properties of many systems, i.e. polymer melts, bitumen, oil, organic solvents, etc. (some examples include works by Cappelle, 1981; Neale et al., 1987; Isaacs et al., 1989; Taylor and Schramm, 1990; Touhami et al., 1994; Verma and Kumar, 1998; Elmendorp and DeVos, 1986; Stammer and Wolf, 1998; Visscher and Willemse, 1999; Verdier et al., 2000; Cayias, 1975.) Since the development of the first spinning drop tensiometer by Vonnegut in 1942, there have been several modifications to the spinning drop tensiometer for better temperature control, vibration elimination, precision of measurements, faster measurement times, etc. (Gardner, 1974; Borchardt, 1993; Joseph, 1992). However, there have been reports on the limitations and anomalous observations associated with the spinning drop tensiometer by several authors (Manning and Scriven, 1975; Cappelle, 1981; Currie and Van Nieuwkoop, 1982 and Isaacs et al., 1989). Manning and Scriven pointed out that the operation of the spinning drop tensiometer is very much dependent on gyrostatic equilibrium. This equilibrium can be easily disturbed, especially at low rotation rates. As such, measured interfacial tension is also erroneously affected by gyrostatic disequilibrium. Cappelle and Isaacs found that apparent interfacial tension is dependent on the rotation rate of the drop, even at speeds high enough such that the length of the cylindrical drop is at least four times its equatorial diameter. Currie and Van



Nieuwkoop found that at low rotation rates, buoyancy effects in the spinning drop apparatus become dominant, affecting the measured interfacial tension measurements. All of these observations indicate the existence of errors associated with the spinning drop tensiometer measurement of interfacial tension, which are dependent on how the equipment is operated, as well as the experimental conditions during each measurement.

This chapter is dedicated to investigating the limitations of the spinning drop apparatus observed by the authors mentioned above. This study is a very important section of this thesis project. The objective of this thesis is to investigate thermodynamic phase transitions of high density polyethylene (HDPE) melts in the temperature range of 200 to 230 °C at the surface of the HDPE. Preliminary interfacial tension studies of HDPE using the spinning drop tensiometer showed promising results in detecting the existence of these phase transitions at the surface of the polymer. However, these apparent phase transitions involve a very small change in interfacial tension. If the errors in interfacial tension measurements are bigger than the transition in interfacial tension values, then the observed results may not be significant. Therefore, a large amount of time was allotted to determining the errors associated with the spinning drop tensiometer measurements and quantifying the magnitude of the errors in the measurements. This chapter describes the details of this investigation.

### **3.1 Materials**

In this chapter, two fluid systems were used to perform the error analysis of the spinning drop tensiometer – silicone oil/air and water/air. (The silicone oil/air



systems were chosen as models for high temperature behavior, related to the study of surface properties of HDPE at high temperatures, which will be explained in Chapter 5.) The silicone oil (Dow Corning 710 Fluid) has an average molecular weight of 2,600 g/mol and a specific gravity of 1.10 at 25 °C, and it is specially temperature-stabilized. The water/air systems were used to investigate low-temperature behavior, since most water data in the literature were taken around room temperature. The water used for the latter experiments was Millipore water, which was de-ionized, degassed, doubly distilled and ultra-filtered.

### **3.2 Time for the Drop to Reach an Equilibrium Size (Water/Air and Silicone Oil/Air Systems)**

The time required for a drop of air to reach an equilibrium shape in the surrounding fluid must first be determined before the experiments are begun. Two experiments were conducted for the water/air system at room temperature to investigate the time required for the drop to reach equilibrium. Since most of the experiments for the water/air and silicone oil/air will be conducted over the period of two hours, we need to be sure that under constant experimental conditions, the drop dimensions will not change and lead to an apparent drift in the measured interfacial tension. In the first experiment, the interfacial tensions of water/air and silicone oil/air were measured over a time of hours. For the water/air experiment, the tube filled with the fluids was initially at rest (i.e. no rotation). The rotation rate was then set to 4002 rpm and kept constant over time at room temperature (19 °C). Figure 3.1 shows the interfacial tension of water and air (~71.8mN/m) in the first 180 seconds, and Figure 3.2





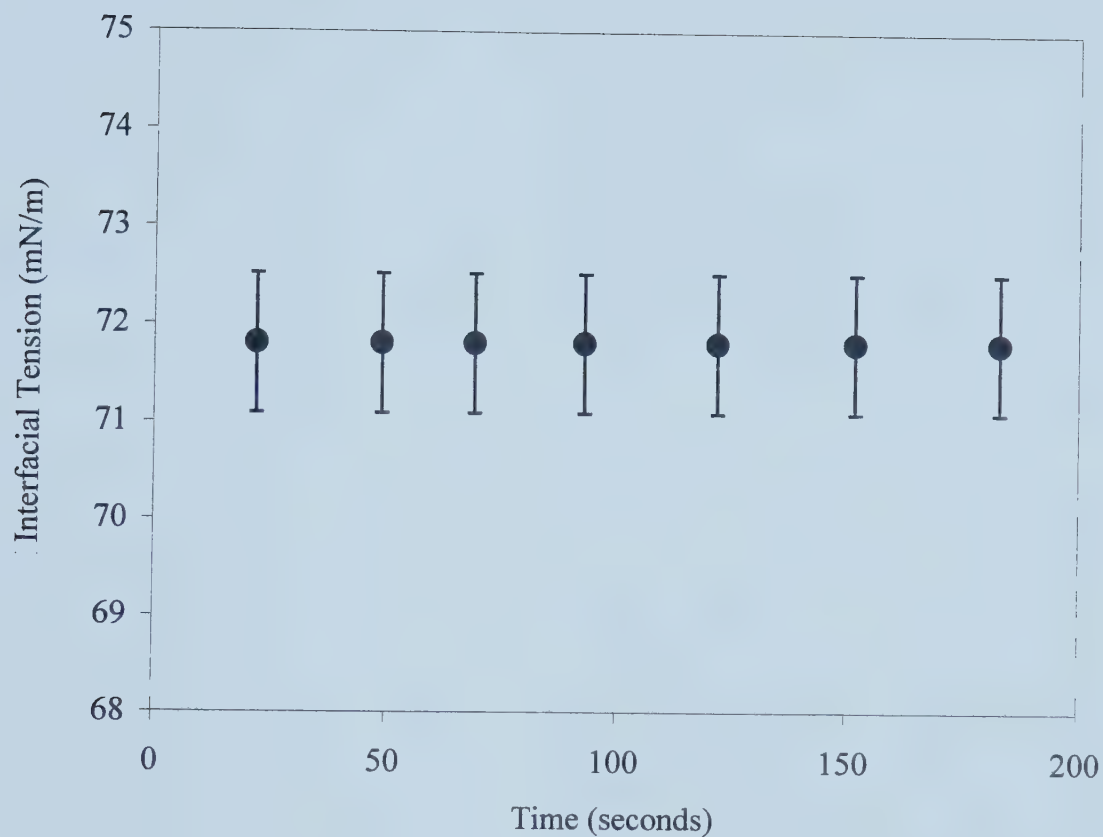


Figure 3.1 The dynamic interfacial tension of water/air as a function of time over a period of 180 seconds at room temperature (19°C). The rotation rate was kept constant at 4002 rpm after a spin up from 0 rpm at time = 0 s.



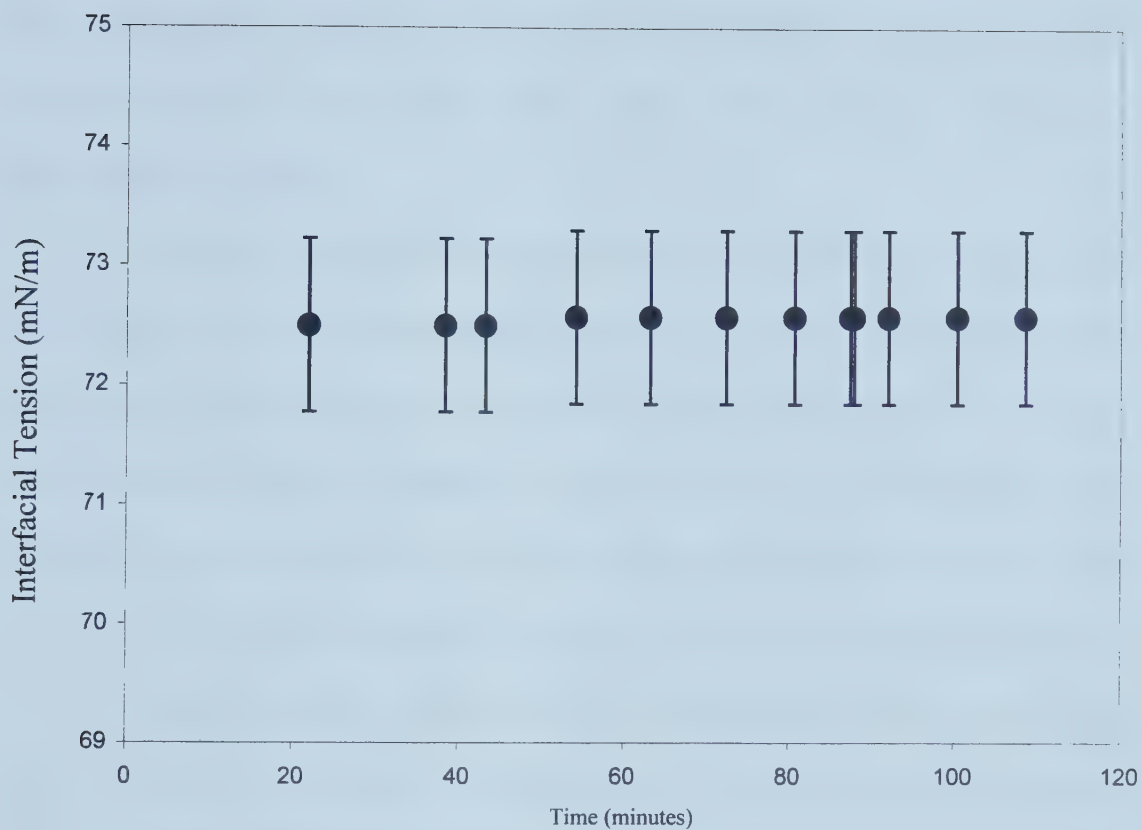


Figure 3.2 The dynamic interfacial tension of water/air as a function time over a period of 120 minutes at room temperature (19°C). The rotation rate was kept constant at 4002 rpm.



shows the interfacial tension of water and air over 2 hours<sup>1</sup>. For the silicone oil/air system, the tube filled with the fluids was initially at rest (i.e. no rotation). The rotation rate was then set to 2840 rpm and kept constant for 2 hours at 19°C. The results are shown in Figure 3.3, and it can be concluded that for the measurement of interfacial tension of the silicone oil/air system, 2000 seconds is sufficient for equilibrium to be reached.

A second set of experiments was conducted to understand the time required for a drop to reach equilibrium during spin-up or spin-down. There are two time scales which govern the rotation motion of the fluid inside a tube when the tube angular velocity is suddenly changed (Hu and Joseph, 1994). The first scale is related to the time required for the fluid to adjust to the new rotation rate caused by viscous diffusion, and the second time scale is the time for the drop to evolve to a new shape.

In this investigation, a tube filled with water and an air-drop was initially rotating at a speed of 4004 rpm. The rotation rate of the tube was suddenly increased from 4004 rpm to 4500 rpm, and the interfacial tension over time was measured. Figure 3.4 shows the interfacial tension as a function of time for three separate runs. For the first two runs, the air-drop reached an equilibrium size after 50 seconds. However, for the third run, equilibrium was reached after 70 seconds. Therefore, we can conclude that for the water and air system at room temperature, the time required to reach equilibrium after a sudden change in its rotation rate by 500 rpm is approximately one minute, and the shorter-time transient maximum should be

---

<sup>1</sup> Figures 3.1 and 3.2 are different sets of experiments, which explains why there is a difference in the interfacial tension of the water/air system.



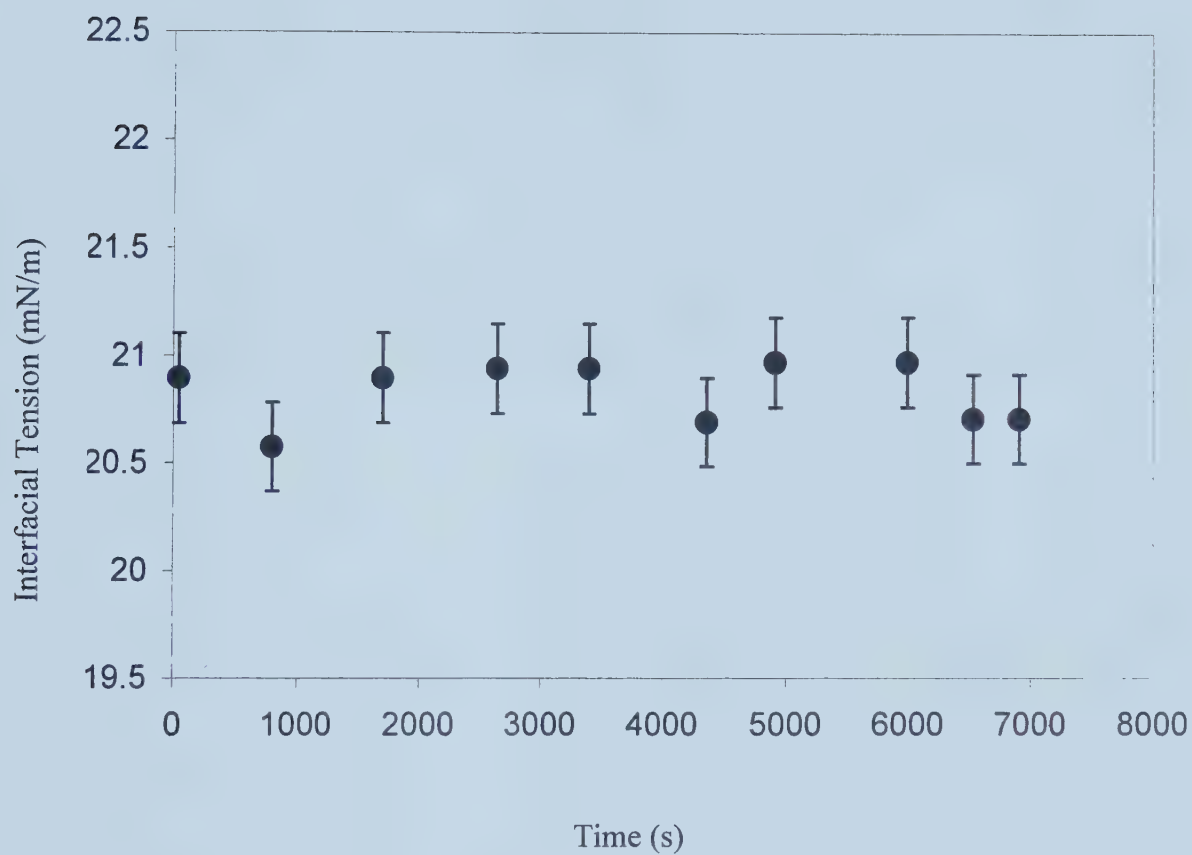


Figure 3.3 The dynamic interfacial tension of silicone oil and air over a period of two hours at room temperature (19°C). The rotation rate was kept constant at 4002 rpm.





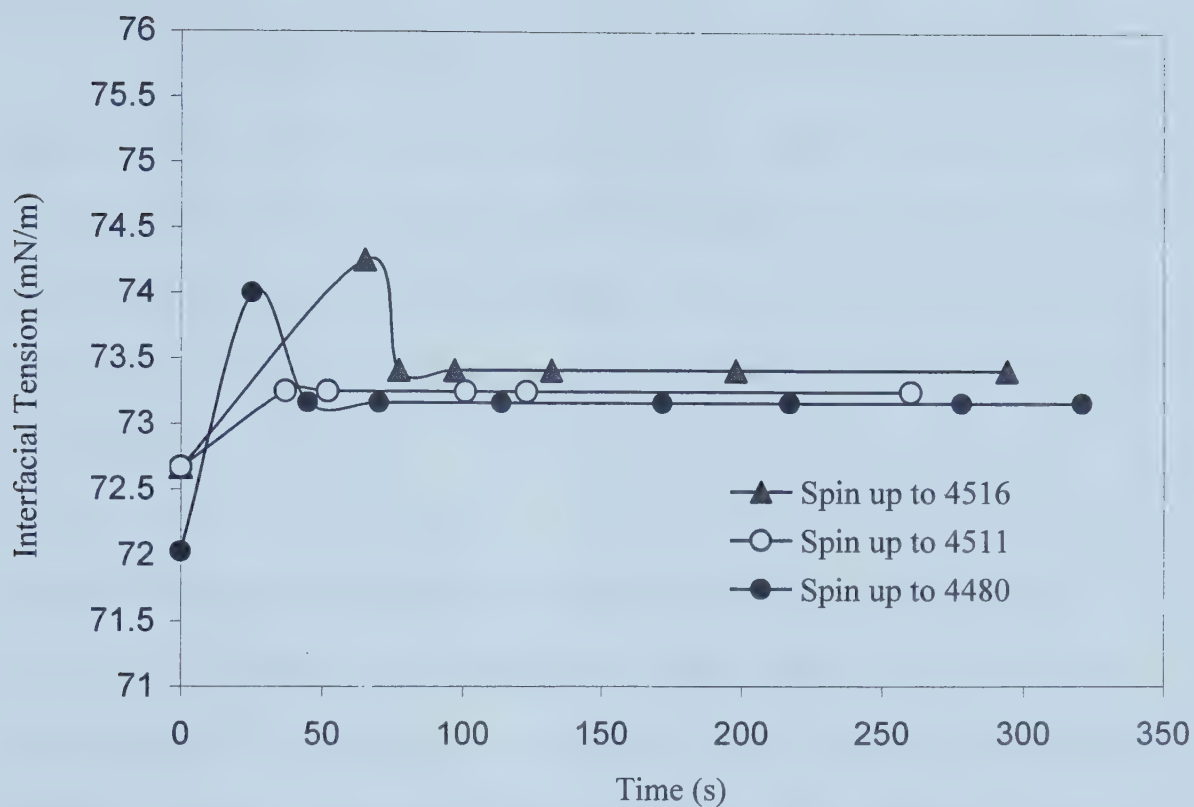


Figure 3.4 The interfacial tension of water/air as a function of time during spin-up to a new rotation rate. The initial rotational rate was 4004 rpm, and the experiment was conducted at room temperature (19°C).



disregarded for the measurement of interfacial tension. (The difference in the peaks observed in Figure 3.4 may be due to the difference in the angular acceleration during the spin up process.)

From the results for the time required for the water/air and silicone oil/air system to be in equilibrium after a spin up, it was decided that for all of the experiments for the water/air and silicone oil/air systems, after an initial spin up or spin down from set rotation rate to a higher or lower rotation rate, three minutes would be sufficient for the systems to reach equilibrium before taking the first measurement.

### **3.3 Measurement Error of the Spinning Drop Tensiometer- Reading Error**

There is a measurement error in the spinning drop tensiometer interfacial tension which includes the accuracy and resolution of the motor controller and the error associated with the measurement of the drop diameter. This measurement error is referred to as the *reading error* in this thesis.

In the initial experiment with the silicone oil/air and the air/water systems, it was found that by changing the rotation rates of the fluids in small incremental or decremental steps, there may not be a visible change in the drop boundary as viewed from the monitor screen. In order to quantify this error, for each measurement, a rotation rate was established such that the diameter of the drop was  $2.00 \text{ mm} \pm 0.05 \text{ mm}$ , which is the same as the diameter of the calibration post. This eliminated the need to correct for possible parallax error when measuring the drop diameter (parallax errors are discussed in the next section.) The rotation rate was then increased in very small steps until it was possible to see a visible decrease in the drop diameter. Then



this rotation rate (and hence the correspondingly calculated interfacial tension) was established as the upper limit of the reading error bar. Similarly, the rotation rate was also decreased in small steps until an increase in the drop diameter was visible. This became the lower limit of the reading error bar. For air/water systems ( $\gamma \sim 71$  mN/m), it was found that the error bar was  $\pm 0.6$  mN/m. A similar experiment was also conducted for the silicone oil/air system. The average interfacial tension value of silicone oil/air from three measurements was 21.3 mN/m, and the reading error was  $\pm 0.6$  mN/m. The relative errors for air/water and air/silicone were 1% and 3% respectively. These values are established as the reading error for the system. It is recommended that a reading error be established for systems other than water/air or silicone oil/air as the refractive index difference is system-dependent and may lead to a different appearance of the interface, and hence change the reading error in the drop diameter.

### 3.4 Interfacial Tension as a Function of Rotation Rate

Recall from Chapter 2 that the basic equation for interfacial tension from the spinning drop tensiometer as derived by Vonnegut (1942) is

$$\gamma = \frac{(\rho_1 - \rho_2)\omega^2 D^3}{32} \quad (3.1)$$

When the angular velocity ( $\omega$ ) is changed, the diameter of the drop changes as well, such that the product  $D^3\omega^2$  is a constant in Vonnegut's equation for a constant interfacial tension value. *This means that under constant experimental conditions (i.e. temperature, fluid properties), the interfacial tension should not change if the*





*rotation rate of the system is varied.* Of course, this equation is only valid when the length to diameter ratio of the drop is greater than 4 ( $L/D > 4$ .)

Despite the discussion above, Capelle (1981) and Isaacs et al. (1988) observed the dependence of apparent interfacial tension on rotation rate of the fluids in the spinning drop tensiometer. Capelle measured the interfacial tension of crude oil and formation water (with added surfactants) at 35 °C, and the rotation rate was varied between 4000 to 9600 rpm. Capelle attributed the dependence of interfacial tension on rotation rate to the “changing composition” of the system due to flow or gravitational effects. However, in his paper, it was unclear whether there were diffusion effects (diffusion of surfactants from formation water into crude oil) over time which would have affected the composition of the crude oil and formation water. Moreover, the author did not report whether the experiment was conducted at high enough rotation rates such that  $L/D > 4$ . This condition is very important, as Currie and Van Nieuwkoop (1982) found that at low rotation rate (where  $L/D < 4$ ) buoyancy effects due to gravitational forces can no longer be neglected and this will have an effect on apparent interfacial tension values.

Isaacs et al. (1989) conducted interfacial tension measurement of n-butanol/water at 30 °C using the spinning drop tensiometer, and the dependence of interfacial tension values on rotation rate was also observed. They also observed that the size of the tube used for the experiment has an effect on the relationship between rotation rate and interfacial tension: the larger the tube, the greater the effect of rotation rate on interfacial tension. The tubes used in the experiment of Isaacs et al. had inner diameters of 0.2 cm and 0.4 cm, while the glass tubes used in our interfacial tension experiments in the lab had an inner diameter of 1.2 cm. This difference in the



size of the glass tube may have a profound effect on the dependence of apparent interfacial tension on rotation rate.

Thus, based on what was reported in the literature and the uncertainty as to whether or not the same observations can be found with our spinning drop tensiometer, several experiments were conducted with water/air and silicone oil/air to see whether the apparent dependence of interfacial tension on rotation rate *exists*. All of these experiments were conducted under high enough rotation rates such that the lengths of the drops were at least four times their equatorial diameters.

#### ***3.4.1 Silicone Oil/Air Systems***

Initially, two different sets of experiments were conducted for the silicone oil and air systems. For the first set of experiments, the diameter readings were calibrated with the 2 mm calibration post<sup>t</sup>. The interfacial tension value obtained for the drop diameter of 2 mm was 21.49 mN/m. The drop diameter was increased from 1.7 mm to 3.1 mm and then decreased in small steps back to 1.7 mm (by increasing or decreasing rotation speed in the range of 1400 to 3600rpm). The incremental/decremental step size was 200 rpm, and the drop was allowed to equilibrate for three minutes after a new rotation rate was set before taking a measurement in order to ensure that the drop was in equilibrium. The interfacial tension of the system was calculated for each corresponding rotation rate, and the relationship between the rotation rate and apparent interfacial tension was examined. See Figure 3.5.

The same tube of silicone oil/air was used for the second experiment, where the diameter readings were calibrated with the 3mm diameter post and the



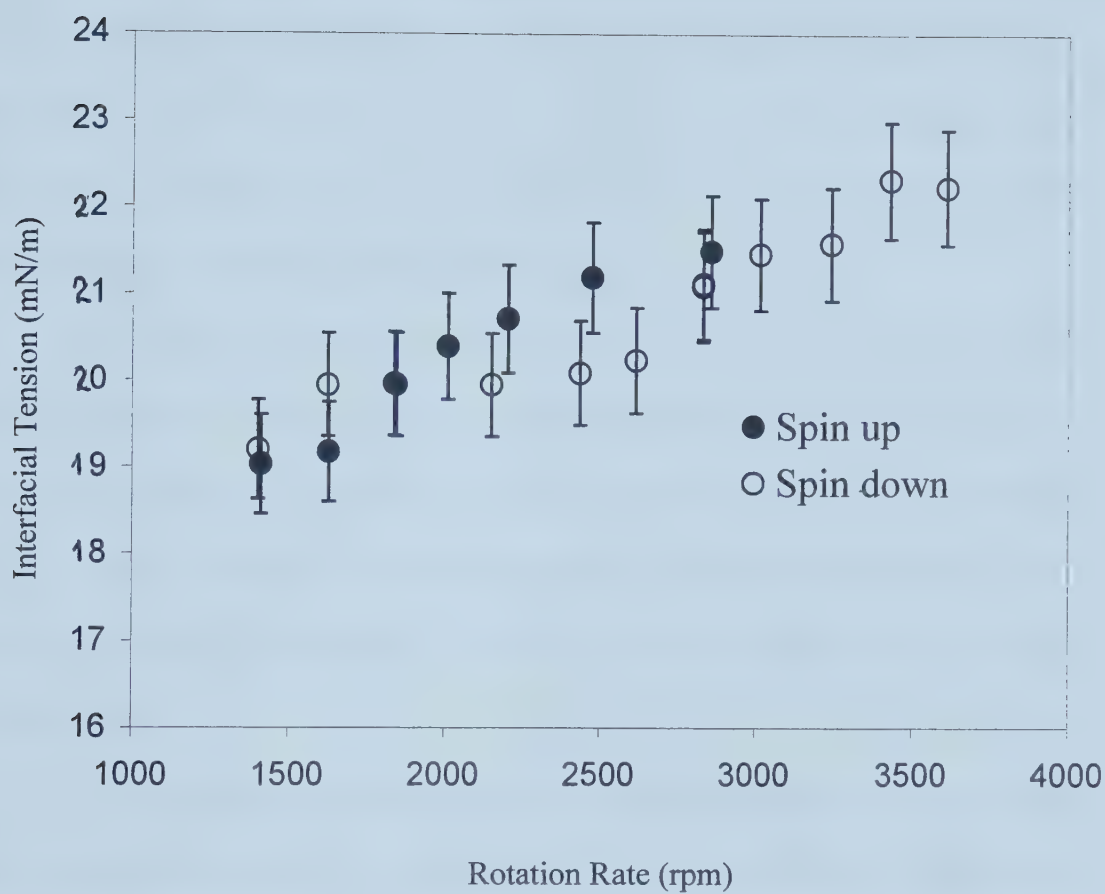


Figure 3.5 The interfacial tension of silicone oil and air as a function of rotation rate when the measuring system is calibrated with the 2mm calibration post. The experiment was conducted at a room temperature of 19°C.



procedure for obtaining a relationship between rotation rate and interfacial tension was the same as that in the first set of experiments. The results are presented in Figure 3.6. The open circles on both figures represents a spin down (increasing drop diameter) during the experiment, and the filled circles represent a spin up process (decreasing drop diameter). The time required for both experiments was approximately one hour. Figure 3.7 shows the data calibrated with the 2 mm and 3 mm calibration post superimposed upon each other.

For both sets of experiments, the interfacial tension was found to be an increasing function of rotation rate. The interfacial tension values varied from 18 mN/m to 22 mN/m for drop diameters ranging from 1000 to 4000 rpm (diameters of 1.7 to 3.4 mm) regardless of whether the system was calibrated with the 2 mm diameter or the 3 mm diameter post. The interfacial tensions agree within the errors at all rotation rates.

In the next step, the interfacial tension of silicone oil/air was measured using the duNuoy Ring method. The value obtained from this method will be taken as the *true* interfacial tension value and can be compared with the interfacial tension values from the spinning drop experiments. The same silicone oil used in the spinning drop tensiometer was used for the ring experiment, and the same cleaning procedure for the spinning drop tensiometer was also used for the duNuoy Ring experiment. Three interfacial tension measurements were made using the duNuoy Ring method; the average value obtained was 20.5 mN/m with a standard deviation of 0.1 mN/m. In Figures 3.8 and 3.9, this value was then taken as the real value of the interfacial tension and the error relative to this value was calculated for the different drop diameters in the spinning drop tensiometer experiments.





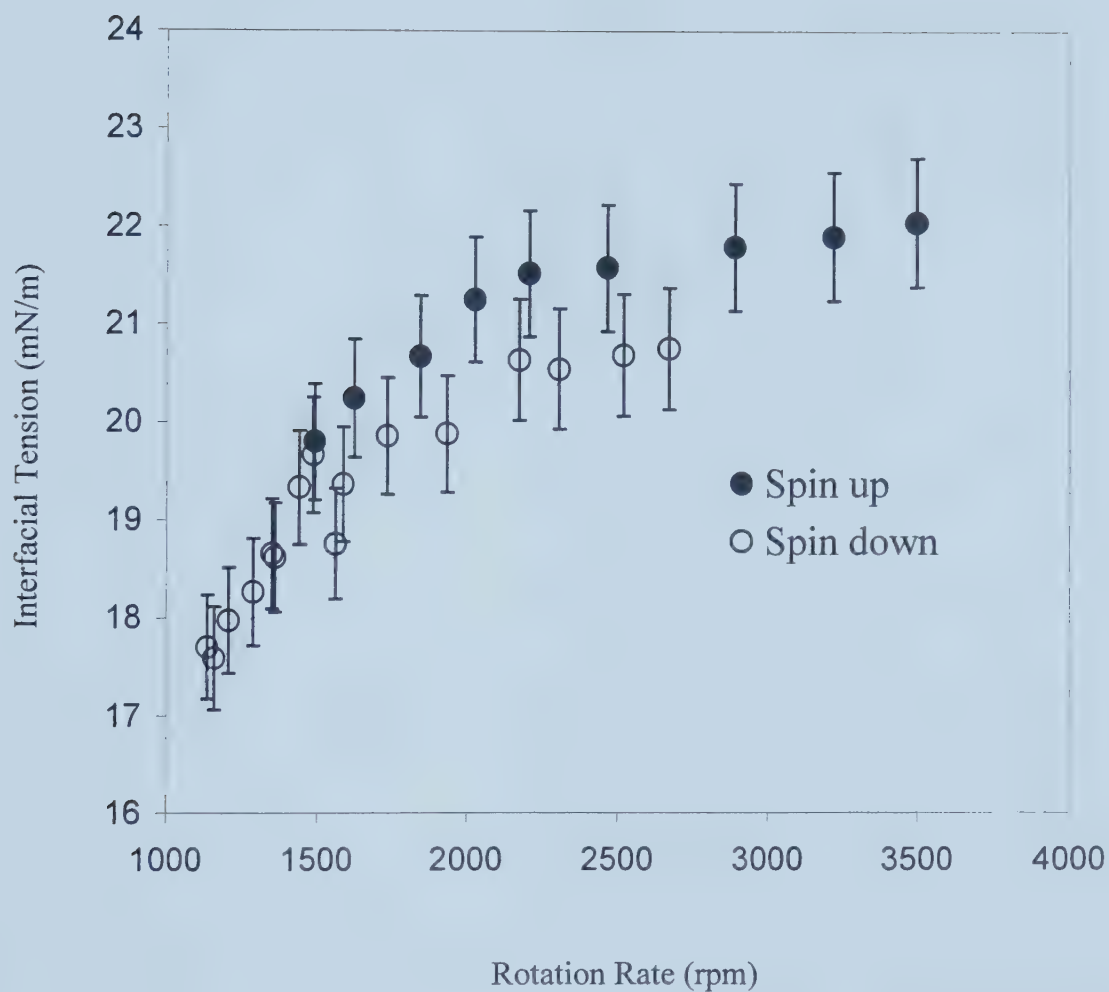


Figure 3.6 The interfacial tension of silicone oil and air as a function of rotation rate when the measuring system is calibrated with the 3mm calibration post. The experiment was conducted at a room temperature of 19°C.



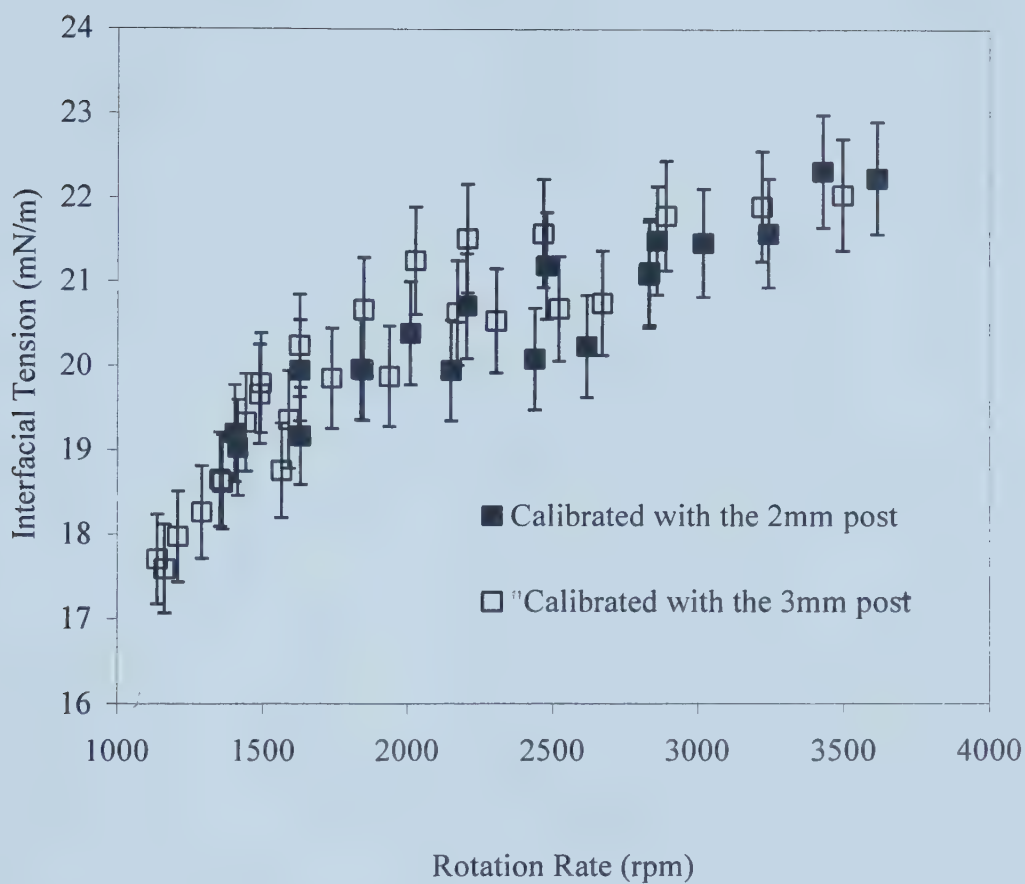


Figure 3.7 The interfacial tension of silicone oil and air as a function of rotation rate when the measuring system was calibrated with the 3 mm and the 2 mm calibration posts. The experiments were conducted at a room temperature of 19°C.



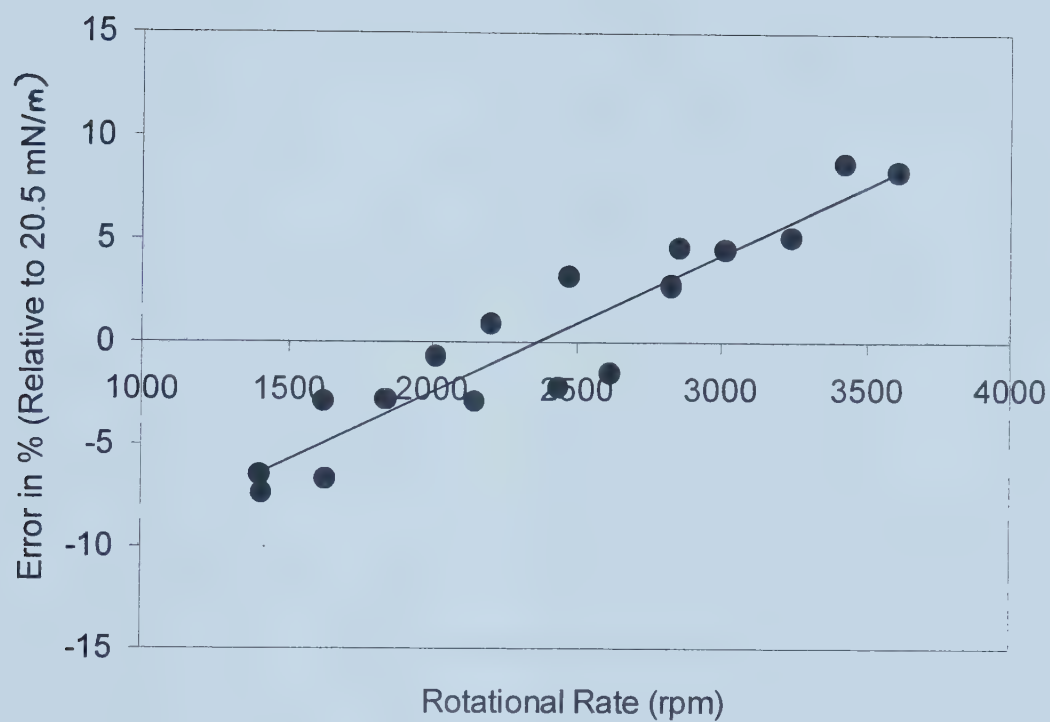


Figure 3.8 The percentage error of SDT interfacial tension value relative to the interfacial tension value obtained from the duNuoy Ring method. This silicone oil/air system was calibrated with the 2 mm calibration post.





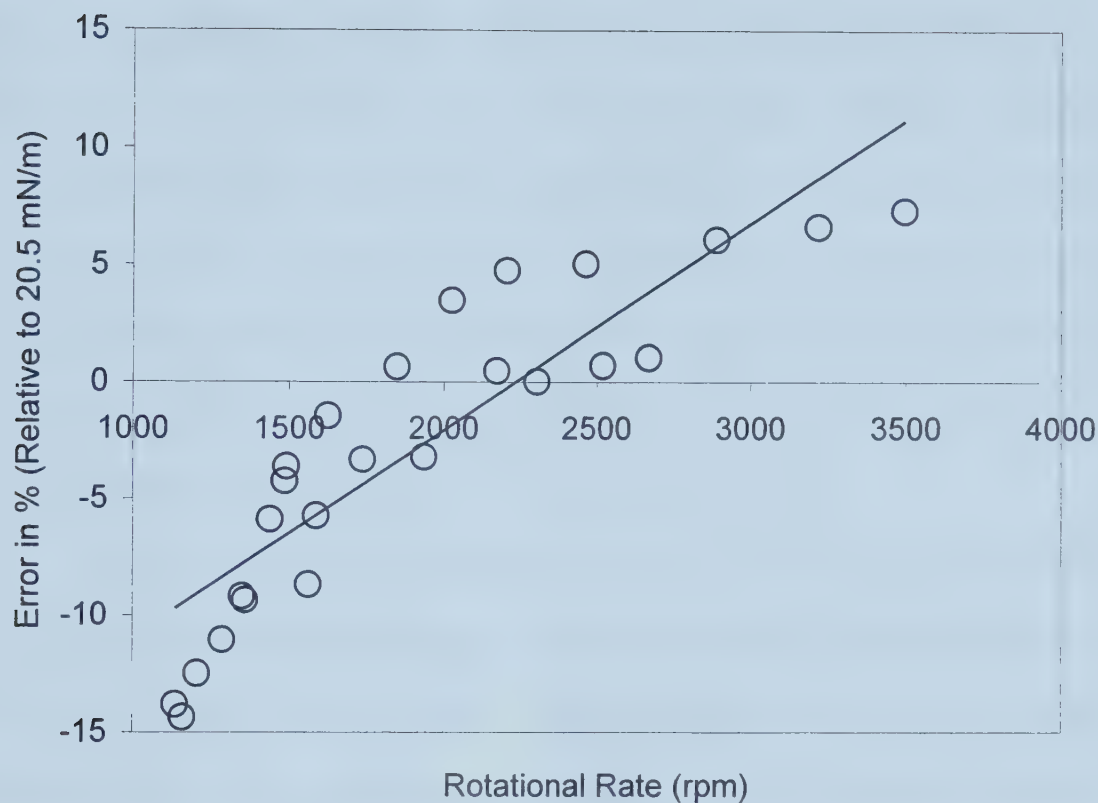


Figure 3.9 The percentage error of SDT interfacial tension relative to the interfacial tension obtained from the duNuoy Ring method. This silicone oil/air system was calibrated with the 3 mm calibration post.



It is interesting to note that for both sets of experiments, the error approaches zero at approximately the same place, between 2000 and 2500 rpm, regardless of whether the reading was calibrated with the 2 mm or 3 mm calibration post. From this observation, it was concluded for the silicone oil/air system, that the decreasing relationship between interfacial tension and drop diameter is independent of which calibration posts the measuring system is calibrated against. It appears that the measured *interfacial tension is directly affected by rotation rate*, even at high enough rotation rates such that the drop's length is at least four times its equatorial diameter.

### **3.4.2 Water/Air Systems**

Three sets of spinning drop experiments were performed for the water/air system, and the effect of rotation rate on measured interfacial tension in the range of 4000 rpm to 7400 rpm was examined. The three experiments were conducted on different days, but the experimental conditions were kept the same for each experiment. The measuring system was calibrated with the 2 mm calibration post at the beginning of each experiment before any measurements were taken. The initial rotation rate was 4000 rpm and the rotation rate was increased in 300 rpm incremental steps. The tube filled with the water and air was rotated at 4000 rpm for 20 minutes before the first measurement was taken, and each measurement was taken three minutes after adjusting to a new rotation rate. From the results in section 3.2, it is assumed that this time length of three minutes will be sufficient for the drop to reach a new equilibrium after a disturbance in its environment. Fresh (new) Millipore water was used for each experiment, and the results of the three experiments are shown in Figure 3.10, Figure 3.11 and Figure 3.12. The results from all three experiments were plotted together on the same graph shown in Figure 3.13.



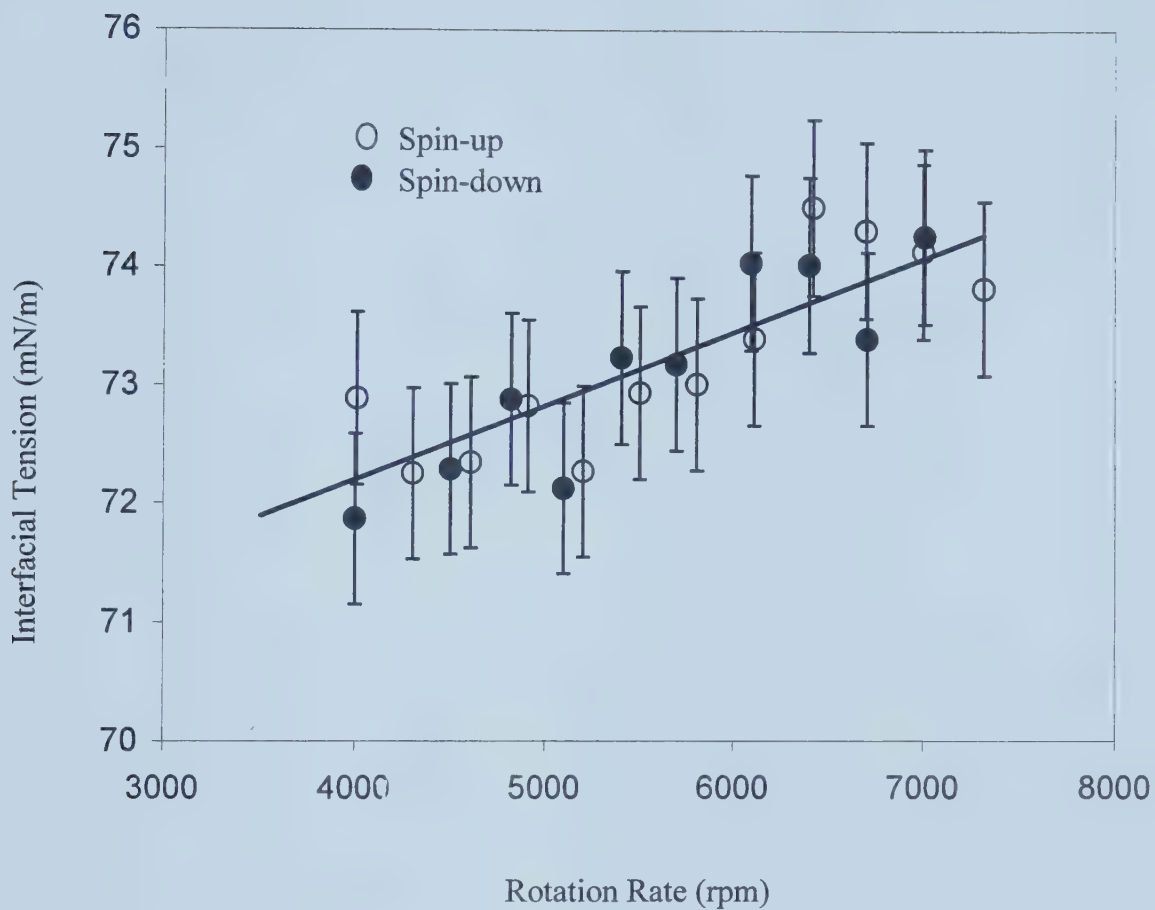


Figure 3.10 Water/air 1 - The effect of rotation rate on interfacial tension for water/air at 17°C. The measuring system was calibrated with the 2 mm calibration post.



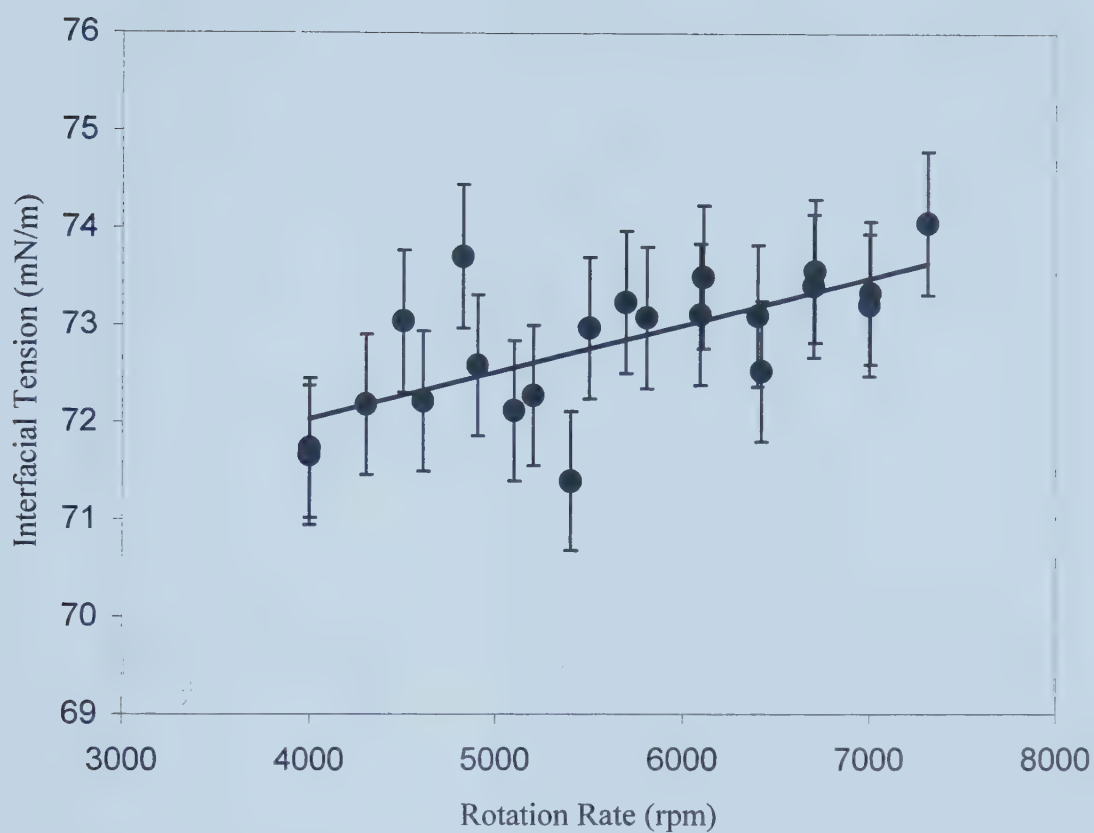


Figure 3.11 Water/air 2 - The effect of rotation rate on interfacial tension for water/air at 17°C. The measuring system was calibrated with the 2 mm calibration post.





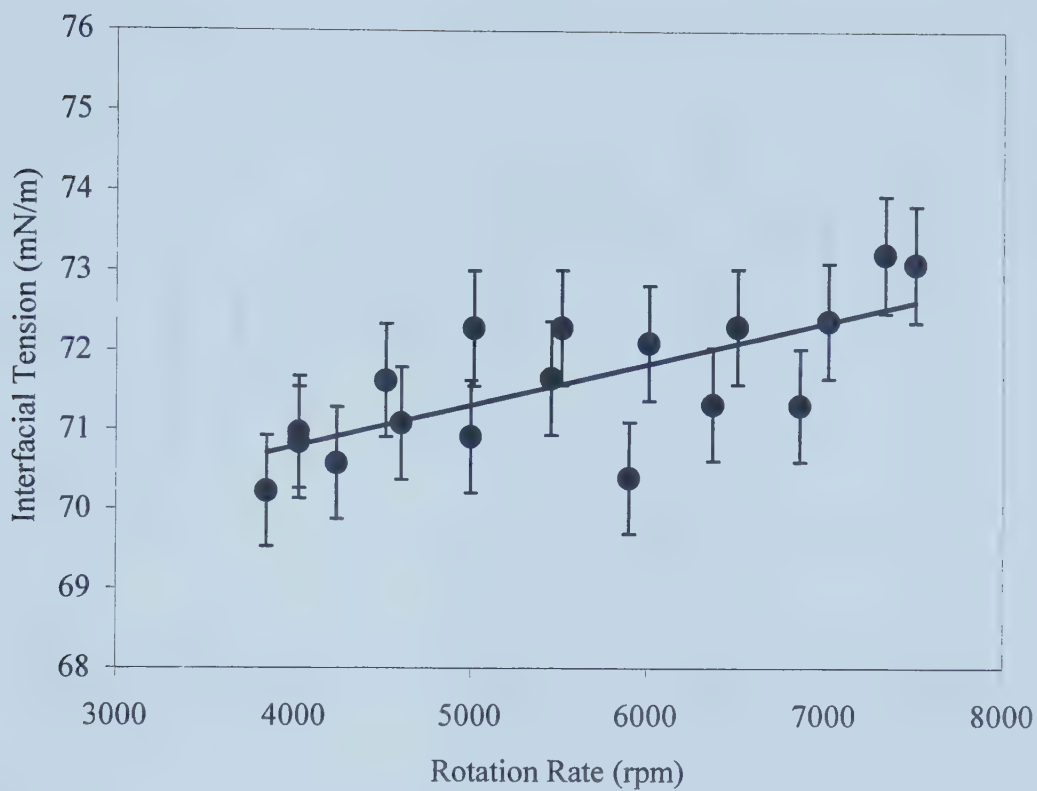


Figure 3.12 Water/air 3 - The effect of rotation rate on interfacial tension for water/air at 17°C. The measuring system was calibrated with the 2 mm calibration post.



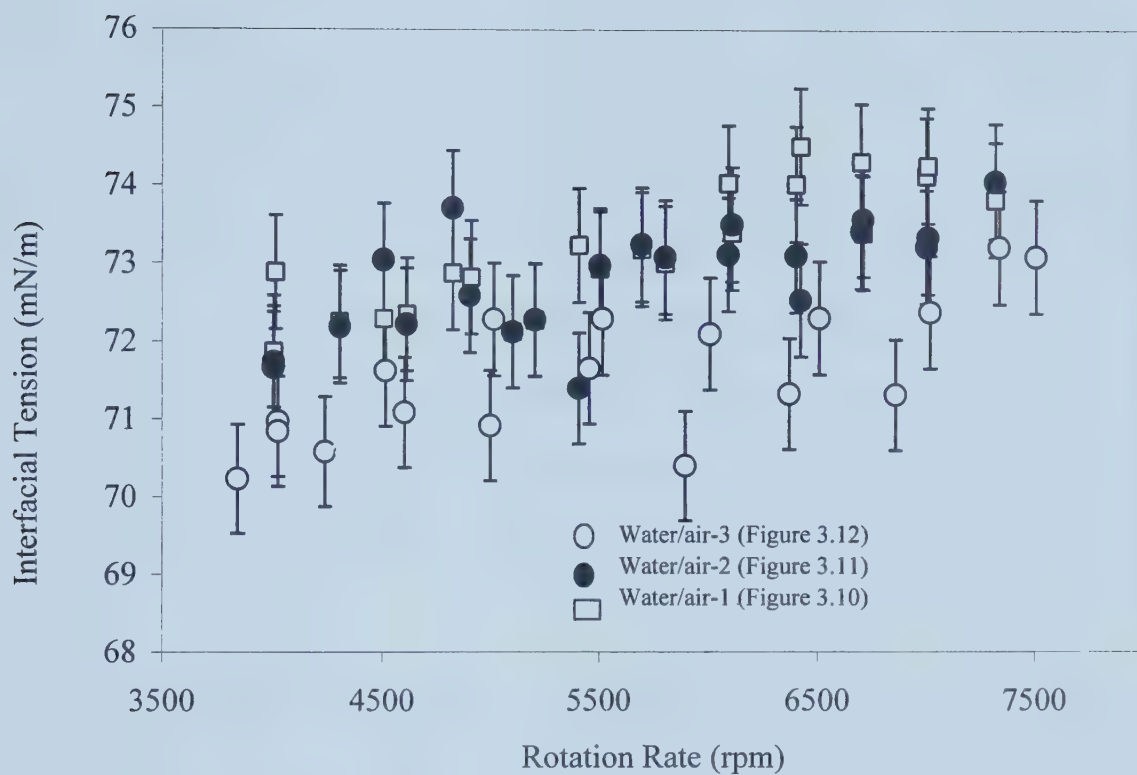


Figure 3.13 - (Water/air 1,2,3 on the same graph) The interfacial tension of water/air at 17°C.



Another set of experiments was conducted for which the measuring system was calibrated with the 1 mm, 2 mm and the 3 mm calibration posts. The results are shown in Figure 3.14.

All of the results shown for the water/air system indicate that there is a trend similar to that observed for the silicone oil/air system (Figure 3.7). Measured interfacial tension was found to increase with increasing rotation rate, regardless of the type of fluid used or the diameter of the calibration post against which the measuring system was calibrated. In all of the silicone oil/air and water/air experiments discussed in the previous sections, the  $L/D$  ratio was greater than 4, in the range where Vonnegut's equation should work well. The effect of the rotation rate on interfacial tension is not caused by neglecting the  $(2R/3L)$  term in Equation 2.18 because increasing the rotation rate will cause the  $(2R/3L)$  term to become smaller, thus the apparent interfacial tension should not increase as rotation rate increases.

In the range of the rotation rates studied for the water/air system, the interfacial tension values obtained varied from 71.5 to 74.5 mN/m for the experiments conducted at a room temperature of 17 °C. These values are approximately within 3% of the water/air interfacial tension value of 73.3 mN/m as published in the CRC Handbook of Chemistry and Physics (2000). It appears that the effect of rotation rate on interfacial tension value is relatively small. Nonetheless, since we are interested in measuring the interfacial tension of polymer melts using the spinning drop tensiometer, we need to understand and to reduce the possible errors associated with the apparatus. The rest of this chapter is dedicated to examining this effect of



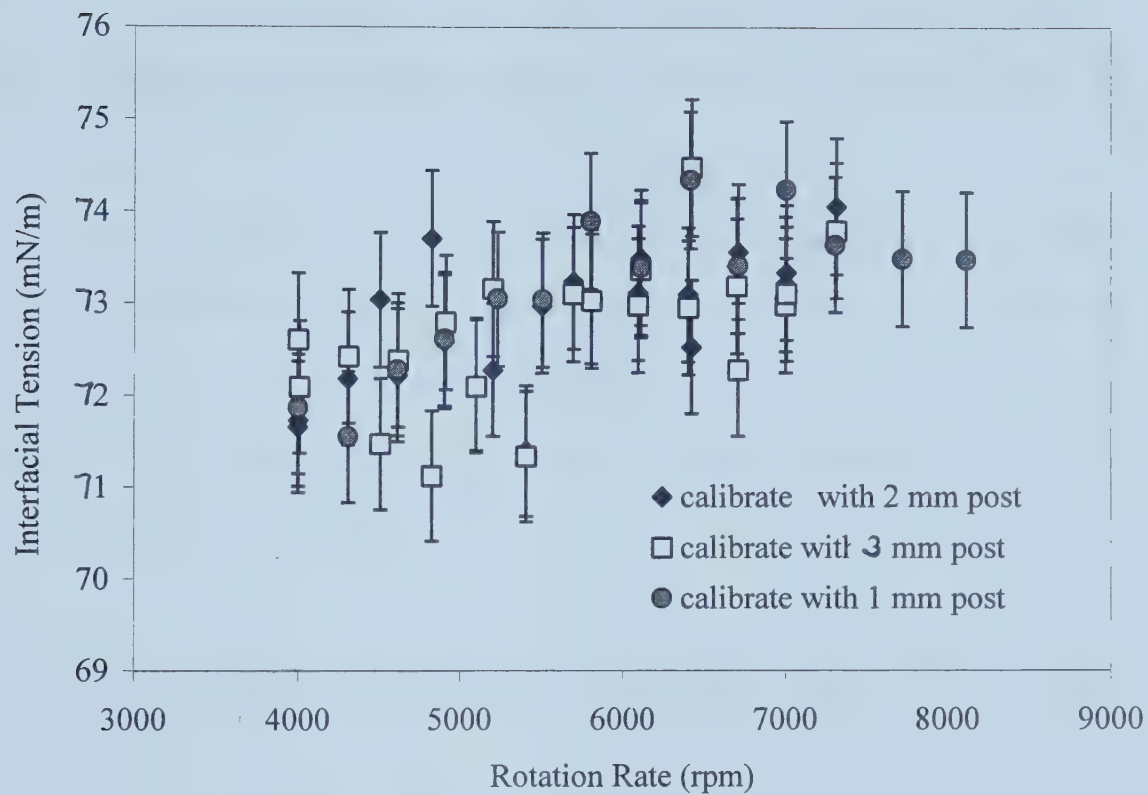


Figure 3.14 Interfacial tension of water/air as a function of rotation rate at 17°C for the experiments calibrated with the 1 mm, 2 mm and 3 mm calibration posts.





rotation rate on the calculated interfacial tension and to investigating the possible reasons why rotation rate has an effect on apparent interfacial tension.

### **3.5 Investigation of the Effect of Rotation Rate on Calculated Interfacial Tension**

Several possibilities that may cause the observed relationship between rotation rate and apparent interfacial tension of the fluids were examined. For all of these experiments, water/air and silicone oil/air were chosen as the systems of interest. Most of the measurements were conducted at room temperature, which was approximately 17 – 19 °C.

#### **3.5.1 The Possibility of Gyrostatic Disequilibrium Inside the Tube Under Rotation**

As a first possibility for the reason that rotation rate effects interfacial tension, we investigated the possibility that under the experimental conditions, the system in the spinning drop tensiometer was not in gyrostatic equilibrium. The principle of operation of the spinning drop tensiometer is based on the assumption of gyrostatic equilibrium of the less dense and the denser fluids when both are subjected to rotation in a tube. Manning and Scriven (1975) defined gyrostatic equilibrium as "a state of uniform rotation in which every bit of fluid inside a spinning rigid container is at rest with respect to the container wall." The authors contended that there may be two reasons which cause a rotating system to deviate from gyrostatic equilibrium in a spinning drop tensiometer. One reason is gravity-induced, where the effects of the buoyancy due to gravity displace vertically the less-dense drop away from its axis of



rotation. This displacement allows for possible flow layers around the drop, which affects the angular velocity of the drop. The effect of gravity is most likely dominant when the  $L/D < 4$ . Secondly, the authors point out that the spinning fluids possess

*“...rotation stiffness, where the field lines of angular momentum and vorticity fields lie nearly parallel to the rotation axis and the fluids behave as if they are more or less bound to these lines. That is, fluid elements do not easily cross the field lines. This effect lays the drop and the surrounding liquid open to various oscillatory motions and secondary flows that can be excited by small perturbing influences.”*(Manning and Scriven, 1975)

Under such conditions, it can be difficult for gyrostatic equilibrium to be reached in a spinning drop tensiometer.

There are several methods suggested by the afore-mentioned authors which test whether or not the rotating fluids in a tube approach gyrostatic equilibrium. Dimensional analysis of the fluids under operation can be performed to do this. The following are the dimensionless numbers for the spinning drop (Manning and Scriven, 1975):

$$\text{Bond Number} = \frac{\text{centrifugal buoyancy force}}{\text{interfacial tension force}} = \frac{\omega^2 R^3 \Delta\rho}{\gamma}$$

$$\text{Rotation Froude Number} = \frac{\text{centripetal acceleration}}{\text{gravitational acceleration}} = \frac{\omega^2 R}{g}$$

$$\text{Reynolds Number} = \frac{\text{inertial forces}}{\text{viscous forces}} = \frac{\omega R^2}{\nu}$$



Where  $R$  is the radius of the drop,  $\gamma$  is interfacial tension,  $g$  is gravitational acceleration, and  $\nu$  is the kinematic viscosity of the drop.

Manning and Scriven suggested that for gyrostatic equilibrium to be approached as closely as possible, the Froude Number should be sufficiently large such that its inverse is less than 1 (Torza, 1975). Also, the Reynolds number should be as small as possible, and the Bond number should be small in comparison to the Reynolds number. These three dimensionless numbers were calculated for the water and air data seen in Figure 3.10, and the values are shown in Table 3.1. It can be seen that the Froude number is relatively large, and thus the centripetal acceleration is a more dominant force than the gravitational force. Also the rotation Reynolds number is small, and the Bond number is even smaller in comparison. Thus, the spinning drop appears to be *approaching* the gyrostatic equilibrium in the spinning drop tensiometer.

One of the “small perturbing influences” suggested by Manning and Scriven is the possibility of a misalignment of the drop’s horizontal axis of rotation. The authors showed through a visualization experiment with the spinning drop tensiometer that the movement of the drop along the horizontal axis causes secondary flows (non-radial) around the drop, disturbing the gyrostatic equilibrium of the system. There is a level on the equipment which was carefully leveled before using the spinning drop tensiometer. In order to check whether or not the rotation axis of our spinning drop tensiometer is aligned, an experiment with water and air was conducted at room temperature, where the fluids were rotated at constant rotation rate of 5000 rpm for approximately 20 minutes. The drop’s horizontal placement was then measured before and after the experiment with the digital ruler attached to the



Table 3.1. Dimensionless Numbers for the Water and Air System in a Spinning Drop Tensiometer. All data from this table are the same data given in Figure 3.10.

Air Drop Diameter (mm)	Glass Tube Rotational Rate (rpm)	Interfacial Tension (mN/m)	Froude Number	Bond Number	Reynolds Number
2.37	4010	72.9	21	4	31
2.37	4010	72.9	21	4	31
2.25	4307	72.2	23	4	30
2.15	4614	72.3	26	4	29
2.07	4912	72.8	28	4	29
1.98	5205	72.3	30	4	28
1.92	5504	72.9	32	4	28
1.85	5807	73.0	35	4	27
1.79	6109	73.4	37	4	27
1.74	6422	74.5	40	4	27
1.69	6700	74.3	42	4	26
1.64	7000	74.1	45	4	26
1.59	7317	73.8	48	4	26
1.64	7006	74.3	45	4	26
1.68	6708	73.4	42	4	26
1.74	6401	74.0	40	4	27
1.80	6093	74.0	37	4	27
1.88	5698	73.2	34	4	28
1.94	5409	73.2	32	4	28
2.01	5103	72.1	29	4	28
2.09	4826	72.9	27	4	29
2.18	4507	72.3	25	4	30
2.36	4003	71.9	21	4	31





video camera. It was found that the final horizontal displacement of the air drop at the end of the experiment was different than the original displacement by less than 0.1mm. With such a small difference, we can say that the rotation axis of the tube is not misaligned.

### 3.5.2 The Possibility of Non-Rigid Body Rotation of the Fluids

The effect of rotation rate on interfacial tension values obtained from a spinning drop tensiometer was also observed by Isaacs et al. (1988), who studied the interfacial tension of bitumen and D<sub>2</sub>O. In their investigation of the spinning drop apparatus, the authors also measured the interfacial tensions of the water/butanol system at 30 °C at different rotation rates ranging from 4050 rpm to 13,460 rpm. Two different tube sizes were used for the experiments, one with an inner diameter of 0.2 cm, and the other with an inner diameter of 0.4 cm. It was found that for the 0.4 cm tube, the interfacial tension of water/butanol increased from 1.73 mN/m to 2.2 mN/m as the rotation rate of the tube was increased. However, the same was *not* observed for the 0.2 cm tube, where interfacial tension value remained relatively constant at 1.73 mN/m as rotation rate was increased. The authors' explanation of these observations was as follows (Isaacs, 1989):

*" It is apparent that with the larger diameter tubes, at high frequencies the drop diameter lags behind the rotation speed of the tube causing an apparent increase in tension... With a more viscous oleic phase as in this study (bitumen +D<sub>2</sub>O), smaller diameter drops, and lower tension systems ( $\gamma \sim 1.7 \text{ mN/m}$ ), lagging should be more severe and result in higher apparent tensions."*



The lag of the drop surface behind the tube suggests that there is non-rigid body rotation of the fluid, hence, gyrostatic equilibrium was not achieved in the operation of the spinning drop tensiometer.

The lagging of the drop interface behind the actual rotation rate of the tube has been initially observed by Manning and Scriven (1975). The authors conducted visualization experiments for the water and butanol system at room temperature using the spinning drop method. Fine carbon particles and lycopodium spores were placed inside the tube filled with water and butanol. As the tube rotated, the small particles migrated to the surface of the butanol drop and acted as markers for the rotation of the drop. A stroboscope light was placed behind the rotating tube, and thus the rotation rate of the drop could be measured and compared to the rotation rate of the glass tube. From these experiments, Manning and Scriven observed that if the tube rotation rate was less than 4700 rpm, the drop surface lagged behind the tube. As the rotation rate decreased, the lag became more apparent. However, at rotation rates greater than 5000 rpm, the lag was less than 1 rpm behind the glass tube rotation rate. The authors attributed this lag to the fact that the buoyancy effect due to gravity was not negligible for rotation rates less than 5000 rpm, where the length/diameter ratio was less than 4. As such, the system was not operating under gyrostatic equilibrium.

So it appears that according to Manning and Scriven, the lag of the drop is evident because of the non-negligible effects of buoyancy due to gravitational forces, which occurs at  $L/D$  less than 4. In Isaacs et al.'s experiments with butanol and water, the  $L/D$  ratio was *at least* 4, which means that gravitational forces should be negligible in comparison to the centrifugal forces on the drop in the tube. However, for a large tube diameter of 0.4 cm, Isaacs et al. observed an effect of rotation rate on



observed interfacial tension values, and attributed this effect to the lag of the drop interface behind the tube rotation rate. It was also stated in the paper that the large diameter of the tube would cause the lagging to be more severe.

An experiment was carried out to test Isaacs et al.'s hypothesis. The inside diameter of the glass tube used in all of the experiments was 1.27 cm, which is approximately three times greater than the glass tube used in Isaacs et al.'s experiments. In order to investigate the possibility of non-uniform rotation rate of the fluids in the tube, the rotation rate of the fluid near the center axis of the tube must be known. Two plastic straws with outer diameters of 2.6 mm and 3.5 mm were used to simulate the air bubble inside the glass tube filled with water. The straws were burnt at both ends so that the ends were closed off and air was trapped inside the straws. The ends were then filed to a spherical rounded shape to simulate the shape of an elongated drop in the rotating tube filled with water, which is cylindrical with hemispherical ends as per Vonnegut's derivation (Equation 3.1). A piece of small reflective tape was glued on the surface of this plastic drop, and the plastic drop was placed inside the tube filled with water. At rest, the plastic drop was displaced upwards and away from the rotation axis due to buoyancy forces, such that the plastic bubble touched the wall of the glass tube. The tube, along with the plastic drop was then rotated at different speeds ranging from 2000 to 8000 rpm. At high rotation rates, the plastic drop moved to the center of the rotation axis due to centripetal acceleration, and the effects of gravity could be neglected. The rotation rates of the plastic drop were measured with a handheld photo/contact digital tachometer (Fisher Scientific Traceable®). Tables 3.2 and 3.3 present the comparisons of the rotation rates of the plastic drops (OD of 2.6mm and 3.5mm) and the rotation rates of the tube.



Table 3.2. A Comparison Between the Tube Rotation Rate and a 3.5mm OD Plastic Drop Rotation Rate Inside a Tube Filled with Water.

Tube Rotation Rate (RPM)	Plastic Drop Rotation Rate (RPM)
2066	2064
2517	2516
3014	3014
3510	3509
4024	4023
4519	4519
5015	5014
5510	5509
6061	6060
6516	6516
7012	7011
7508	7508
8097	8097

Table 3.3. A Comparison Between the Tube Rotation Rate and a 2.6mm OD Plastic Drop Rotation Rate Inside a Tube Filled with Water.

Tube Rotation Rate (RPM)	Plastic Drop Rotation Rate (RPM)
2045	2045
2509	2509
3008	3008
3568	3568
4096	4096
4513	4514
5031	5030
5514	5514
6035	6034
3576	3575
7007	7007
7522	7522
8022	8022







The rotation rate of the tube was obtained from the motor readout. Separate experiments confirmed that the rotation rates of the tube and the motor readout were the same (as described in section 3.5.4). The accuracy of the handheld tachometer and the spinning drop tensiometer motor are each  $\pm 1$  RPM (as according to the Fisher Scientific Traceable<sup>®</sup>Tachometer manual and the Vinagre 1998 SDT Manual).

As the Tables 3.2 and 3.3 show, the rotation rate of the plastic drop is the same as the rotation rate of the tube. This means that the fluid angular velocity near the plastic drop interface and at the interface of the air bubble in the rotating fluid is exactly the same as the tube velocity, i.e. there is *no* lagging of drop diameter behind the tube rotation rate. The increase in the apparent interfacial tension as rotation rate increases is not due to a lagging of the drop, but rather to some other phenomena.

### **3.5.3 Possible Calibration Error Due to Parallax Error in the Spinning Drop Tensiometer**

The second measurement error may be associated with the calibration of drop diameters. The spinning drop tensiometer is equipped with three calibration posts (1 mm, 2 mm and 3 mm). In order to obtain the diameter of the drop, one needs first to convert the number of pixels into actual distances in millimeters, and this is done by calibration against the calibration posts of known diameters. However, since the glass tubes are cylindrical, there may be parallax errors associated with readings for drop diameters that are not exactly the diameter of the calibration post. Moreover, there may be a possibility that there is a calculation or calibration error embedded in the spinning drop tensiometer software. If this were true, then the calculated interfacial tension value will be erroneous when the rotation rate is changed causing



the drop diameter to stray further from the size of the calibration post. To test this hypothesis, another method of calculating the interfacial tension of the silicone oil and air system was used instead of using the equations already embedded in the SDT32 software. If there were truly an error in the SDT32 software causing the trend with rotation rate, then one would not see a similar trend if another method is used to obtain interfacial tension values.

The volume-length method suggested by Princen et al. (1967) was used. Unlike Vonnegut's method which was based on a mathematically approximate method, Princen et al. derived an exact method using elliptic integrals to calculate the interfacial tension of two fluids under rotation. Two parameters were needed for this calculation, the length and the volume of the drop. The length of the drop can be easily obtained from the spinning drop tensiometer, as the video camera is equipped with a digital ruler which allows the operator to measure the length of the drop. The volume of the drop (approximately  $0.20 \pm 0.05$  ml) was controlled as carefully as possible by inserting a syringe filled with a known volume of air into the silicone oil in the glass tube. The rotation rates studied were between 1500 and 4000 rpm. The interfacial tension obtained using this volume/length method was compared with the interfacial tension obtained using the spinning drop tensiometer software. Figure 3.15 and Figure 3.16 show the interfacial tension as a function of rotation speed and length of the drop using the volume/length method. Based on Princen's equations, the uncertainty of  $\pm 0.05$  ml in the volume of the air translated to a 12% uncertainty in the interfacial tension of air/silicone oil, which are applied to Figures 3.15 and 3.16. Figure 3.17 shows the interfacial tension as a function of rotation speed of the drop as obtained from the spinning drop tensiometer software. We observed that the trend



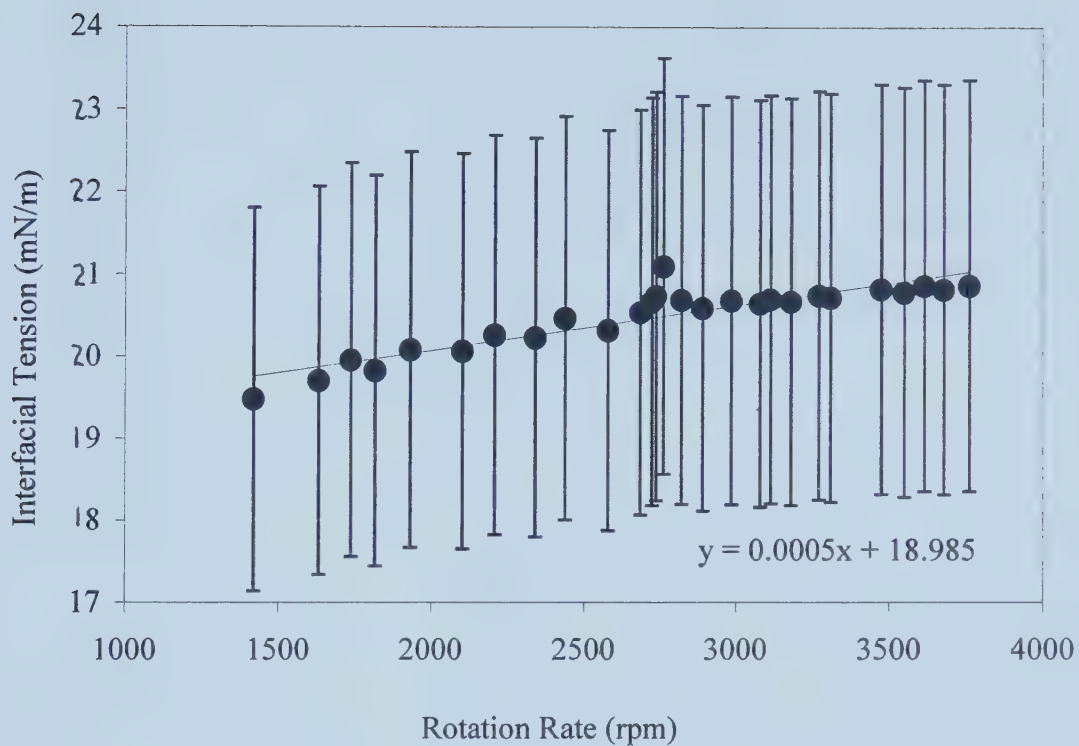


Figure 3.15 The interfacial tension of silicone oil/air as a function of rotation rate at room temperature (19°C) using the volume/length method by Princen.



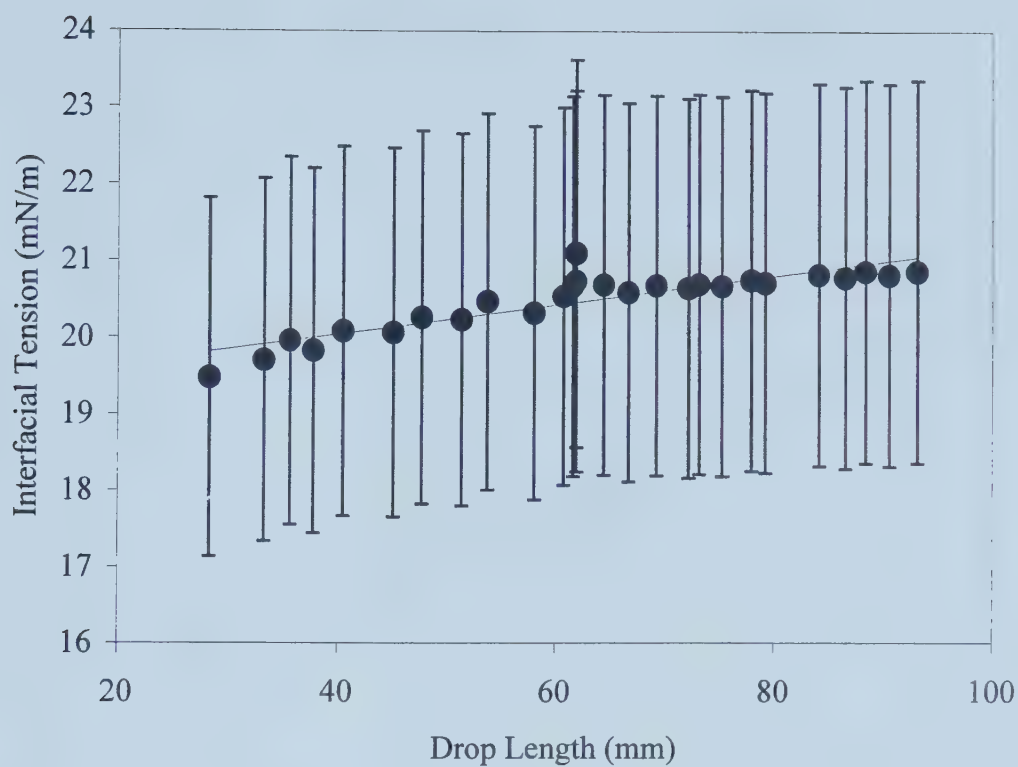


Figure 3.16 The interfacial tension of silicone oil/air as a function of air drop length using the volume/length method by Princen.





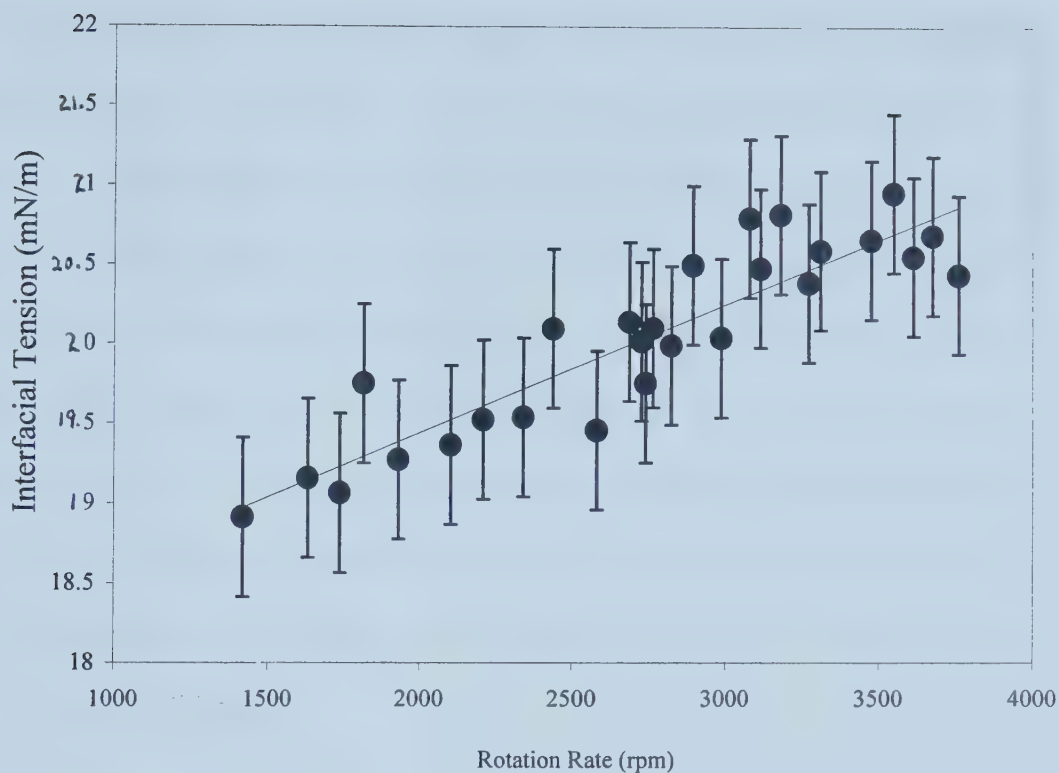


Figure 3.17 The interfacial tension of silicone oil/air as a function of rotation rate. Interfacial tension values were calculated by the SDT32 software. The same sample used for the experiment in Figure 3.16 was used for this experiment, and conducted under the same experimental conditions.



found in the volume/length method was the same as that observed in the spinning drop tensiometer method, regardless of the method of interfacial tension calculation used, i.e. the interfacial tension is an increasing function of rotation speed. Although the magnitude of the error bars were large, this error was consistent throughout the experiment (i.e. even though the exact volume is not known accurately, the same volume was used throughout the experiment). Therefore, the trend of increasing interfacial tension with increasing rotation rate can be believed. Based on these observations, the possibility that there was an error in the calibration equation embedded in the SDT32 software causing the trend was discarded. The problem now is to find out why such a trend exists, for it is not a function of reading error, parallax error or calibration error. Rather, rotation rate directly has an effect on the equilibrium shape of the drop.

#### **3.5.4 Possible Error in the Motor Controller or Rotation Rate**

Another possible explanation as to why there is a trend/relationship between interfacial tension and rotation rate of the sample could be that the digital display of the motor controller is not reporting the true value of the rotation rate of the glass tube. This would mean that the value of the rotation rate used in Equation 3.8 is either higher or lower than the actual rotation rate of the fluids, causing an error in the calculated interfacial tension value. To examine this, a handheld photo/contact digital tachometer by Fisher Scientific (Traceable<sup>®</sup>) was used to check the rotation rate of the sample and compared with the motor controller display.

A small piece of reflective tape was placed on the motor shaft and glass tube. (The glass tube was filled with water.) The tachometer was pointed toward the



reflective tape as the motor/glass tube was rotating and readings of the rotation rates of the glass tube and the motor shaft were then obtained. Table 3.4 shows the comparisons between the motor controller readout and the glass tube/motor shaft readout. As the results show, the rotation rate reported by the motor controller is an accurate representation of the actual rotation rate of the sample.

### 3.5.5 Possible Pressure Effects on Interfacial Tension for Liquid –Gas Systems

When the rotation rate of the fluids inside the glass tube changes, the pressure at various locations inside the tube changes as well. The relationship between rotation rate and liquid pressure ( $P_L$ ) is given by

$$P_L = P_o + \frac{1}{2} \rho_L \omega^2 r^2 \quad (3.2)$$

where  $P_o$  is the pressure on the center line in the liquid. Eriksson (1967) collected a set of experimental data on the relationship between interfacial tension and pressure at room temperature for several gas- liquid systems. Most of the systems (including water and nitrogen gas) showed that interfacial tension *decreases* with increasing pressure.

The possibility of the effect of pressure on interfacial tension is investigated in this section. Before we began, the relationship between the liquid pressure inside the tube and the interfacial tension at different rotation rates was first derived. A spinning drop experiment with varying rotation rate was again conducted for the air-water system at room temperature. The change of interfacial tension with the change in pressure for this system can be obtained and compared to the data presented by Eriksson (1967). If the two values are of the same order of magnitude, then there is a



Table 3.4. A Comparison between the Rotation Rate of the Glass Tube and the Rotation Rate of the Motor Controller Digital Display.

Controller Readout (RPM)	Tachometer Readout for Motor Shaft (RPM)	Tachometer Readout for Glass Tube (RPM)
1000	1000	1000
2000	2000	2000
3017	3017	3017
4040	4040	4040
5063	5062	5063
6054	6054	6054
7078	7077	7077
8039	8038	8038
9053	9053	9053





possibility that the relationship between interfacial tension and rotation rate as seen in Figures 3. 10-3.15 is caused by the pressure effect.

### 3.5.5a The Derivation of the Relationship between Liquid Pressure and Rotation Rate

This derivation is based on a force balance on the end plug of the glass tube, as shown in Figure 3.18. The force of the liquid ( $F_L$ ) acting on the surface area of the end plug ( $A_P$ ) can be written as:

$$F_L = \int_0^R P_L dA_P \quad (3.4)$$

$$F_L = \int_0^R \left( P_o + \frac{1}{2} \rho_L \omega^2 r^2 \right) 2\pi r dr \quad (3.5)$$

$$F_L = \int_0^R (2\pi P_o r + \pi \rho_L \omega^2 r^3) dr \quad (3.6)$$

$$F_L = P_o \pi R^2 + \frac{\pi}{4} \rho_L \omega^2 R^4 \quad (3.7)$$

The force of atmospheric air plus any friction force acting on the end plug is:

$$F_o = A_P P_{atm} + F_{Friction} \quad (3.8)$$



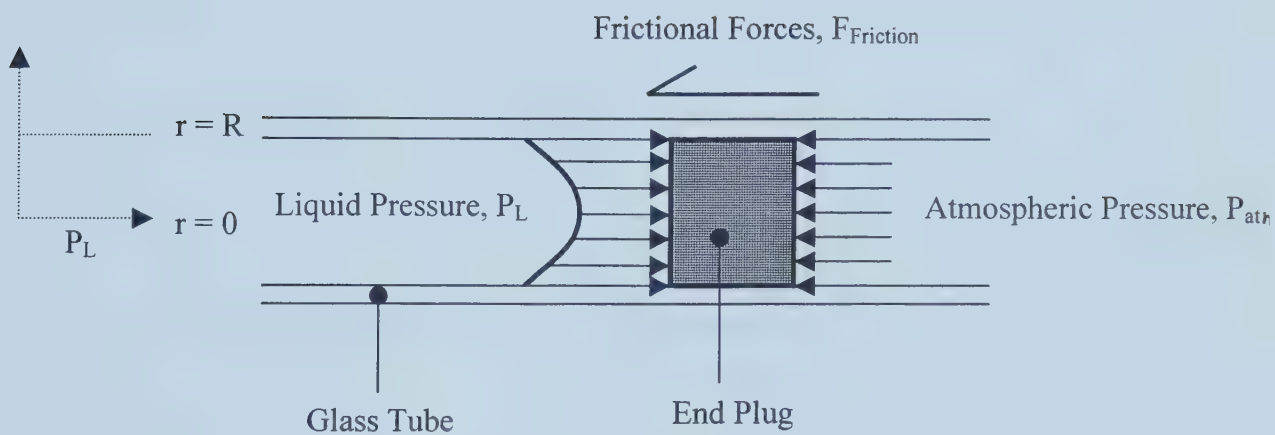


Figure 3.18 A schematic diagram of the forces acting on the end plug in a glass tube filled with liquid. Note that the liquid pressure acting on the plug is parabolic with radius ( $r$ ), while the atmospheric pressure is uniform and constant across the surface of the plug. The surface area ( $A_p$ ) of the circular end plug is given by  $A_p = \pi R^2$ .



The force balance on the end plug can be obtained by equating Equations 3.6 and 3.7:

$$F_o = F_L \quad (3.8)$$

$$P_o \pi R^2 + \frac{\pi}{4} \rho_L \omega^2 R^4 = P_{atm} \pi R^2 + F_{Friction} \quad (3.9)$$

$$P_o = \frac{P_{atm} \pi R^2 + F_{Friction} - \frac{\pi}{4} \rho_L \omega^2 R^4}{\pi R^2} \quad (3.10)$$

Therefore, by substituting Equation 3.10 into 3.2, the liquid pressure inside the tube is

$$P_L = \frac{P_{atm} \pi R^2 + F_{Friction} - \frac{\pi}{4} \rho_L \omega^2 R^4}{\pi R^2} + \frac{1}{2} \rho_L \omega^2 r^2 \quad (3.11)$$

Simplifying, the liquid pressure at the interface is

$$P_{Ll} = P_{atm} + \frac{F_{Friction}}{\pi R^2} + \frac{1}{2} \rho_L \omega^2 \left[ r_l^2 - \frac{R^2}{2} \right] \quad (3.12)$$

where  $r_l$  is the radius of the drop.



During a spin-up process, as rotation rate ( $\omega$ ) increases, the radius of the drop,  $r_1$  decreases. As such, from equation 3.12, pressure  $P_{LI}$  at the interface ( $r_1$ ) decreases as well. From the previous experimental results (Figures 3.10-3.15), interfacial tension increases with increasing  $\omega$ , indicating that increasing pressure in the tube decreases interfacial tension.

The interfacial tensions of water and air at different rotation rates (4000 rpm – 7500 rpm) and at a room temperature of 19 °C were measured. Equation 3.12 is used to calculate the pressure at the water/air interface ( $r$ ) at the different rotation rates. This pressure is based on an arbitrary friction force acting on the end plug,  $F_{\text{Friction}}$ , and it is assumed to be constant (corresponding to 1 atm) throughout the experiment. Figure 3.19 shows interfacial tension of the water/air system as a function of pressure at the interface as rotation rate is changed. The slope of this relationship (change in interfacial tension over change in pressure,  $dy/dP$ ) is  $-45.4\text{mN/m/atm}$ . The change in the interfacial tension over the change in pressure for water and nitrogen as reported by Eriksson (Eriksson, 1967) is  $-0.075\text{mN/m/atm}^2$ . This is a difference of three orders of magnitude, which is an indication that the effect of rotation rate on interfacial tension observed cannot be accounted for by pressure effects.

### 3.5.6 Possible Effects of Heat Generated in the Bearing Housings of the Motor

All of the experiments shown earlier were conducted at ambient temperatures ranging from 17 to 19 °C. There may be a possibility that at different rotation rates,

---

<sup>2</sup> Since air is composed of 79% nitrogen gas, we assume that Eriksson's data for water/nitrogen can be used as a comparison to our data for the water/air system.





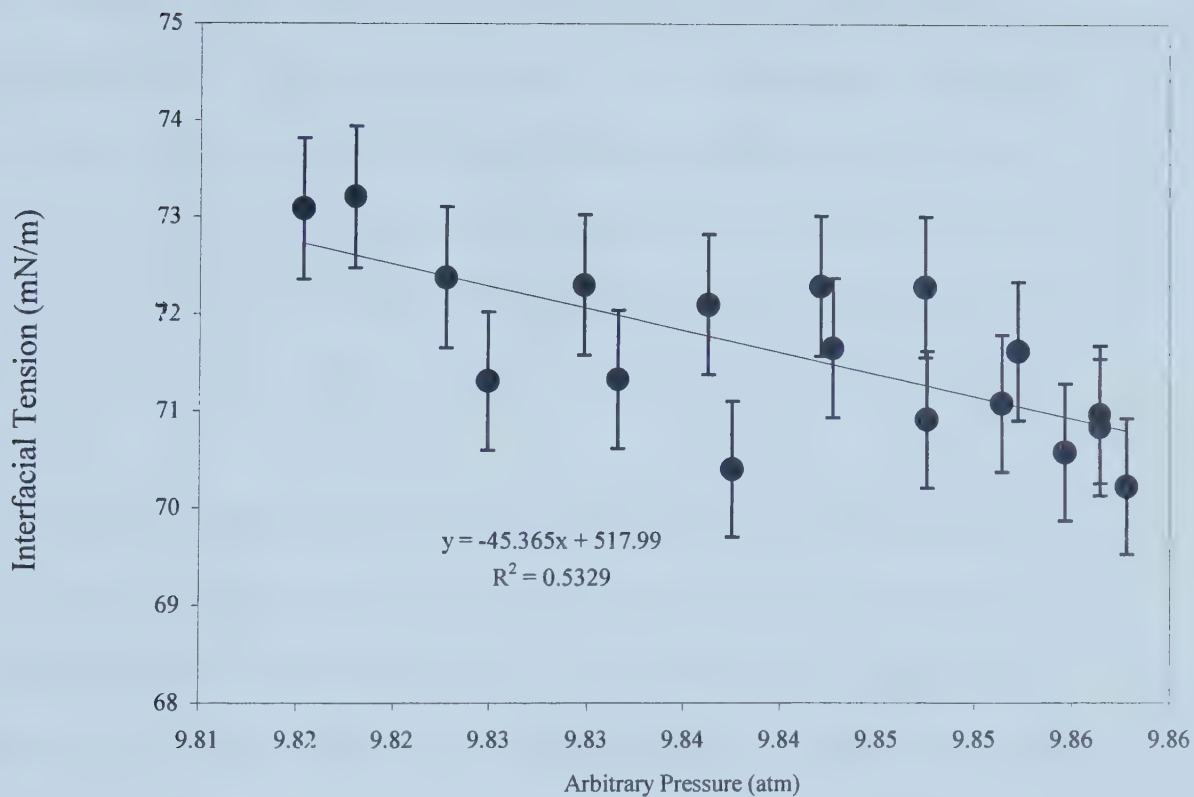


Figure 3.19 The interfacial tension of water/air (at room temperature) as a function of arbitrary pressure at the interface.



the heat generated in the bearing housings may affect the temperature of the fluid near the interface. Manning and Scriven (1975) found that the temperature at the bearing housing of their spinning drop tensiometer was 5 to 10 °C higher than their surrounding air bath. Non-uniform temperature of the fluids inside the tube will create a density gradient, which induces multidimensional flow patterns in the tube. This, of course, will have a direct effect on the equilibrium shape of the drop (Manning and Scriven, 1975). There is also the possibility that the temperature of the fluids inside the tube is a function of rotation rate, which will also affect interfacial tension.

Therefore, interfacial tension measurements of a water and air system at a uniform controlled temperature of 40 °C were conducted at various rotation rates. This temperature was chosen because it is at least 20 °C higher than the room temperature, and it is most likely higher than the temperature increase in the glass tube at room temperature due to heat generated in the bearing housings. The system was calibrated against a 2 mm calibration post. As Figure 3.20 shows, even at a higher temperature, interfacial tension was an increasing function of rotation rate, ranging from 67.0 mN/m to 69.5 mN/m for a rotation rate of 3500 rpm to 6500 rpm. According to the CRC Handbook of Chemistry and Physics (2000, p. 115), the value of the interfacial tension of the water/air system at 40°C is 69.5 mN/m. The interfacial tension values shown in Figure 3.20 are also in close agreement with the literature value.



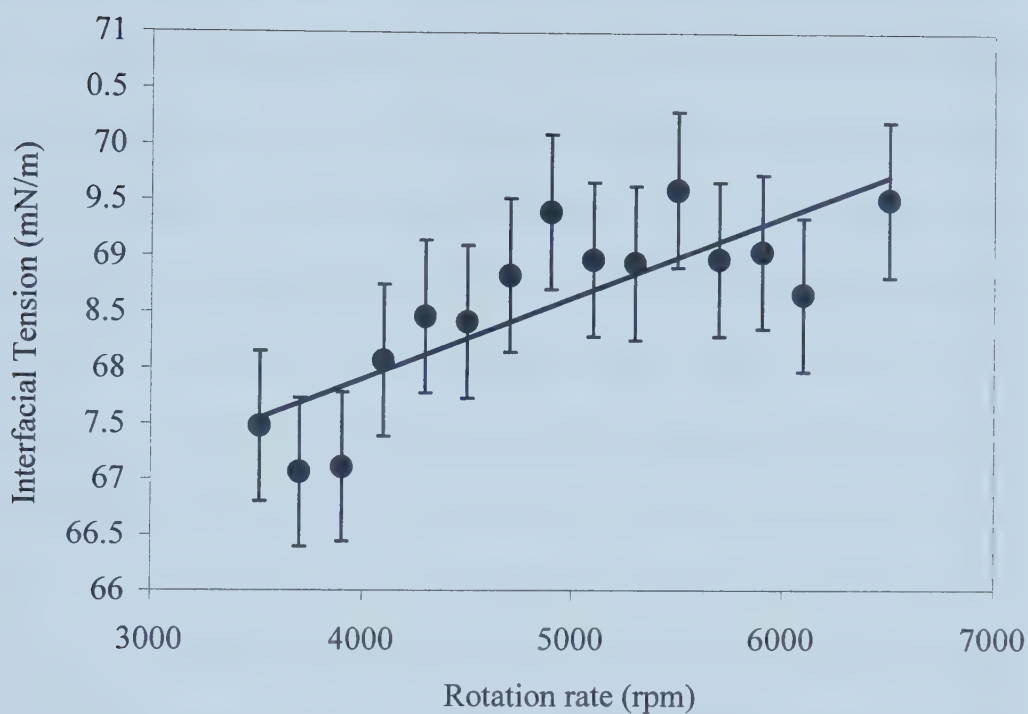


Figure 3.20 The interfacial tension of water/air as a function of rotation rate at a higher temperature of 40°C.



### 3.5.7 Possible Effect of Different Reticule Placement Methods

When one operates the spinning drop tensiometer, the image of an elongated rotating drop in a tube is projected onto the computer monitor via a video camera. Two reticules appear on the computer monitor, allowing the operator to move the reticules to the edges of the drop. The SDT32 software converts the numbers of pixels between the reticules into actual distances in millimeters after the system has been calibrated against a known post diameter. The image of the drop on the black and white screen of the computer monitor has an unclear region of gray "shadow" around the boundaries of the drop. The width of this shadow region is a reading error associated with the system. In all of the measurements discussed so far, the diameter of the drop was measured by placing the reticules on the outside edge of the drop, as shown previously in Figure 2.7. When the rotation rate of the fluid is large, the drop will have a smaller diameter. When the operator places the reticule on the outside edge of the shadow region, then the measured diameter would be bigger than the actual diameter, resulting in a higher apparent interfacial tension by a certain percent error. When the drop is subjected to higher rotation rate, the drop diameter will become smaller, but the width of the unclear region remains constant since it is caused by the lighting and refractive index difference of the two fluids. As such, the apparent diameter is bigger than the actual diameter by a larger percentage. If the rotation rate is increased, the drop diameter decreases and the positive error in the diameter will increase, thus causing an increase in apparent interfacial tension as rotation rate increases (see Vonnegut equation, Eq. 3.1). This possibility is shown in Figure 3.21.





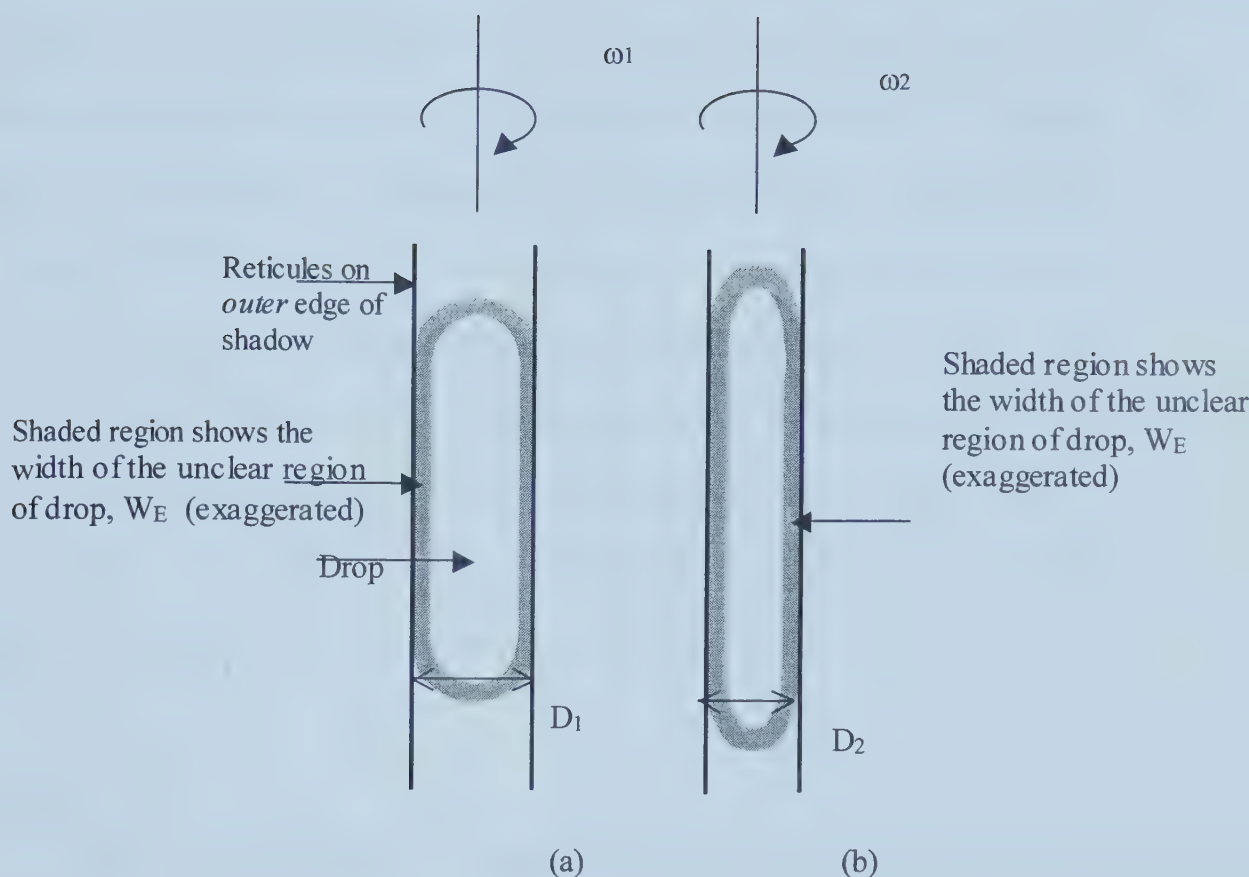


Figure 3.21 The measurement of drop diameter by placing the reticules on the *outside* edges of the drop. The width of the unclear region of the drop is the same regardless of the diameter of the drop. The actual diameter of the drop is somewhere between the inner and outer edges of the drop. In (a), the rotation rate  $\omega_1$  is low, hence the drop diameter,  $D_1$  is larger. The fractional error in diameter ( $W_E/D_1$ ), and corresponding interfacial tension is  $E_1$ . In (b), the rotation rate  $\omega_2$  is higher, hence the drop diameter,  $D_2$  is smaller than  $D_1$ . The fractional error in diameter ( $W_E/D_2$ ), and corresponding interfacial tension is  $E_2$ . Since  $W_E$  is constant for both drop diameters,  $E_2$  will be bigger than  $E_1$  in a *positive* direction, i.e.  $E$  increases as  $\omega$  increases. Thus the apparent interfacial tension will increase with increasing rotation rate.



In order to investigate this possible explanation, a different method of measuring drop diameter was used in which the diameter of the drop was measured by placing the reticules on the *inside* edge of the drop. We would expect the reverse trend to be observed, i.e. the magnitude of the error due to reading error will be increasing as rotation rate increases, but it will be in a negative direction so that the interfacial tension would be expected to decrease with increasing rotation rate. This is explained in more detail in Figure 3.22. The interfacial tension of water and air was measured at room temperature using the method suggested above and is shown in Figure 3.23. From this figure, interfacial tension is once again found to be an increasing function of rotation rate, regardless of which method of reticule placement was used. As such, the possibility of the effect of reticule placement as the cause of the relationship between interfacial tension and rotation rate is discarded.

### 3.6 Discussion

Non-cylindrical shapes of the drop are also another indication that “perturbing influences are present in the system” (Manning and Scriven). However, vibrations or odd shaped drops were not observed while the experiments for Figures 3.5 to 3.13 were conducted. So it appears that if indeed the effect of rotation rate on inferred interfacial tension is caused by non-gyrostatic equilibrium in the system, then the disturbance in the system cannot be visually observed.

Manning and Scriven (1975) observed several flow patterns in directions other than the radial direction, and there is a possibility that secondary flows in the system will affect the equilibrium shape of the drop. Many factors may cause this secondary flow; dimensions of the tube or even the geometry of the end plugs that seal the tube,



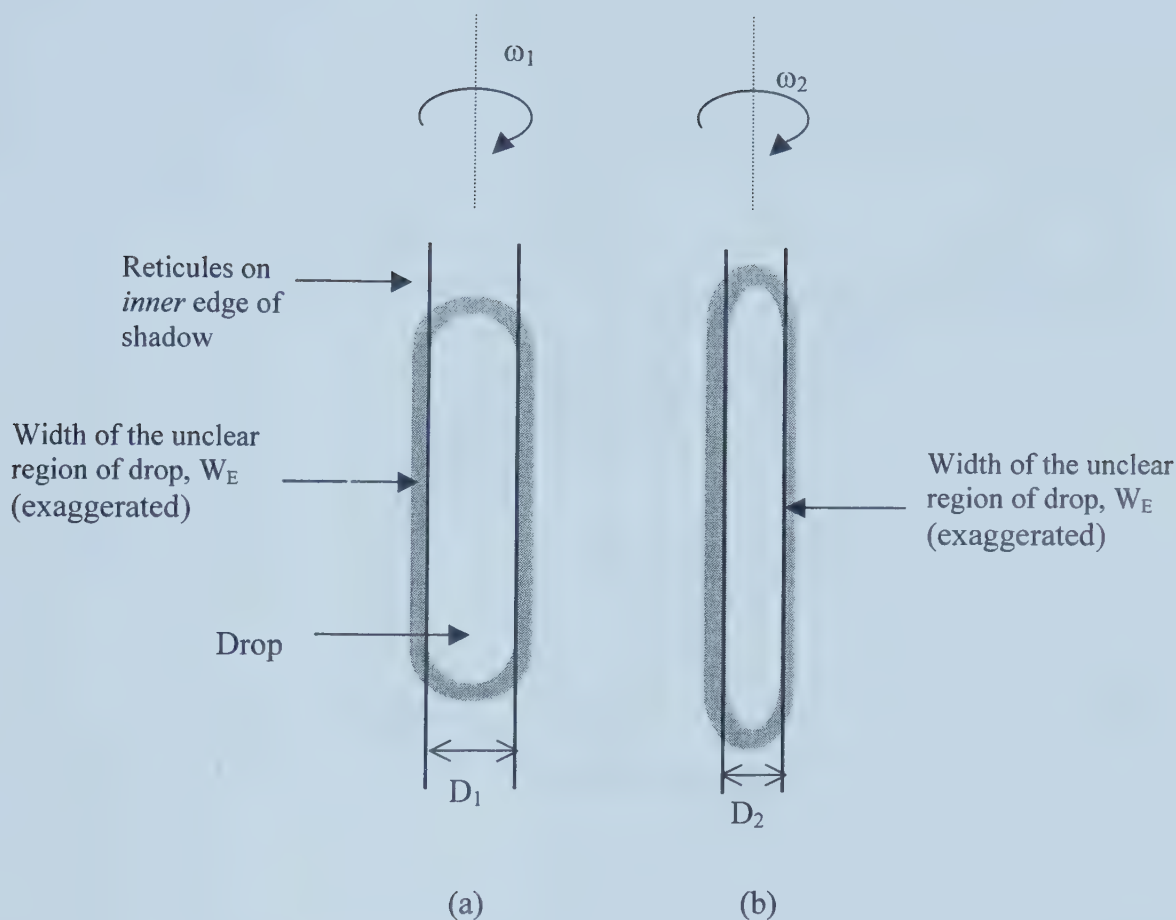


Figure 3.22 The measurement of drop diameter by placing the reticules on the *inside* edges of the drop. The width of the unclear region of the drop is the same regardless of the diameter of the drop. The actual diameter of the drop is somewhere between the inner and outer edges of the drop. In (a), the rotational rate  $\omega_1$  is low, hence the drop diameter,  $D_1$  is larger. The fractional error in diameter ( $W_E/D_1$ ), and corresponding interfacial tension is  $E_1$ . In (b), the rotational rate  $\omega_2$  is higher, hence the drop diameter,  $D_2$  is smaller than  $D_1$ . The fractional error in diameter ( $W_E/D_2$ ), and corresponding interfacial tension is  $E_2$ . Since  $W_E$  is constant for both drop diameters,  $|E_1|$  will be smaller than  $|E_2|$ , but the error is negative. Thus, the apparent interfacial tension will decrease with increasing rotational rate.



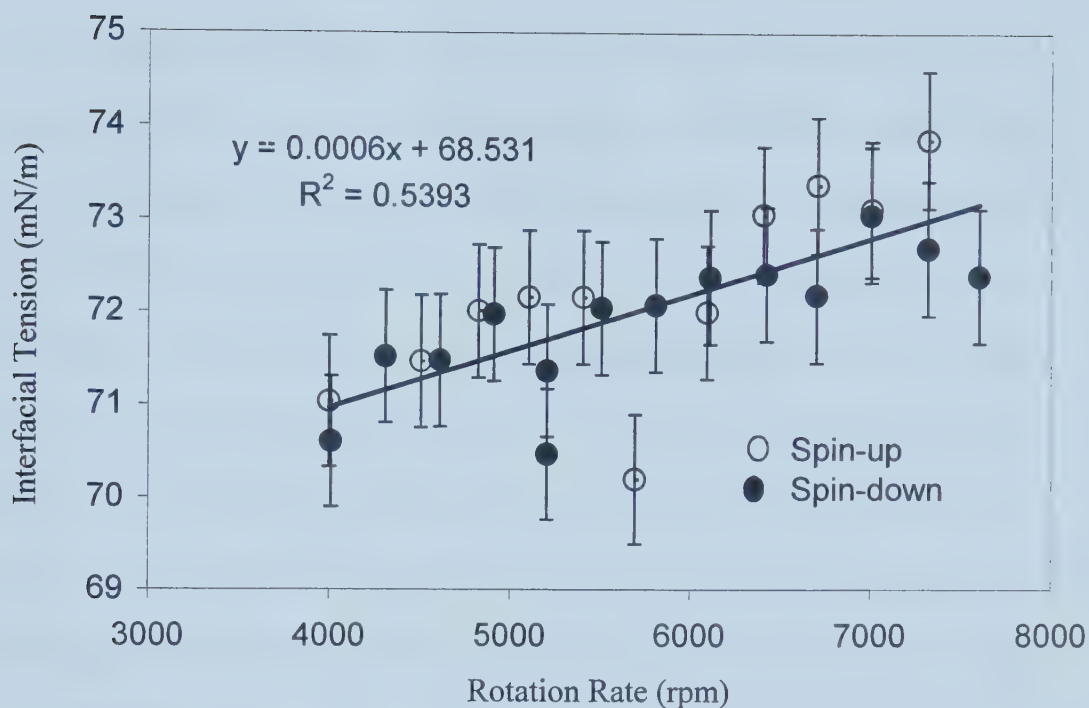


Figure 3.23 The interfacial tension of water/air (at room temperature of 17°C) as a function of rotation rate with the reticules placed on the inside edge of the drop shadow during the measurement of drop diameter.





viscosity of the fluids and density difference are a few possibilities suggested by the authors. Isaacs (1989) mentioned that a larger drop diameter and a possibly lower rotation rate and less viscous fluid may reduce the effect of increasing interfacial tension values. All these variables will have an effect on apparent interfacial tension if the flow of the fluid in the tube is not one-dimensional, but multidimensional, i.e in the radial as well as the vertical direction. So it appears that the multidimensional flow pattern of the fluid in the tube under rotation may be what is causing the effect of rotation rate on interfacial tension values. Unfortunately, the investigation of this possibility is beyond the scope of this project. However, in experiments to be described later in this thesis, where the objective is to measure the interfacial tension of polymer systems at different temperatures, we kept the rotation rate constant for each set of experiments so that the effect of rotation rate on interfacial tension would not need to be considered.

### **3.7 Conclusions**

- The reading error associated with the operation of the spinning drop tensiometer was found to be 1% and 3% for water/air and silicone oil/air systems respectively.
- Rotation rate of the fluids was found to have a real effect on interfacial tension values measured. Increasing rotation rate appears to increase interfacial tension.
- Rotation rate affects apparent interfacial tension when conditions investigated by Manning and Scriven for gyrostatic equilibrium were met, and when the bubble has the same rotation rate as the tube wall (Isaacs).



- Several possibilities were investigated and discarded as causing the effect of rotation rate on the obtained interfacial tension value, e.g. possibility of pressure effects, gyrostatic disequilibrium, non-uniform temperature, different reticule placement method, calibration and parallax error in the spinning drop tensiometer software and non-rigid rotation. None of these possibilities could explain the effect of rotation rate on obtained interfacial tension values.
- The fluids in the spinning drop tensiometer may not be under gyrostatic equilibrium due to complicated multidimensional flow phenomena inside the tube under rotation which may cause the effect of rotation rate on apparent interfacial tension. The investigation of this possibility is beyond the scope of this project.
- In experiments to be described later in this thesis, where the objective is to measure the interfacial tension of polymer systems at different temperatures, the rotation rates of the fluids were kept constant in each set of measurements so that the effect of rotation rate on interfacial tension does not need to be considered.



## CHAPTER 4

### DENSITY MEASUREMENTS OF POLYETHYLENE MELTS

---

#### 4.1 Introduction

This chapter describes the experimental methods for obtaining the density of the polyethylene melt at high temperatures. Recall from Chapter 2 that quite a few of the interfacial tension measurement methods, including the spinning drop method, required the density data of the less dense and the denser fluid at the temperature and pressure at which interfacial tension is to be measured (see Equation 2.19). Moreover, Hussein (PhD Thesis, 1999) carried out the density measurement of a sample of high density polyethylene ( $M_w = 85,149$ ) between 135 and 250 °C. Interestingly, a thermodynamic transition was observed at 208 °C, where the thermal expansion coefficient changed by 25% after the transition temperature<sup>1</sup>. This transition temperature is in the range of the transitions observed in Hussein and Williams' torque melt experiments as explained in Chapter 1, which suggests the possibility of molecular ordering in the PE melt. Therefore, the objective of this chapter is two-fold: the first objective is to report quantitative density values of a different HDPE melt which will be used for the interfacial tension experiments, and the second objective is to scrutinize the density-temperature [ $\rho(T)$ ] data for possible thermodynamic transitions in the densities of the PE melt between 200 to 230 °C. The

---

<sup>1</sup> The densities of PE melts are conventionally believed to be monotonically decreasing functions of increasing temperature. For example, Tait's empirical correlation of PE melts takes the form  $V(P,T)=V(0,T)\{1-C\ln[1+P/B(T)]\}$ , where  $V$ ,  $P$  and  $T$  are specific volume, pressure and temperature respectively,  $C$  is a universal constant and  $B(T)$  is an experimentally fitted parameter (Rodgers, 1993).



densities of HDPE melts with different molecular weights were measured in the temperature range of 160 to 250 °C. The same experimental method described in Hussein's thesis will be used here.

## 4.2 Materials

The properties of HDPE samples investigated in this chapter are shown in Table 4.1 (Hussein, PhD Thesis). These HDPE samples are Ziegler-Natta type commodity-grade polymers produced by different producers. There were varying amounts of additives and anti-oxidants added to these polymers by the producers. The molecular weights of these polymers were previously characterized by Hussein (PhD. Thesis, 1999) using gel permeation chromatography.

Table 4.1. The properties of the HDPE investigated in this chapter

HDPE producer and product code	Density* (g/cm <sup>3</sup> )	M <sub>n</sub> <sup>(a)</sup> (g/mol)	M <sub>w</sub> <sup>(b)</sup> (g/mol)	M <sub>w</sub> /M <sub>n</sub>	M <sub>z</sub> <sup>(c)</sup> (g/mol)
Paxon	0.960	17,449	82,960	4.76	274,329
Solvay	0.960	16,970	79,689	4.70	264,826
Union Carbide	0.961	13,340	78,292	5.87	224,055
Exxon 6750	0.951	10,823	35,946	3.32	79,871

\* At 25 °C.

(a) Number average molecular weight

(b) Weight average molecular weight

(c) Z-average molecular weight

The available HDPE is in pellet form. For the density measurements, the HDPE pellets were molded into small circular disks with a diameter of approximately 2.5 cm and 0.2 cm in thickness by pressing the polymer at 170 °C in a Carver press, under a load of 2 metric tonnes, and held for 3 minutes. Silicone oil was also required in this experiment. It is Fluid 710 produced by Dow Corning (supplied by EB Peerless Ltd.,





Calgary) with a specific gravity of 1.1 at room temperature and a molecular weight of 2,600 g/mol. The upper limit of the operating temperature of the oil in an open system is 260 °C. For the calibration of the densitometer, distilled water was used. The distilled water was Millipore water, which was double distilled, de-ionized and ultrafiltered.

### 4.3 Experimental Methods

A method for measuring the density of polymer at high temperatures was previously designed and described by Hussein in his PhD thesis. A similar densitometer, with the help of Dr. Xiaosen Li (University of Alberta), was set up in the lab to perform all of the density measurements presented in this chapter. The method of this densitometer is similar to the ASTM D 792 method (Shah, 1984, p.239) which is based on the Archimedes principle. The density of a solid sample ( $\rho_s$ ) can be obtained by measuring its weight in air ( $W_a$ ), and its weight when it is immersed in a liquid ( $W_L$ ) provided that the density of the immersion liquid  $\rho_L$  is known:

$$\rho_s = \frac{\rho_L}{\left(1 - \frac{W_L}{W_a}\right)} \quad (4.1)$$

A diagram of the apparatus is shown in Figure 4.1. The apparatus consists of an electronic balance (Mettler Toledo, precision to the fourth decimal place), a thin copper wire (diameter  $\sim 0.01$ mm) to hang the solid sample from the balance, a beaker to hold the immersion fluid, a high temperature circulator (Haake F3, upper temperature of 350°C)



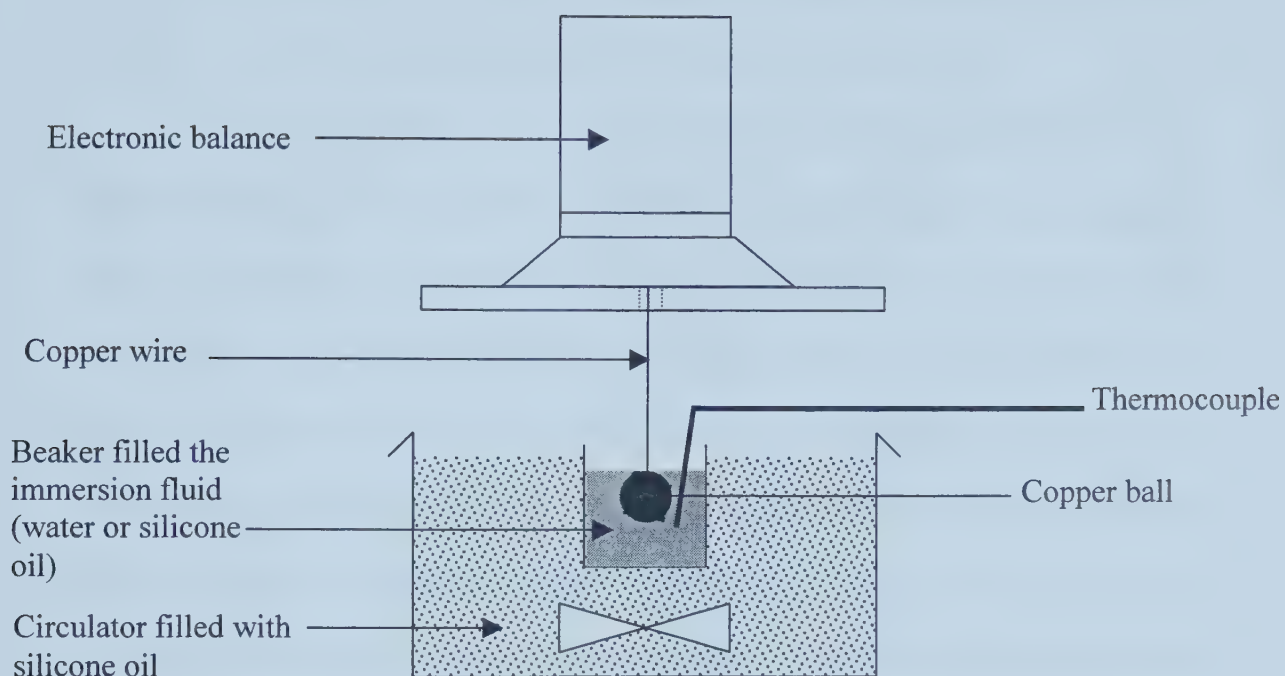


Figure 4.1 A schematic diagram of the densitometer for the measurement of the density of water with a copper ball.



and a thermocouple with a digital display<sup>2</sup>. Silicone oil was used as the heating medium in the circulator. Silicone oil was also used as the immersion fluid for the polyethylene density experiment, which will be described later.

Initially, a long piece of copper wire (with a known density of 8.93 g/cm<sup>3</sup>, Metals Handbook, p. 115) was rolled up in a ball to mimic a copper ball. The copper “ball” was immersed into distilled water at room temperature and the density of the distilled water was measured. However, the measured densities of the distilled water had an average error of 20% higher than the published values, and the quantity of the error was not consistent each time the experiment was repeated. It was suspected that air was trapped between the wires in the rolled-up copper “ball”, and the amount of air trapped was not accounted for in Equation 4.1. Each time the experiment was repeated (by removing the immersed copper “ball” from the water and by changing the distilled water), the amount of air trapped between the copper wires was different from the last experiment. This caused an inconsistency in the density measured for the distilled water.

In order to rectify the error caused by the trapped air between the copper wires, a rectangular copper plate was used in place of the copper ball (as suggested by Dr. Y. Maham, University of Alberta). The copper plate (weight of 13 g) was dipped into the water and removed several times to remove possible air bubbles adhered to the surface of the plate. It was also ensured that the plate was immersed just below the surface of the liquid such that the volume of the hanging copper wire did not need

---

<sup>2</sup> In one experiment with distilled water at 70 °C, the position of the thermocouple was varied. It was found that the temperature of the fluid (within a 3 cm radius of the sample) was the same. Therefore, in all of the density experiments presented in this chapter, the thermocouple was placed as closely to the solid sample as possible (within 3cm of the sample) to ensure that the temperature displayed was as close as possible to the temperature of the sample.



to be accounted for. The apparatus was first used to measure the density of water at a room temperature (22.3 °C). The copper plate hung from the balance was immersed in the beaker filled with distilled water, and the weight of the copper plate ( $W_s$ ) was recorded over a temperature range of 20 °C to 90 °C.

In the calculation of the density of distilled water, Equation 4.1 was modified to correct for the extra volume of the copper wire (approximately  $2 \times 10^{-3} \text{ cm}^3$ ) which was used to hang the copper plate. The densities of distilled water at different temperatures are shown in Figure 4.2. The black data points are the measured densities, and the solid line represents data reported by Kell (1975). The average error of the measured densities (relative to the literature values as reported by Kell) was 0.4% after the correction for the volume of the copper wire. The likely sources of the error in the densitometer are: uncertainty in the temperature readout; uncertainty of the balance readings; error caused by air drafts in the environment, causing fluctuations in the balance reading. The uncertainties in the temperature readout and the balance readings are very small (less than 0.1%). The fluctuations in the balance readings caused by air drafts were likely the largest contributor to the errors in the densitometer. Nonetheless, the error observed with the distilled water experiment appeared to be a systematic error (measured value is consistently higher than the published values), and this error of 0.4% will be applied to all of the measured densities in the rest of this chapter.

Initially, the density of polyethylene was measured with the method of the copper plate similar to the method described above, with the HDPE melt as the





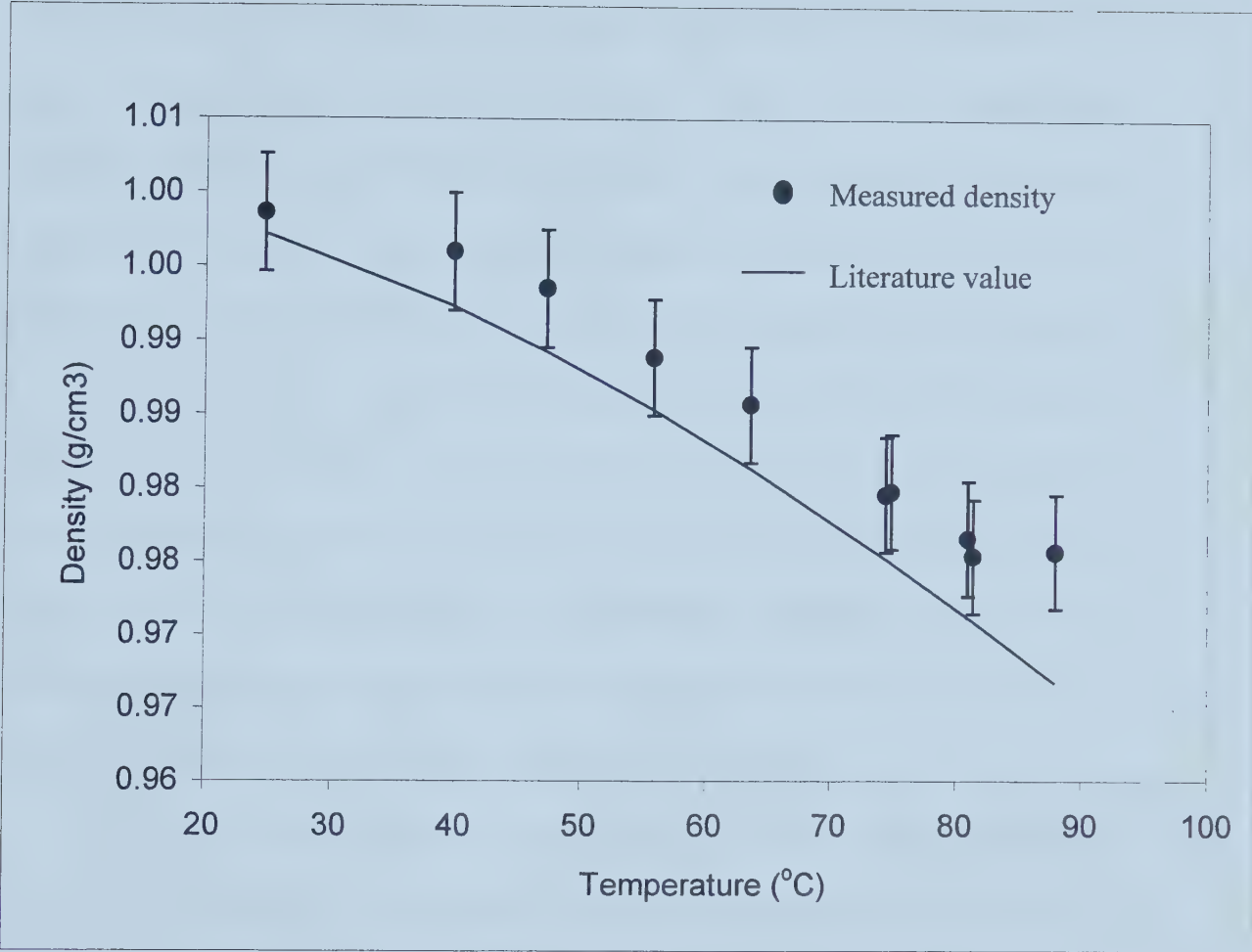


Figure 4.2 The measured density of distilled water at different temperatures compared to the literature value reported by Kell, 1975. The magnitude of the error bar on the density is  $\pm 0.4\%$ .



immersion fluid instead of distilled water. A beaker filled with polyethylene pellets at room temperature was placed in the silicone oil circulator and heated up to a liquid state at 140 °C. The copper plate was then immersed in the molten polyethylene, and, ideally the density of PE,  $\rho_L$  could be calculated using Equation 4.1. However, this method presented some experimental difficulties. First, the densitometer was operated in open air, and the PE melt in the beaker was also exposed to air at high temperatures. Thus, PE was susceptible to oxidation and degradation under the experimental conditions which might alter the physical properties of the polymer. Second, each time the temperature was increased, the volume of the PE expanded, and the height (at which the surface of the PE liquid just covers the copper plate) grew higher such that a portion of the *copper wire* was also immersed along with the copper plate. This created a problem in the calculation of the PE density as it was difficult to approximate the volume of copper wire immersed in the liquid each time, and this volume correction was not accounted for in Equation 4.1.

As a result of the problems discussed above, a method originally used by Hussein (PhD Thesis, 1999) was employed in our density experiments: silicone oil was used as the immersion fluid and PE was the sample to be hung from the balance and immersed into the beaker filled with silicone oil. In this set-up, PE was not exposed to air at all under high temperatures, thus degradation under oxidation was minimized if not prevented entirely. The possibility of diffusion of silicone oil into the PE samples at high temperature was previously investigated by Hussein (PhD Thesis): The samples were scanned using an SEM for the presence of silicon inside after it was immersed in the oil at high temperatures. No silicon was observed inside



the PE, which indicates that silicone oil did not diffuse into the polymer. Hussein hung a small piece of paper clip (approximately 0.1-0.2g) at the end of the PE sample, (as shown in Figure 4.3a) and simultaneously heated the sample and silicone oil to the desired temperature. The weight of the immersed sample was recorded each time a new temperature was reached. Since the density of PE is less than the density of silicone oil, the addition of the paper clip provided enough weight to the PE such that the sample could remain immersed in the oil throughout the experiment. The molecular weight (weight average) of the PE used in Hussein's experiment was 85,129 g/mol, and it was reported that even in the molten state, the PE sample was able to hold the weight of the paper clip. However, when the density experiment for several samples of PE (molecular weights range of 35,946 to 82,960 g/mol - Table 4.1) were conducted in this work, it was found that by hanging the paper clip on all of these PE samples, the PE melt was not strong enough to withstand the weight of the paper clip. In the case of the Union Carbide, the Solvay and the Paxon samples ( $M_w = 78,292, 79,689$  and  $82,960$  g/mol), due to the extra weight of the paper clip, the PE samples were "pulled down" and elongated such that the paper clip touched the bottom of the beaker, as shown in Figure 4.3b. For the Exxon 6750 sample, the PE melt was not able to hold the weight at all, and the paper clip fell through the PE melt. It appears that with a slight decrease in the molecular weight of PE (Hussein's PE had a molecular weight of 85,149 g/mol), the "strength" of the polymer changed as well.

For all of the density measurements of PE presented in this thesis, instead of hanging a paper clip on the PE melt, we wrapped a piece of copper wire (approximately 0.2 g) around the PE melt such that the load of the copper wire is



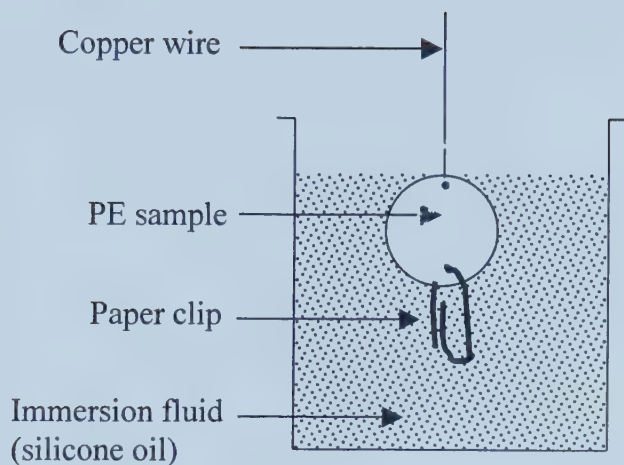


Figure 4.3a A paper clip hanging at the end of the PE sample and immersed in silicone oil.

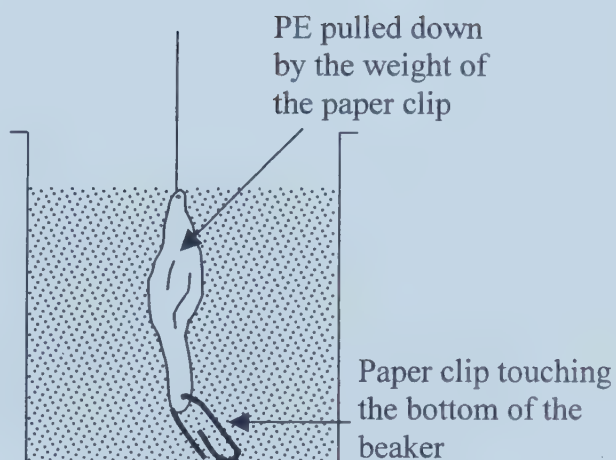


Figure 4.3b PE melt deformed and elongated under the weight of the paper clip. The paper clip touches the bottom of the beaker.

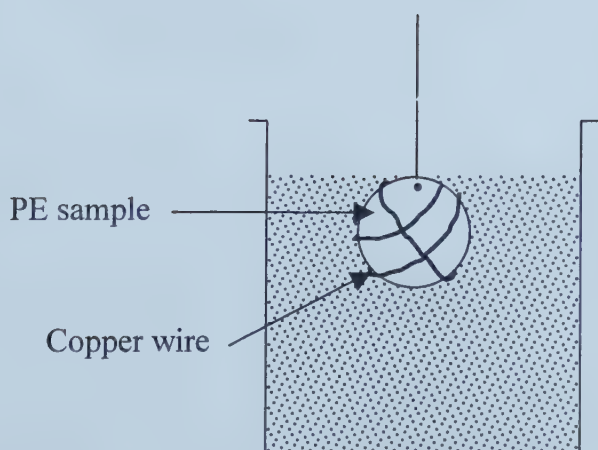


Figure 4.3c A copper wire wrapped around the PE sample and immersed in silicone oil.





distributed and large deformation of the polymer does not occur. This is shown in Figure 4.3c. Before immersing the sample into silicone oil, the copper-wire-wrapped PE sample was dipped in the silicone oil a few times to remove air bubbles that may adhere to the sample. The immersed sample was then simultaneously heated and its weight was recorded for various temperatures in the range of 130 – 250 °C. Equation 4.1 was modified to account for the volume of the copper wire ( $V_{wire}$ ), as shown below in Equation 4.2<sup>3</sup>:

$$\rho_s = w_a \left[ \frac{w_a - w_L}{\rho_L} - V_{wire} \right]^{-1} \quad (4.2)$$

All of the experiments involving the HDPE melts were conducted by heating the samples up to 240 °C and the weights of the immersed sample were measured as it cooled to 130 °C. For temperatures greater than 200 °C, a measurement was taken approximately every 0.6 °C while the measurements were taken approximately every 5 °C for temperatures less than 200 °C.

#### 4.4 Results

The density of silicone oil between 130-250 °C was first measured using the densitometer. Silicone oil was the immersion fluid for the copper plate hanging from the balance. The density of silicone oil as a function of temperature is shown in Figure 4.4. The volumetric expansion coefficient obtained from the experiments

---

<sup>3</sup> The volume of the copper wire was calculated by dividing the mass of the copper wire by its density at different temperatures. The density of copper in the temperature range of 130-250 °C was obtained from the Metals Handbook ( 2<sup>nd</sup> Edition, p. 115).



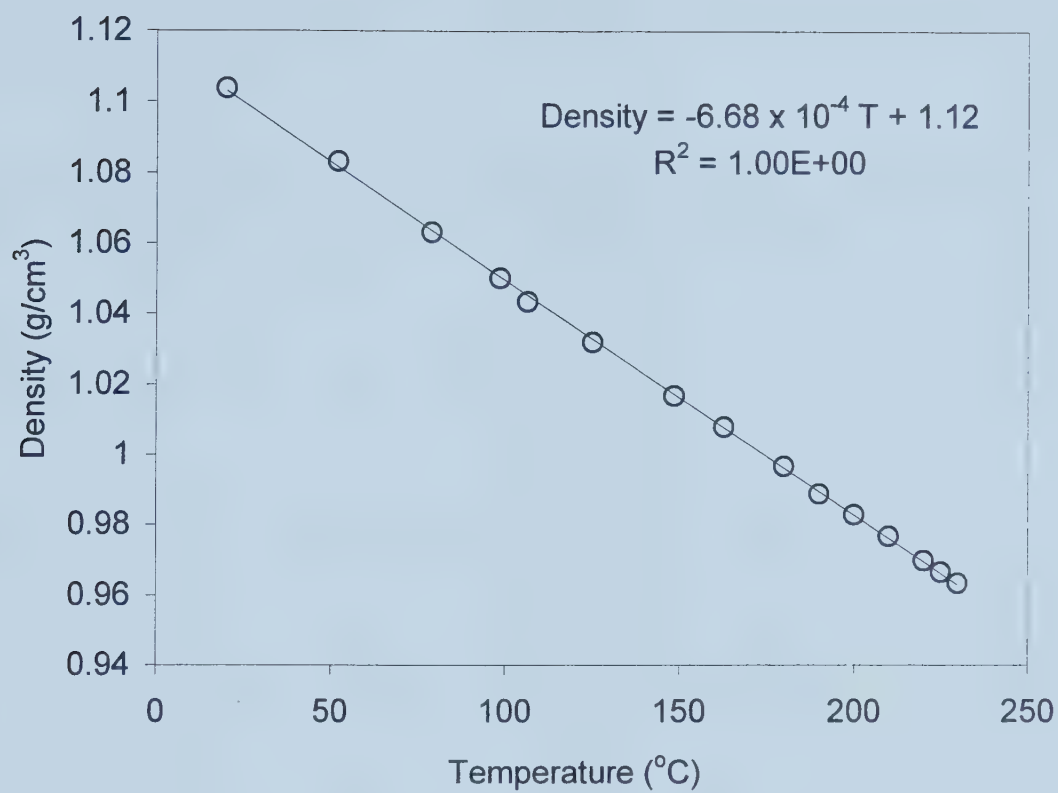


Figure 4.4 The density of the silicone oil at various temperatures.



agreed with the manufacturer's data (the manufacturer's value was 0.7% higher than the value obtained from the experiment in this work).

#### Lower Molecular Weight HDPE - The Exxon 6750 and the Union Carbide Samples

Density experiments with the Exxon 6750 HDPE ( $M_w=35,946$ ) and the Union Carbide HDPE ( $M_w=78,292$ ) were not successful. Once the temperature exceeded approximately 180 °C, the copper wire wrapped around the PE sample could not retain the PE melt, as most of the PE sample escaped into the silicone oil. At the end of each experiment, the silicone oil (which was originally translucent) became milky and gel-like. Initially it was suspected that the PE samples may have emulsified in the silicone oil at the high temperature. However, upon observing a sample of this "altered" silicone oil under a microscope, no emulsion was observed and the texture of the oil was uniform. It is possible that some component of the PE melt may have leached into the silicone oil at high temperatures, therefore changing the physical properties of the oil.

It was also observed that more of the Exxon 6750 HDPE escaped into the oil than did the Union Carbide sample. When the weights of the samples before and after the experiment were compared, the Exxon sample lost at least 95% of its weight while the Union Carbide sample lost approximately 60% its original weight. This suggested that the higher molecular weight of the PE, the stronger the yield "strength" within the polymer<sup>4</sup>. Nonetheless, due to change in the weights of the Exxon and Union Carbide samples during the experiments, the density measurements of the

---

<sup>4</sup> The yield strength denotes the polymer's resistance to deformation due to an external force.



Exxon and Union Carbide HDPE were not successful and no density values were obtained from these experiments.

#### The Higher Molecular Weight HDPE - The Paxon and the Solvay HDPE

The problem described with the lower molecular weight HDPE was not observed with the higher molecular weight samples, even though the differences between the molecular weights of the Union Carbide and the Solvay samples were very small ( $M_w = 78,292$  for the Union Carbide HDPE and  $79,689$  for the Solvay sample). Although deformed from their original circular shape (see Figure 4.5) when they were in the liquid state, the PE samples did not dissolve into the silicone oil at high temperatures. The weights of the samples before and after the experiment were measured and found to be almost the same.

Two density experiments were conducted for the Paxon HDPE and three experiments were conducted for the Solvay HDPE. A 0.5% error bar was placed on all of the data points. In the first experiment with the Paxon sample, an obvious discontinuity in the density curve was observed in the temperature range of 190-205 °C, as shown in Figure 4.6a. When the experiment was performed for a different Paxon specimen (Figure 4.6b), the discontinuity observed in Figure 4.6a could not be observed. Instead, very small transitions were observed between 208-211 °C and 216-221 °C. The density data for the two sets of the Paxon experiments were plotted together and shown on Figure 4.6c. Both sets of data lie within the error bars of each other, indicating good repeatability of the experiment.





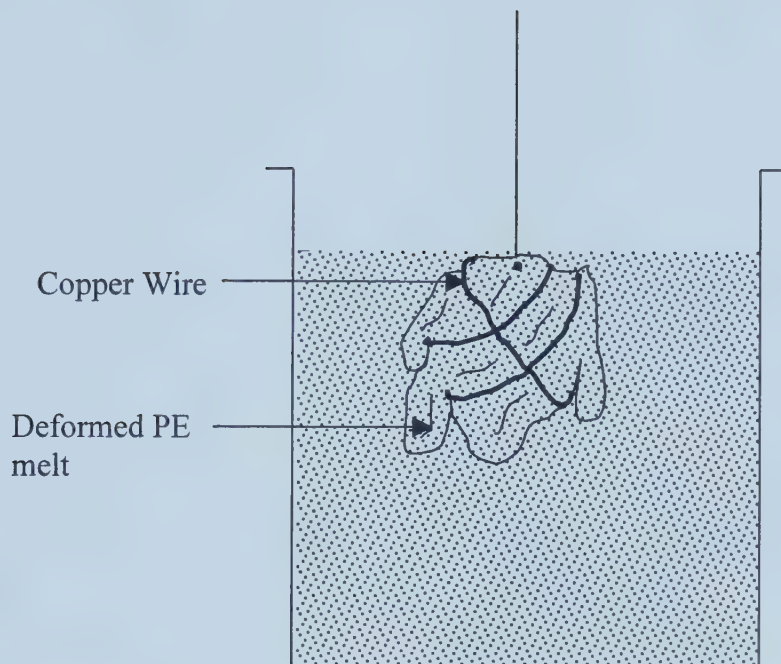


Figure 4.5 The PE melt bounded by a copper wire immersed in silicone oil. Although the shape of the PE was deformed, no PE broke away to dissolve in the silicone oil.



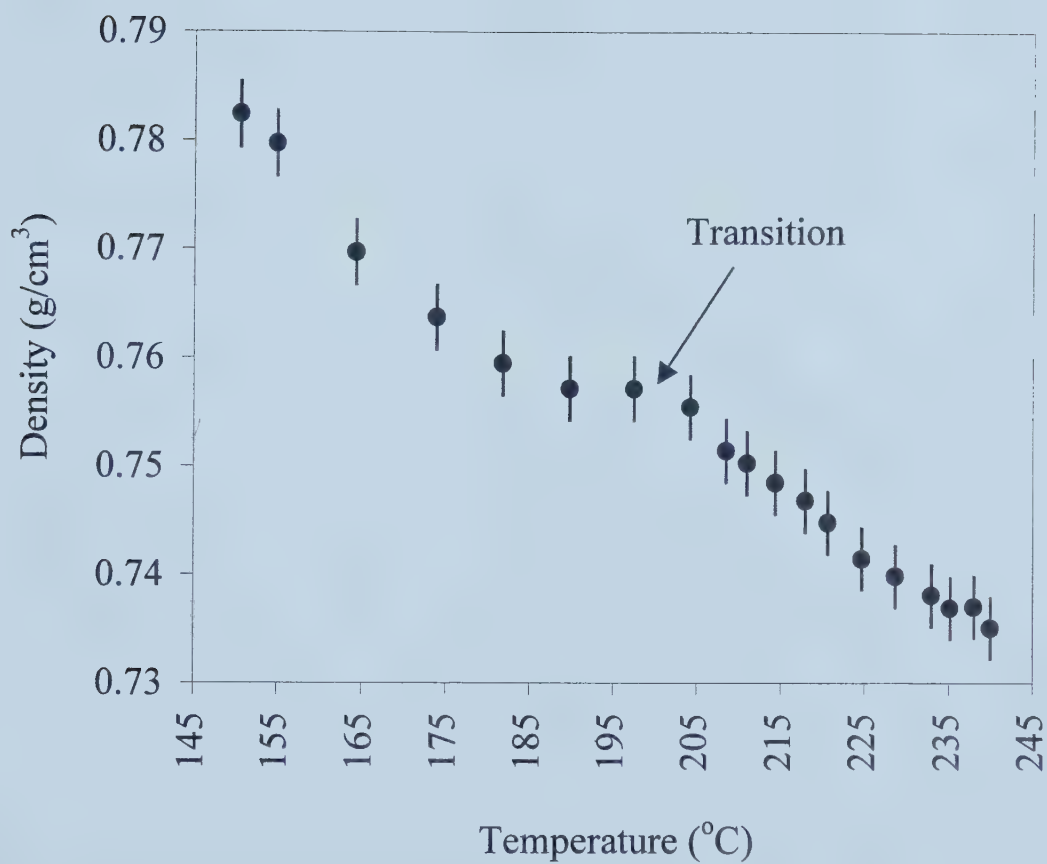


Figure 4.6a The density measurement of the first Paxon HDPE sample between 145 and 245 °C. A discontinuity or a transition is observed between 185 and 205 °C. The error bar on each data point is 0.4%.



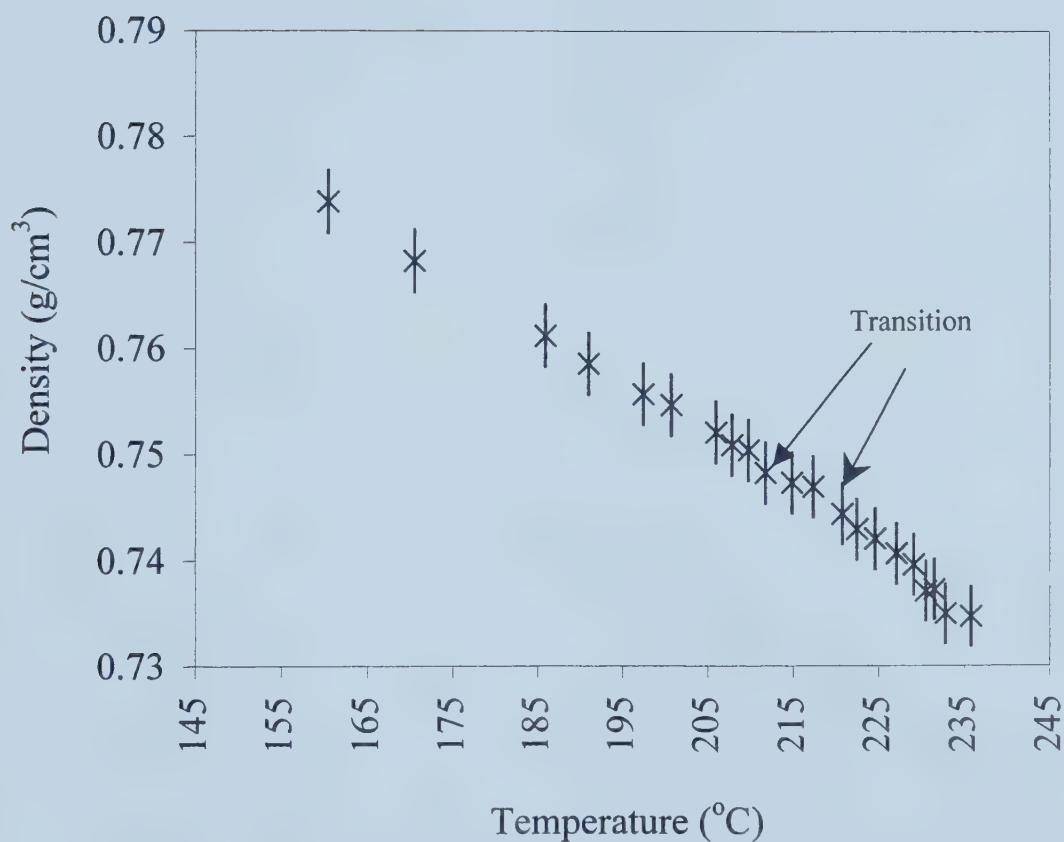


Figure 4.6b The density measurement of the second Paxon HDPE sample between 145 and 245 °C. A discontinuity or transition is observed between 208 - 211 °C and 216 - 221 °C. The error bar on each data point is 0.4%.



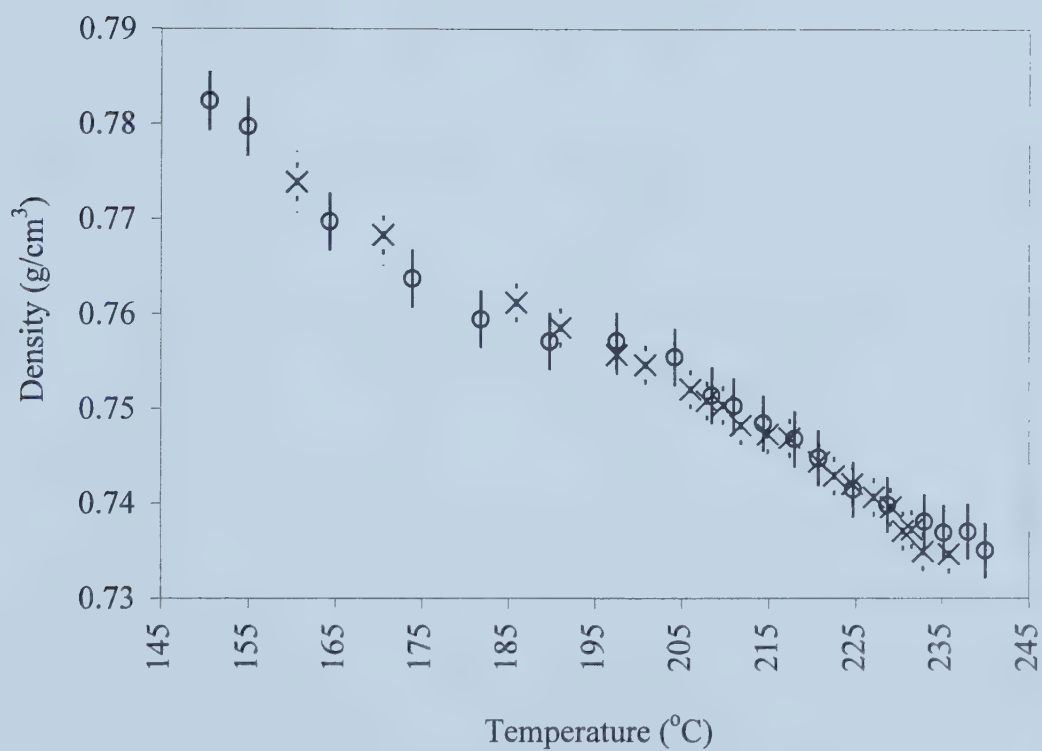


Figure 4.6c The data from Figures 4.6a and 4.6b shown together on the same graph. The open circles indicate data from the first Paxon HDPE experiment while the crosses are data from the second Paxon HDPE experiment.





The three density experiments of the Solvay HDPE are shown in Figures 4.7a, 4.7b and 4.7c. The density data for the two sets of the Paxon experiments were plotted together and shown on Figure 4.7d. All three experiments showed transitions at different temperatures, at approximately 218 °C for Figure 4.7a; at 215 and 220 °C for Figure 4.7b; at 226 °C for Figure 4.7c. Nonetheless, the temperatures at which these transitions were observed are consistent with those observed for the Paxon HDPE.

The density data presented in Figures 4.6abc and 4.7abc are more comprehensive than those reported by Hussein (PhD Thesis, 1999), since here an average of forty measurements were recorded between 130 and 250 °C compared to the thirteen data points in this range presented by Hussein. Nonetheless, the transitions observed with the Paxon and Solvay HDPE in this chapter are consistent with Hussein's density measurements of another HDPE sample ( $M_w=85,149$ ), where a transition was observed at 208 °C.

All of the data transitions observed in Figures 4.6 and 4.7 are within the 0.4% experimental error bar. However, as discussed earlier, this error is not a random error, it is most likely a systematic error. This error is consistent with each measurement and each set of experiment, therefore, we believe that the transitions observed in the density experiments can be believed.



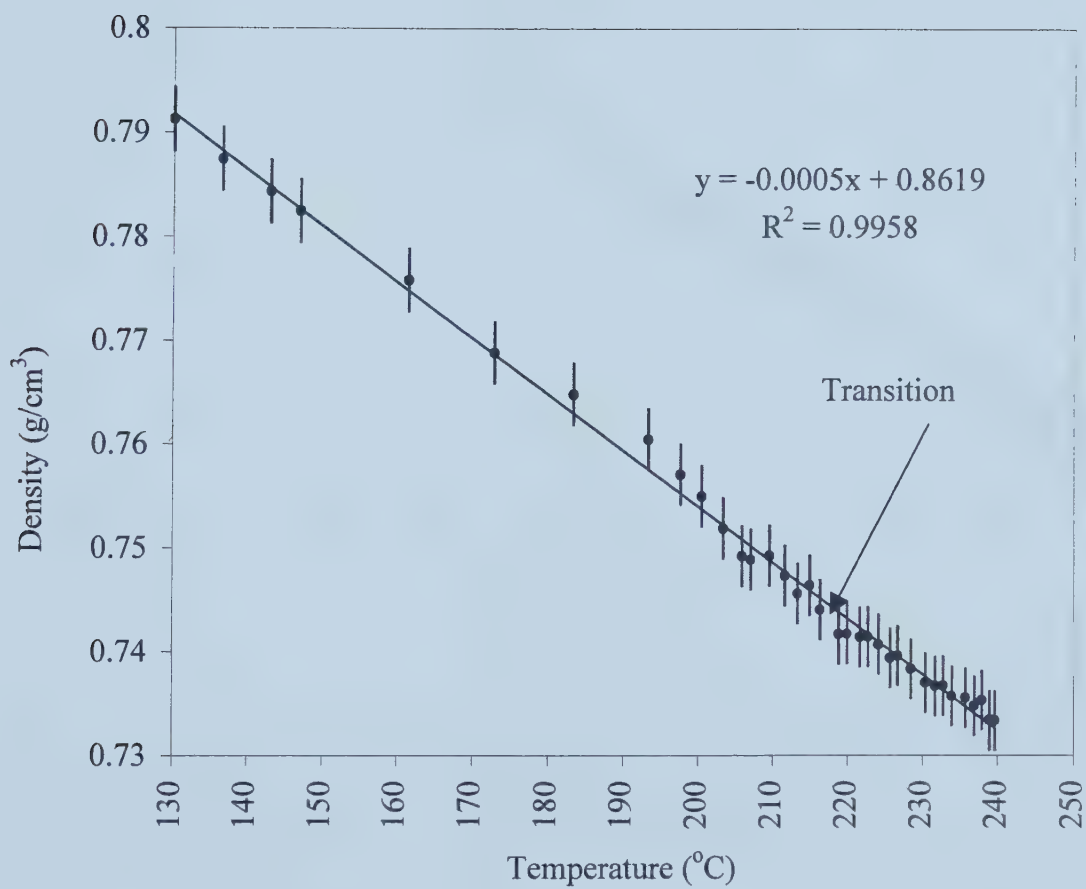


Figure 4.7a The density measurement of the first Solvay HDPE specimen between 130 and 240 °C. The error bar on each data point is 0.4%. The transition arrow identifies where the transition appeared for the Paxton sample (Figure 4.6a)



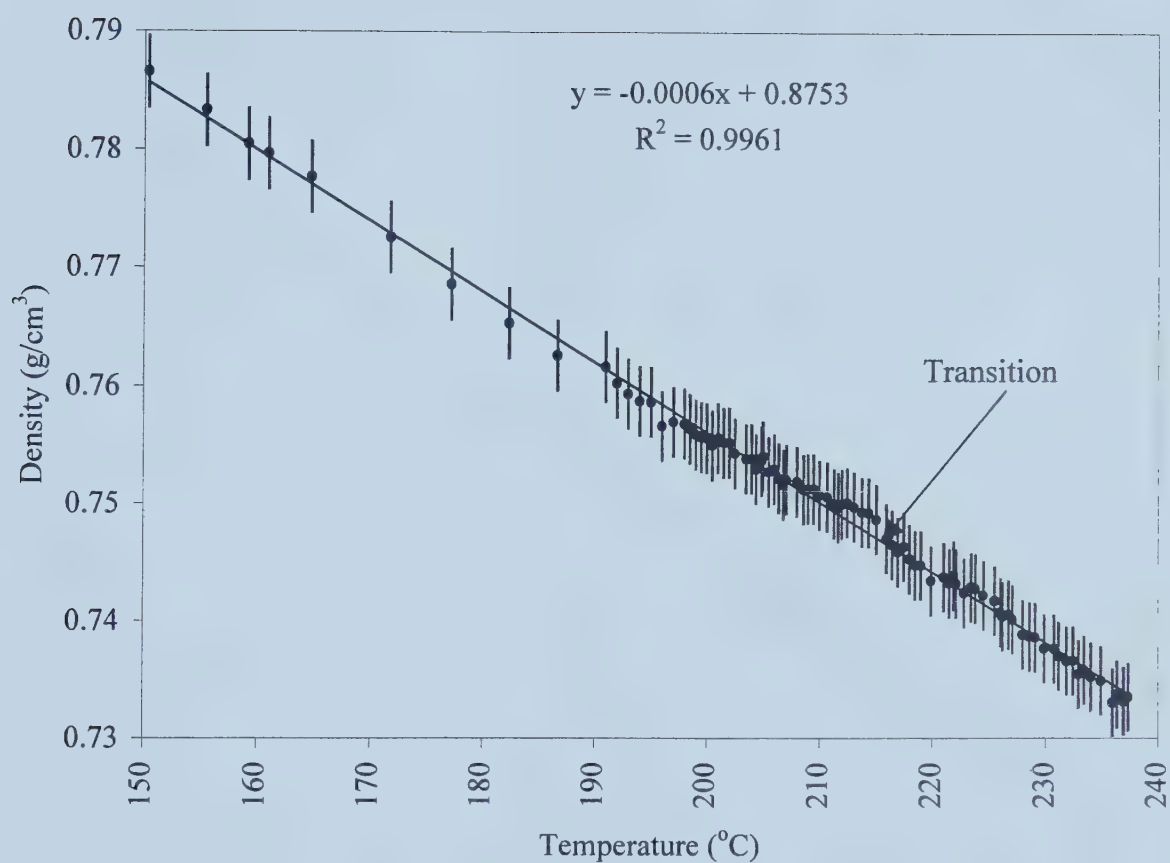


Figure 4.7b The density measurement of the second Solvay HDPE specimen between 150 and 240 °C. The error bar on each data point is 0.4%. The arrow shows the transition for the Solvay sample at approximately 215 °C.



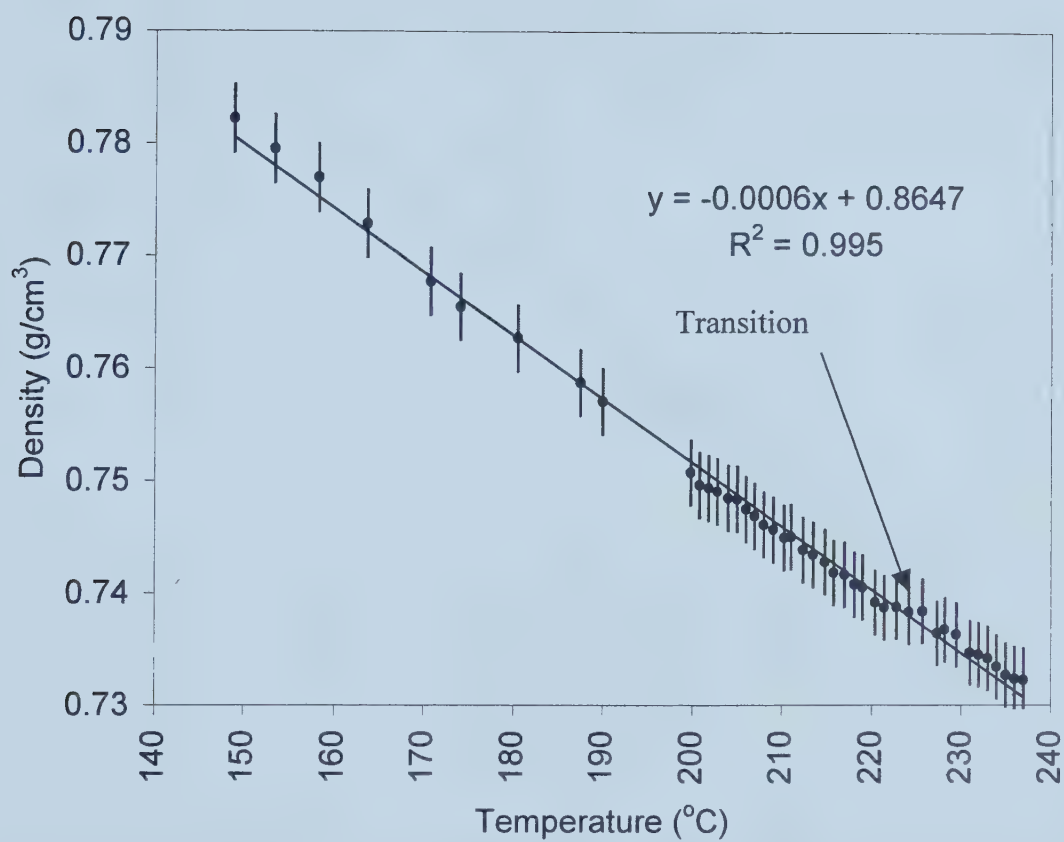


Figure 4.7c The density measurement of the third Solvay HDPE specimen between 150 and 240 °C. The error bar on each data point is 0.4%. The arrow shows the transition for the Solvay sample at approximately 228 °C.





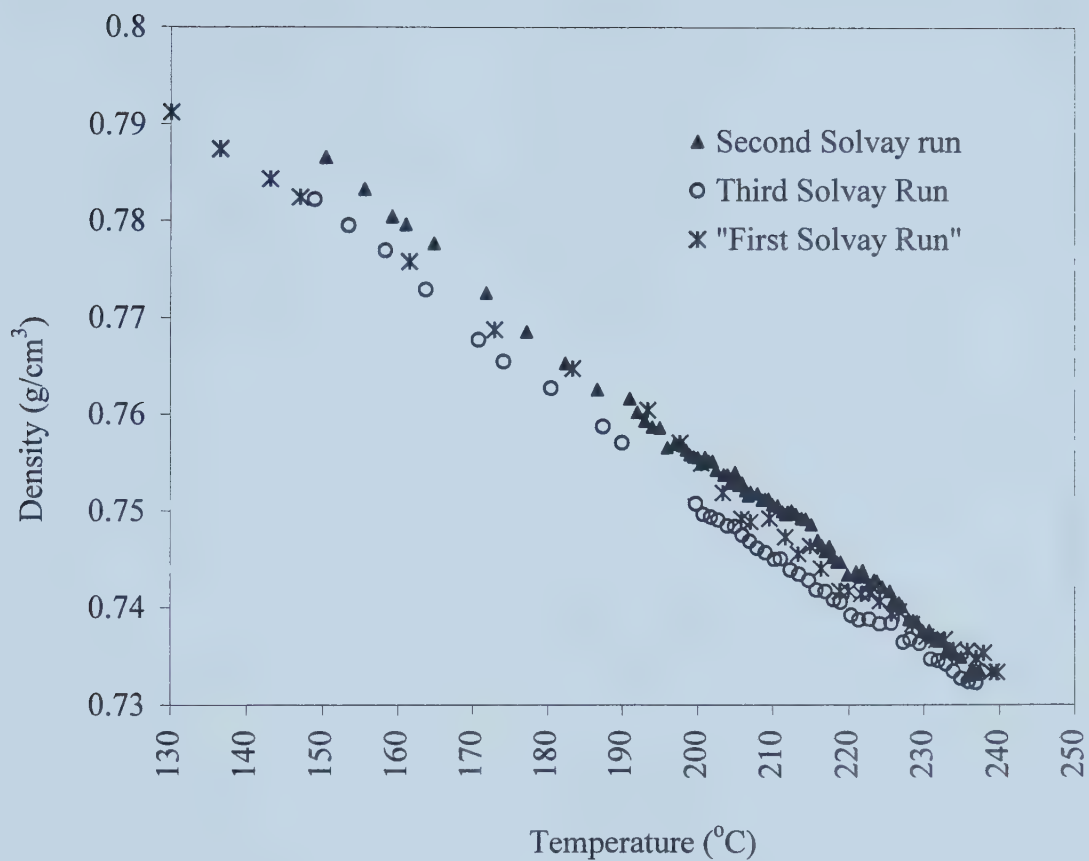


Figure 4.7d The density measurement of all three Solvay HDPE samples between 130 and 240 °C.



## 4.5 Conclusions

- The higher the molecular weight of the PE, the stronger the yield “strength” within the polymer.
- A transition in the temperature range of 215 - 230 °C was observed in the densities of all five HDPE samples. This is consistent with Hussein’s density measurements.



## CHAPTER 5

### INTERFACIAL TENSION MEASUREMENTS AND EVIDENCE OF ORDER IN POLYETHYLENE MELT

---

#### 5.1 Introduction

It is conventionally believed that above the melting temperature ( $T_m$ ) of 135-140 °C, PE undergoes a change from the semi-crystalline to a melt amorphous phase with no long range molecular order i.e. a classical random coil (Flory, 1953). However, there is increasing evidence from rheological, DSC and NMR studies which suggests the presence of microstructural order in the bulk of PE melts. The objective of this thesis is to investigate further the existence of these so-called “ordered” phases in the PE melts by examining the surface properties of the PE melt at high temperatures. The interfacial tensions of amorphous polymer melts are known to be monotonically decreasing with increasing temperature (Wu, 1982), whereas the interfacial tensions of ordered anisotropic phases are known to behave non-monotonically when their ordered molecules undergo a thermodynamic transition to isotropic phases. These thermodynamic transitions are easily identified by a maximum in the interfacial tension at the transition temperature (George and Mohandas, 1995). This chapter is therefore dedicated to the investigation of the existence of the ordered phases in HDPE, LDPE and LLDPE melts through interfacial tension studies of the melts in the temperature range of 180-240 °C. Due to the experimental ease associated with the measurement of interfacial tension using a spinning drop tensiometer, the data



presented in this chapter will be the most comprehensive study of the interfacial tension of PE melts at different temperatures to date.

## **5.2 Review of Literature**

### **5.2.a Evidence of Structural Order in PE Melts**

The number of reports in the literature regarding the anomalous behavior and the possible evidence of microstructural order in PE melt is compelling. Kruger et al. (1980) conducted acoustic tests (using Brillouin spectroscopy) to study the hypersonic properties of low molecular weight linear PE ( $M_w = 6,600$ ) from 130 to 390 °C. They discovered an anomalous transition at 230 °C in the sound velocity of the PE melts. Other experiments by the same authors also found discontinuities in the volume expansion coefficient and refractive index of the PE melt at high temperatures. These discontinuities also occurred at 230 °C. The authors attributed these anomalous observations to possible transitions from a locally nematic state to an isotropic state in the PE melt, similar to that found in liquid crystal polymers.

Kamel and Charlesby (1981) conducted NMR spin-spin relaxation studies on commercial HDPE ( $M_w = 20,000$ ) from 140-205 °C, and found that the PE melt was composed of three different types of components: a structured or ordered component where the chains have little mobility; an entangled yet mobile component; and a “free segment” of molecules which are too short to be entangled or form a network. As such, the conventional idea of an “amorphous” PE melt could not explain the existence of the structured packing as identified by the NMR studies.





Bremner and Rudin (1992) conducted a similar NMR study on LDPE and HDPE from 40 to 200 °C. The authors also found three components present in the PE at temperatures higher than  $T_m$ : a region with high segment density, i.e. a close packed ordered region; an entangled network material; and a non-network amorphous material. The authors speculated that the ordered component is “a portion of the polymer which retains its order while passing from the crystalline solid to melt state.” They also found that the volume fraction of the ordered material is dependent on the particular polymer and its previous thermal history (ie. cooling and annealing rates).

Wang and Drda (1996) studied the temperature dependence and the molecular characteristics of the stick-slip transitions of HDPE melt from 200 to 260 °C through a capillary rheometer. The authors observed a systematic anomalous behavior of the stick-slip transition at the PE melt/die wall interface at 200 °C, and speculated that the anomalous behavior may be due to possible ordered phases (such as the nematic phase) that existed in the PE melt.

Hussein and Williams (1998) conducted torque-melt experiments in a blender for a sample of molten HDPE ( $M_w = 78,030$ ,  $M_n = 16,540$ ) in the temperature range of 160 to 260 °C. One or more thermal transitions were observed in the torque in the narrow temperature range of 200 to 230 °C. The same discontinuity was not observed for the polystyrene (PS) sample, which is normally believed to be amorphous (PS is used as a reference or comparison to the behavior of PE to rule out the possibility of artifacts in the experimental apparatus.) This anomalous transition was thought to resemble the rheology of liquid crystal polymers, which undergo a microstructural transition at a transition temperature.



The thermal/microstructural transitions of HDPE, LLDPE and LDPE in the temperature range of 208 to 227 °C were also observed in the DSC experiments conducted by Hussein and Williams (2000). These transition temperatures were similar to their torque melt experiments (Hussein and Williams, 1998) discussed earlier, and provided more evidence of microstructural order in the PE melt.

### **5.2b Interfacial Tension of Polyethylene Melts**

Despite the importance of the knowledge of the interfacial tension of polymer melts in polymer blending processes, little data and information is available in the literature on the dependence of interfacial tension on temperature (Anastasiadis et al., 1986, Kamal et al., 1994, Carriere et al., 2000). This is most likely attributed to the experimental difficulties associated with the polymer melts, such as the long equilibration time for the polymer and the high temperatures involved (as discussed in Chapter 2). For the limited data available on the interfacial tension of PE melts, few data points are available for temperatures as high as 240 °C, and most experiments are conducted by using large temperature steps i.e. a measurement was made every 10 °C (Wu, 1982; Chen and White, 1993; Pham and Carriere, 1997; Garmabi et al., 1998; Arashiro and Dermalquette, 1999; Carriere et al., 2000; Chapleau et al., 2000). This again is probably due to the experimental difficulties associated with measurements of the interfacial tension of PE melts, as well as attempts to avoid degradation of the PE during the experiment. Most methods used by the afore-mentioned authors (such as the pendant drop method, breaking thread method and the imbedded fiber retraction method) make it very difficult to measure



interfacial tension in a continuous manner at different temperatures (as discussed in Chapter 2). Moreover, it is generally accepted that PE melts behave like isotropic liquids, where interfacial tensions decrease monotonically with increasing temperature. Wu (1982) tabulated a series of interfacial tension of PE melts at 100, 140 and 180 °C and it was shown that interfacial tension decreased linearly with increasing temperature with a constant temperature coefficient ( $dy/dT$ ) on the order of 0.01 mN/m °C. As such, most of the authors (Wu, 1982; Carriere et al.; Chen and White, 1993; Pham and Carriere, 1997; Garmabi et al., 1998; Arashiro and Dermalquette, 1999; Carriere et al., 2000; Chapleau et al., 2000) measured only very few data points in their experiments, and then fit a linear regression line through the data to obtain the temperature coefficient for the interfacial tension. Because of the lack of data points, it is sometimes difficult to ascertain whether the data over the temperature range actually represents a monotonic linear function or the scatter in the data represents a non-continuous curve.

Due to the conventional belief that PE melts behave like an isotropic liquid (with interfacial tension decreasing monotonically with increasing temperature) some experimentalists have overlooked some anomalous observations in their measurements of the interfacial tension of PE melts at high temperature. Pham and Carriere (1997) measured the interfacial tensions of polycarbonate/polyethylene (polyethylene  $M_w = 70,000$ ) using the imbedded fiber retraction method from 210 to 240 °C where a peak was observed at 220 °C. However, due to the large standard deviation associated with the measurement at that temperature, the authors fitted a linear regression line through all data points and offered no explanation for the



observed peak. Pham and Carriere's data for the interfacial tension between PC and PE are shown in Table 5.1. The shaded box in the table represents the temperature where a peak in the interfacial tension was reported.

**Table 5.1. Data from Pham and Carriere (1997) on the Interfacial Tension of the PC/PE at different temperatures**

<i>Temperature (°C)</i>	<i>Interfacial Tension (mN/m)</i>
210	$2.77 \pm 0.24$
220	$3.18 \pm 0.68$
320	$2.56 \pm 0.44$
240	$2.13 \pm 0.33$

Rao (M.Sc. Thesis, 1998) measured the interfacial tension of polypropylene and LLDPE at 200, 220 and 260 °C using the breaking thread method. A peak in the interfacial tension was observed at 220 °C for all three measurements. The author suggested that the peak was likely due to a different experimental procedure applied for the measurements at 220 °C, but could not point out the specific cause of the observed peak.

Carriere et al. (2000) measured the temperature dependence of the interfacial tension of PS/PMMA, PS/PE and PMMA/PE (PE molecular weight = 135,000) using the imbedded fiber retraction method. The range of temperature studies was from 140 to 220 °C. For the PS/PE system, a peak in the interfacial tension similar to the observation of Pham and Carriere (1997) was observed at 180 °C, where the





interfacial tension value at these temperatures were higher than the others. For the PMMA/PE system, a discontinuity in the interfacial tension was also observed at 200 °C. However, a peak was not observed for the PS/PMMA pair. Again, due to the large standard deviation associated with the measurement at that temperature, the authors also fitted a linear regression line through all data points and offered no explanation for the observed peak or discontinuity with the PS/PE and PMMA/PE systems.

### **5.3 Materials**

For the measurement of the interfacial tension using the spinning drop tensiometer, PE melt was the less dense fluid and silicone oil was the denser fluid of the system. Polyethylene was chosen for the obvious reasons that we are interested in examining the phase transitions at the polymer's interface between 200-230 °C. Silicone oil was chosen as the denser medium for several reasons. Firstly, silicone oil is known to be an isotropic fluid. As such, during the measurement of the interfacial tension of PE/silicone oil, any thermal variation observed will be due to PE alone, and not contributed to by the silicone oil. Secondly, silicone oil is denser than the PE, thus allowing easier loading of the samples into the spinning drop tensiometer (this will be discussed further in section 5.4). Thirdly, silicone oil (Fluid 710) is heat stabilized at high temperatures, with upper temperature limits of 260 °C for open systems and 315 °C for closed systems. Finally, previous experiments by Hussein (PhD Thesis, 1999) showed that silicone oil did not diffuse into the polymer in the temperature range of 200-230 °C, thus ensuring that the silicone oil is an inert medium for the PE.



The PEs used to investigate the possible phase transitions at the interface at high temperatures were the high-density polyethylene, the low-density polyethylene and the linear low-density polyethylene. The available PEs were in pellet forms, and each pellet was approximately 0.03 cm<sup>3</sup> at room temperature. The properties of these PEs are shown in Table 5.2. The properties of silicone oil can be found in Section 4.2.

**Table 5.2 The properties of the PE investigated in this chapter**

PE producer and product code	Density (at 25 °C) g/cm <sup>3</sup>	M <sub>n</sub>	M <sub>w</sub>	M <sub>w</sub> /M <sub>n</sub>	M <sub>z</sub>
HDPE – Paxon	0.960	17,449	82,960	4.76	274,329
HDPE – Solvay	0.960	16,970	79,689	4.70	264,826
HDPE – Exxon 6750	0.951	10,823	35,946	3.32	79,871
LDPE – S231	0.918	13,377	71,797	5.37	182,785
LLDPE – S237	0.918	-	110,000	-	-

## 5.4 Experimental Methods

### *5.4.1 The Measurement of the Interfacial Tension of Silicone Oil and PE Melt*

As discussed earlier in section 5.2b, most of the data available in the literature are collected in a small temperature range and with few data points. As such, it is sometimes difficult to be sure that the interfacial tension of the particular PE and polymer pair is indeed decreasing monotonically with increasing temperature as with isotropic fluids, even though most experimentalists would fit a linear regression line through the limited data points. In this Chapter, the interfacial tensions of silicone oil and PE melt were measured over a large temperature range (180-240 °C) with



temperature increments of 5 °C and 10 °C. The small temperature increment was chosen so that any anomalous variation in the interfacial tension of the PE melt would be captured.

As discussed earlier in Chapter 2, the measurement of interfacial tension using the spinning drop tensiometer requires a small drop of the less dense fluid embedded in the matrix of denser fluid (Vonnegut, 1942). For the measurement of the interfacial tension of polymer systems (most polymers are in the solid state at room temperature), it is necessary to machine the solid polymer sample such that the geometry of the polymer fits the glass tube exactly (Vinagre 1998 SDT Manual). This solid-solid (polymer) loading process is tedious and is subject to possible contamination in the polymer systems since the samples have to be machined. In this thesis, we developed a novel technique of liquid-solid loading. Silicone oil, which is a denser fluid than the PE we examined in this thesis, was loaded first into the glass tube at room temperature (silicone oil is in liquid state in all of the temperatures investigated in this thesis). Two PE solid pellets were then placed inside the glass tube filled with the silicone oil, also at room temperature. Air bubbles inside the silicone oil were removed by gently tapping on the glass tube before sealing the end of the tube with an end plug. The glass tube filled with silicone oil and PE pellets was then loaded on the spinning drop tensiometer and the samples were simultaneously heated to 180°C for the first measurement of the interfacial tension between the silicone oil and the HDPE melt<sup>1</sup>. During this heating process, the rotation rate of the glass tube was adjusted to 1000 rpm to ensure even heating throughout the samples in the glass tube. It took 15 minutes for the oven to reach



180 °C, and approximately 5 minutes more for the HDPE pellets to be in a liquid state. The transition of the HDPE from the solid to liquid state was visible through the glass tube, and once this transition was observed, the rotation rate of the samples was adjusted to 5000 rpm for 35 minutes before the first interfacial tension was measured at 180 °C. A rotation rate of 5000 rpm was chosen for all of the measurements (from 180 °C to 250 °C) in all of the experiments for silicone oil and HDPE melt because it was found from previous preliminary experiments that at this rotation rate, the diameter of the HDPE drop was approximately 2 mm, which is the same as the diameter of one of the calibration posts. Therefore, the measuring system was calibrated against the 2 mm post to reduce possible parallax errors (this was previously explained in Chapter 3). Previous preliminary experiments also showed that a period of 35 minutes was required for the HDPE drop to reach an equilibrium size after a spin up from 1000 rpm to 5000 rpm: the dynamic interfacial tensions of samples were measured and the values were found to be constant after 35 minutes.

After the first measurement at 180 °C, the temperature of the samples was increased by 5 °C or 10 °C, depending on the experiment. After each temperature increment, the samples were given 10 minutes so that at the new temperature the temperature of the sample was the same as the oven temperature. This thermal equilibration time was tested and confirmed by measurement of the dynamic interfacial tension of the samples at each new temperature.

---

<sup>1</sup>The melting point of HDPE is approximately 140°C.





#### ***5.4.2 Degradation of PE and the Blending of Anti-Oxidants into HDPE***

The degradation of PE usually is caused by a chemical modification to the molecules by the environment, such as the presence of heat, UV radiation, mechanical stress or by reactive chemicals. The most prevalent degradation process for PE is the chain-oxidation reaction which involves oxygen. The rate of this degradation process can be greatly enhanced by an energy source such as heat. Anti-oxidants are commonly added in commercial PE as stabilizers to prevent or reduce the degradation of the polymer. The commercial PE samples used in my work surely contained some anti-oxidant, but the composition and amount were unknown.

In this chapter, the total time for each of the interfacial tension experiments was approximately two hours. Under such a long period of time and at such high temperatures, the HDPE samples showed signs of degradation, i.e. browning of the originally white sample after the experiment. In an attempt to reduce or prevent degradation, various amounts of anti-oxidants were blended with the HDPE samples before the commencement of the interfacial tension experiments. The Haake Rheocord 90 melt blender was used to blend the anti-oxidants into HDPE. As recommended by Ciba-Geigy Inc., the anti-oxidant used in all of the experiments in this chapter was a 1:1 blend of Irganox 1010 [Phenol B, tetrakis[methylene 3-(3', 5' – di-t-butylphenol) propionate]methane,  $M_w=1178$ ] and Irgafos 168 [P-1, tris[2,4-di-t-butylphenol] phosphite,  $M_w=646$ ]. The amounts of the anti-oxidants added varied from 1000 ppm to 20,000 ppm. This will be described later. Fifty grams of HDPE were loaded into the blender along with the anti-oxidants. The samples were blended at 150 °C with a rotor speed of 50 rpm for 10 minutes. The blender was not air tight;



during the blending process, the samples were exposed to the air in the room. When the samples were subjected to shear stress at high temperature in the presence of oxygen, there was a high possibility that the samples might be subjected to oxidative degradation during the process. Moreover, when the blending process was completed, the samples needed to be removed from the blender when it was still in the liquid state in order to prevent damage to the blender. Two spatulas were used to “scoop” the HDPE melt from the blender into a storage container. During this process, the HDPE melt was exposed to not only oxygen, but it was also exposed to air-born contaminants in the room which will alter the surface properties of the polymer.

In order to prevent the degradation and exposure to contamination during the blending process, nitrogen gas was kept blowing on top of the blender bowl to “purge” the oxygen from the samples during the blending process. After blending was complete, the PE melt was then immediately quenched in liquid nitrogen. During the transfer of the PE melt from the blender to the liquid nitrogen, a stream of nitrogen gas was kept as close to the sample as possible in an attempt to minimize the exposure of the samples to air. Moreover, in order to ensure that the specimen used for the interfacial experiment was not exposed to the air, the HDPE specimen was cut from the middle of the quenched PE sample.

#### ***5.4.3 The Densities of PE and Silicone Oil for the Calculation of the Interfacial Tension of the Polymer Melts***

The densities for all HDPE, LDPE and LLDPE used for the calculation of the interfacial tension of PE in this chapter are monotonically decreasing functions of



increasing temperature. The densities of the HDPE in the temperature range of 180-250 °C are obtained from the density experiments shown in Figure 4.7c as described in Chapter 4. The specific volumes of liquid LDPE and LLDPE are obtained from Tait's equation (Rodgers, 1993):

$$\text{LDPE:} \quad V = 1.1944 + 2.841 \times 10^{-4} T + 1.872 \times 10^{-6} T^2 \quad (5.1)$$

$$\text{LLDPE:} \quad V = 1.1516 \exp(6.730 \times 10^{-4} T) \quad (5.2)$$

where  $V$  is the specific volume in  $\text{cm}^3/\text{g}$  and  $T$  is temperature in °C. Two different silicone oils purchased from Dow Corning on different dates were used<sup>2</sup> for the interfacial tension experiments. In the rest of this chapter, they will be designated as *silicone oil A* and *silicone oil B*. The density of silicone oil A was previously measured by I.A. Hussein (Hussein, PhD. thesis, 1999) and the density of silicone oil B was measured as described in Chapter 4:

$$\text{Silicone oil A:} \quad \rho \text{ (g/cm}^3\text{)} = 0.9811 - 8.34 \times 10^{-4} T \quad (5.3)$$

$$\text{Silicone oil B:} \quad \rho \text{ (g/cm}^3\text{)} = 1.116 - 6.68 \times 10^{-4} T \quad (5.4)$$

Where  $T$  is the temperature in degree Celcius. Equations 5.3 and 5.4 are valid up to 260 °C.

---

<sup>2</sup> The first batch of silicone oil (Fluid 710) ordered in 1998 was used up in the middle of the experiments. Hence more silicone oil (also 710 Fluid) was ordered from the same manufacturer in



## 5.5 Results and Discussion

### 5.5.1 Interfacial Tensions of HDPE Without Additional Anti-Oxidant

#### Solvay and Paxon HDPE ( $M_w=82,960, 79,689$ )

The interfacial tension measurements of the two higher molecular weight HDPEs (compared to the Exxon HDPE) could not be performed. Recall from Chapter 2 that the measurement of interfacial tension using the spinning drop method is valid if the less dense fluid drop assumes a cylindrical shape with hemispherical ends. However, the higher molecular weight Solvay and Paxon HDPE drops could not assume the cylindrical profile in the spinning drop tensiometer. There appeared to be a yield stress present within the polymer which prevented the HDPE drop from “stretching out” to become cylindrical. This observation is consistent with the findings in the density experiments where the higher molecular weight HDPE also appeared to exhibit yield strength (see Chapter 4).

#### Exxon 6750 HDPE ( $M_w = 35,946$ )

The persisting yield stress observed in the Solvay and Paxon HDPE was not observed with the lower molecular weight Exxon HDPE. Six runs were conducted for the Exxon HDPE from 160 °C to 250 °C, three sets at approximately 5300 rpm and three sets at a higher rotation rate of 8400 rpm. Silicone oil A was used in these experiments. For temperatures less than 190 °C, a measurement was made every 10 °C while at temperatures higher than 190 °C a measurement was made every 5 °C.

---

2000. However, the viscosity and density of the latter silicone oil ordered were different from the silicone oil ordered in 1998.





The results for all six runs, as shown in Figure 5.1, revealed that the interfacial tension of PE/silicone oil-A is not a monotonic function of temperature. For temperatures *less than* 200 °C, the interfacial tension of PE/silicone oil decreases linearly as temperature increases. The average  $d\gamma/dT$  for all six runs in the temperature range of 160 to 200 °C is 0.012 mN/m/°C. This temperature coefficient agrees well with the data collected by Wu (1982), where the  $d\gamma/dT$  for most polymer pairs was found to be on the order of 0.01 mN/m/°C (Wu, 1982). A peak in the interfacial tension was observed for all six runs between 200 and 230 °C, where the interfacial tensions were increasing with increasing temperature. After reaching the peak, interfacial tension again became a decreasing function of temperature. It is interesting to note that although the interfacial properties of PE/silicone oil sets were similar at  $T < 200$  °C, each of the six experiments yielded different transition behavior between 200 and 230 °C; i.e., the peak in the interfacial tension occurred at different temperatures. Moreover, after the transition temperatures, some runs exhibited a larger  $d\gamma/dT$  than others.

Several attempts were made to measure the interfacial tensions of the HDPE with a decreasing temperature sequence from the higher temperature of 250 °C to a cooler temperature of 190 °C. However, all of the attempts failed because when the silicone oil was cooled from 250 °C by 10 °C or 5 °C steps, the silicone oil contracted to produce suction within the tube, and as a result air entered between the tube wall and the sealing plugs. The air bubbles present in the glass tube disrupted the experiments and no measurements could be made.



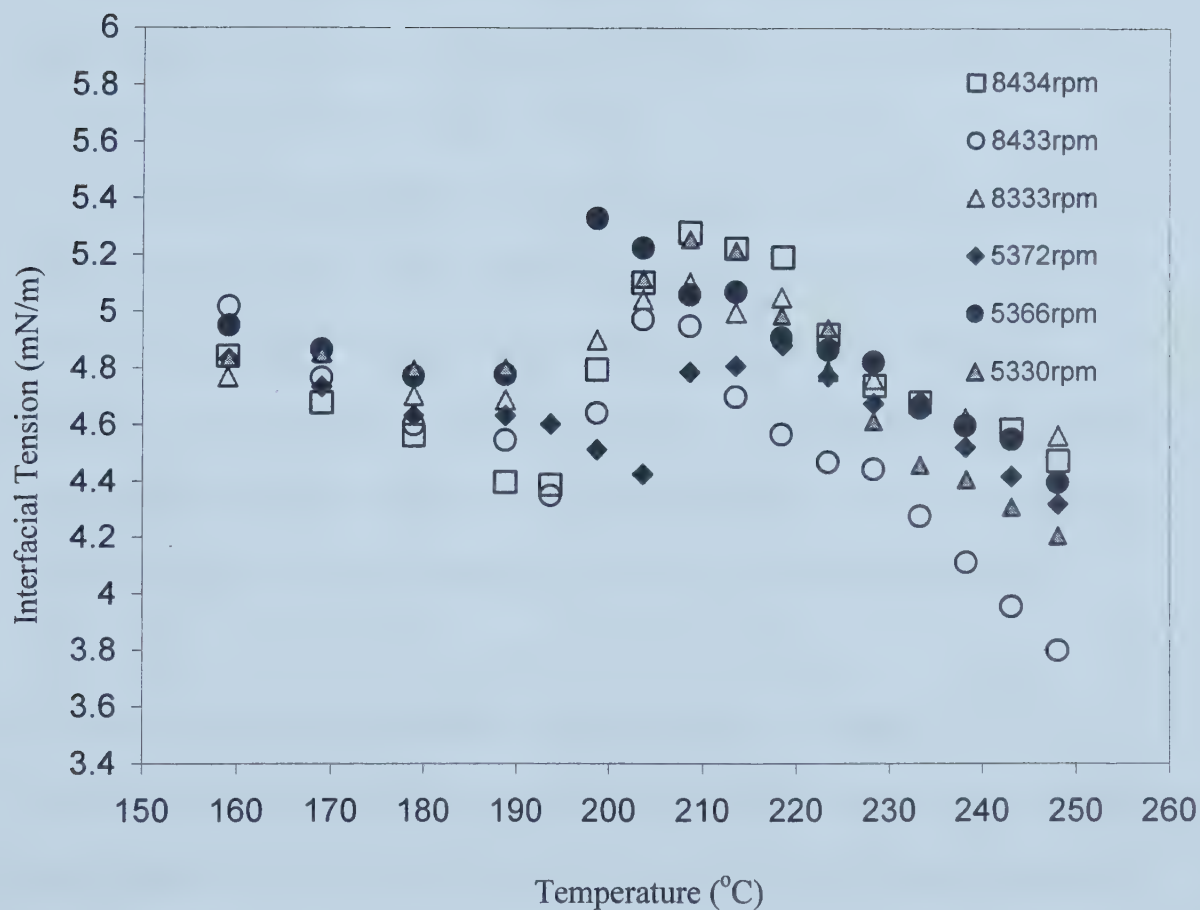


Figure 5.1 The interfacial tension of the Exxon 6750 HDPE (no additional anti-oxidant) and silicone oil-A from 150 to 250 °C. A total of six experiments are shown in this graph. The filled data points indicate experiments conducted at a rotation rate of 5000 rpm, while the open data points indicate experiments conducted at 8300 rpm.



The total time for each set of experiments was approximately two and a half hours. After each experiment, browning was observed for all of the HDPE samples. An additional experiment was conducted to test whether or not silicone oil degraded under the experimental conditions, thus causing the browning observed in the HDPE samples. A tube filled with silicone oil (without HDPE pellets) was subjected to the same rotation rate, temperature increments and experimental time described for the HDPE/silicone oil experiments in a spinning drop tensiometer. At the end of this experiment, no discolouring was observed for the silicone oil, i.e. the silicone oil did not degrade under the experimental conditions.

At the end of each HDPE/silicone oil experiment, it was also observed that the HDPE drop became very rigid, such that when the rotation rate of the samples were increased or decreased, the drop diameter did not change. This rigidity may have been due to crosslinking of the HDPE molecules – an indication that thermal degradation had altered the physical properties of the HDPE. This is also supported by the browning of the HDPE samples observed after each of the experiments.

### **5.5.2 Interfacial Tensions of HDPE with Additional Anti-Oxidant**

Additional anti-oxidant was blended with the Exxon HDPE in an attempt to reduce or prevent degradation of the polymer sample during the interfacial tension experiment. The interfacial tensions of HDPE with varying amounts of extra anti-oxidant (7,000 ppm, 10,000 ppm and 20,000 ppm) and silicone oil were measured over a temperature range of 190 to 250 °C with a temperature step of 10 °C. This smaller temperature range and larger step size was chosen to reduce the experimentation time so that



thermal degradation could be minimized. (These experiments will be referred to as the 7,000 ppm, 10,000 ppm and 20,000 ppm experiments in the rest of this chapter).

The 7,000 and 10,000 ppm experiments were conducted with silicone oil-A. For the 7,000 ppm experiment, interfacial tensions for all three runs were not linear functions of temperature, as shown in Figure 5.2. A discontinuity in the interfacial tension was observed for all of the experiments. However, the discontinuity occurred at different temperatures of 200, 220 and 240 °C. For the 10,000 ppm anti-oxidant experiment, interfacial tensions were again not a linear function of temperature, as shown in Figure 5.3. Unlike the 7,000 ppm experiments, a peak in the interfacial tension was observed in the same temperature range of 210-220 °C for all three sets of experiments.

The total experiment time for the 7,000 ppm and 10,000 ppm experiments were approximately 1.5 hours, which is less than the experiments where no additional anti-oxidant was added. However, browning was still observed for all of the samples after each experiment. The HDPE samples with additional anti-oxidants were less rigid than the HDPE without additional anti-oxidants (HDPE w/o AO); unlike the HDPE w/o AO, the diameter of the HDPE drops changed with ease when the rotation rate of the samples was changed at the end of the experiments. All these indicate that although degradation was not prevented even with the shorter experimentation time and additional anti-oxidants (since browning was still observed for all of the samples), according to the rigidity observations, the degradation of the HDPE samples was *reduced* for the 7,000 ppm and the 10,000 ppm experiments.





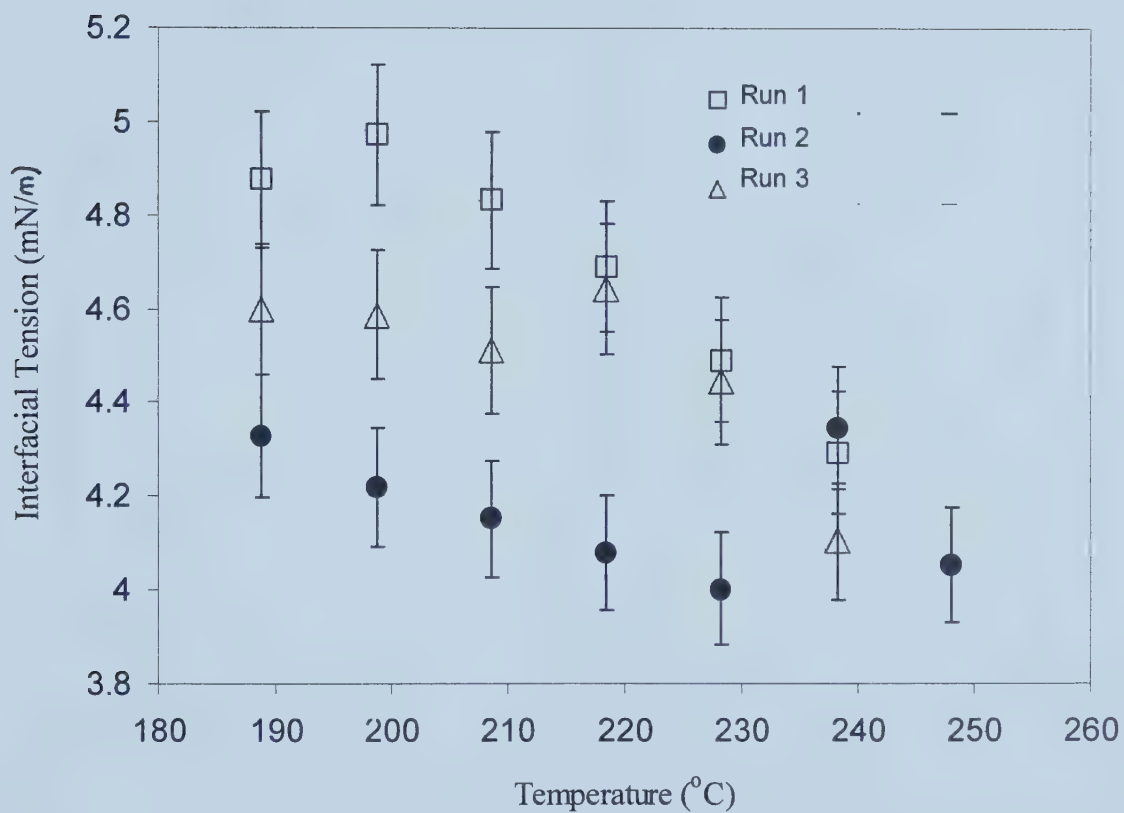


Figure 5.2 The interfacial tension of the Exxon 6750 HDPE with the addition of 7,000 ppm anti-oxidant and silicone oil - A from 190 to 250 °C. A measurement was made every 10 °C.



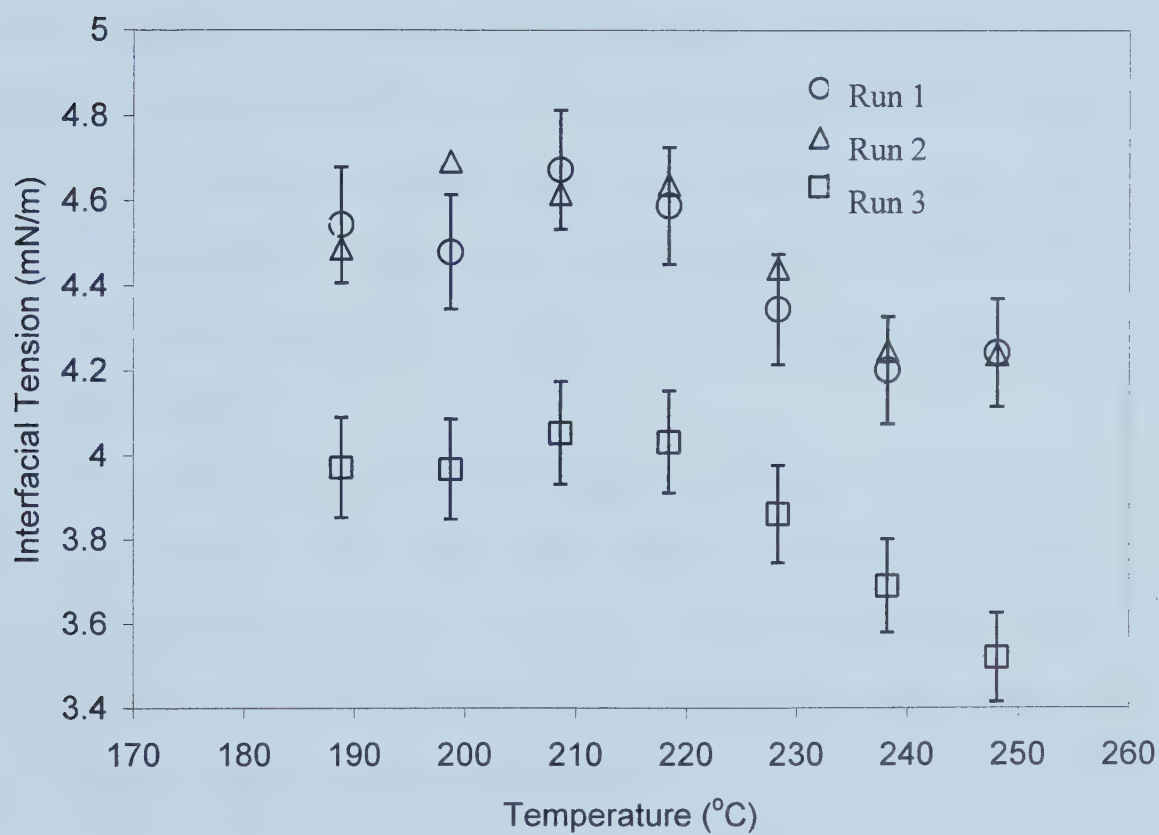


Figure 5.3 The interfacial tension of the Exxon 6750 HDPE with the addition of 10,000 ppm anti-oxidant and silicone oil - A from 190 to 250 °C. A measurement was made every 10 °C.



The 20,000 ppm experiment was conducted with silicone oil-B, and the results for the two sets of experiments with 20,000 ppm anti-oxidant are shown in Figures 5.4a and 5.4b. Unlike the 7,000 ppm and 10,000 ppm experiments, a peak was not observed in the interfacial tensions as temperatures were increased. However, Figures 5.4a and 5.4b clearly show a discontinuity in the temperature coefficients of interfacial tension between 200 and 220 °C. Browning was still observed for the samples after each of the experiments, and similar to the 7,000 and 10,000 ppm experiments, the diameter of the HDPE drop changed easily with a change in the rotation rate at the end of each experiments. As such, it appeared that the addition of 20,000 ppm did not further reduce the degradation observed with the 7,000 and 10,000 ppm experiments.

The interfacial tensions of the 20,000 ppm shown in Figures 5.4a and 5.4b are in the range of 2.4 to 3.4 mN/m between 190 and 250 °C, which are lower than the interfacial tensions shown in Figures 5.1 to 5.4. These lower interfacial tension values were most likely due to the difference in the properties of silicone oil used and also the addition of large amounts of anti-oxidant.



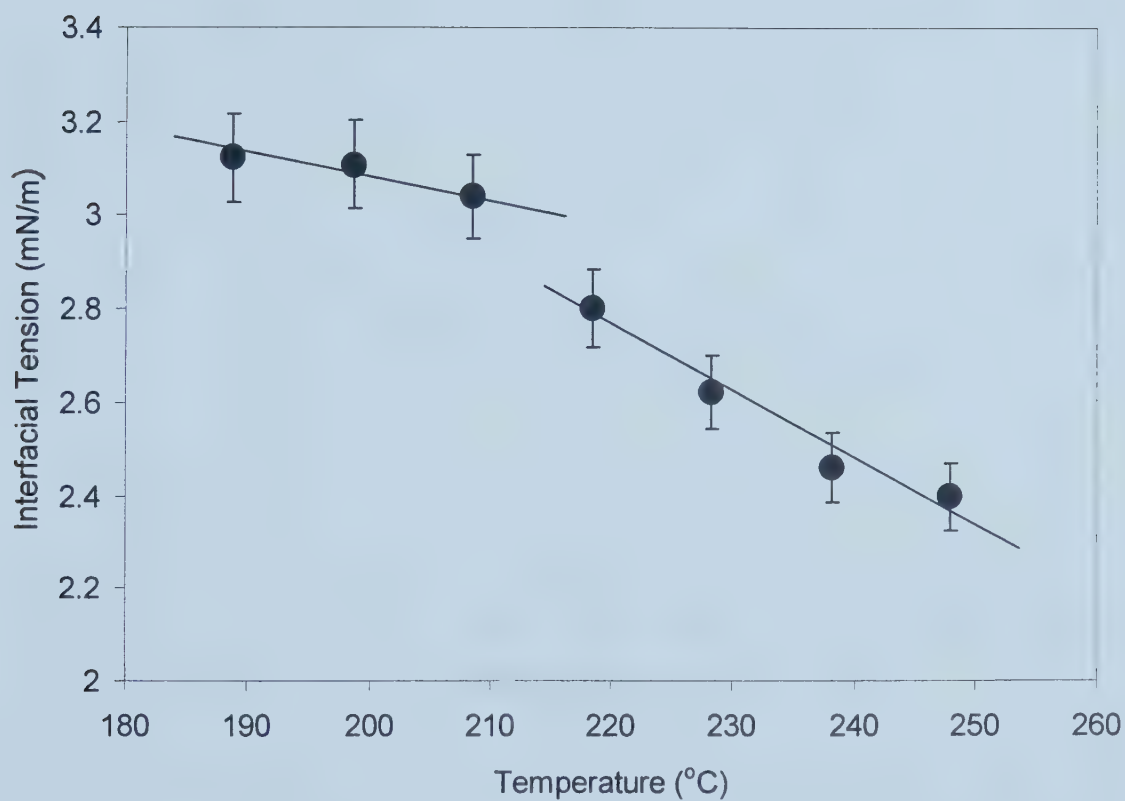


Figure 5.4a Run 1: The interfacial tension of the Exxon 6750 HDPE with the addition of 20,000 ppm anti-oxidant and silicone oil - B from 190 to 250 °C. A measurement was made every 10 °C.





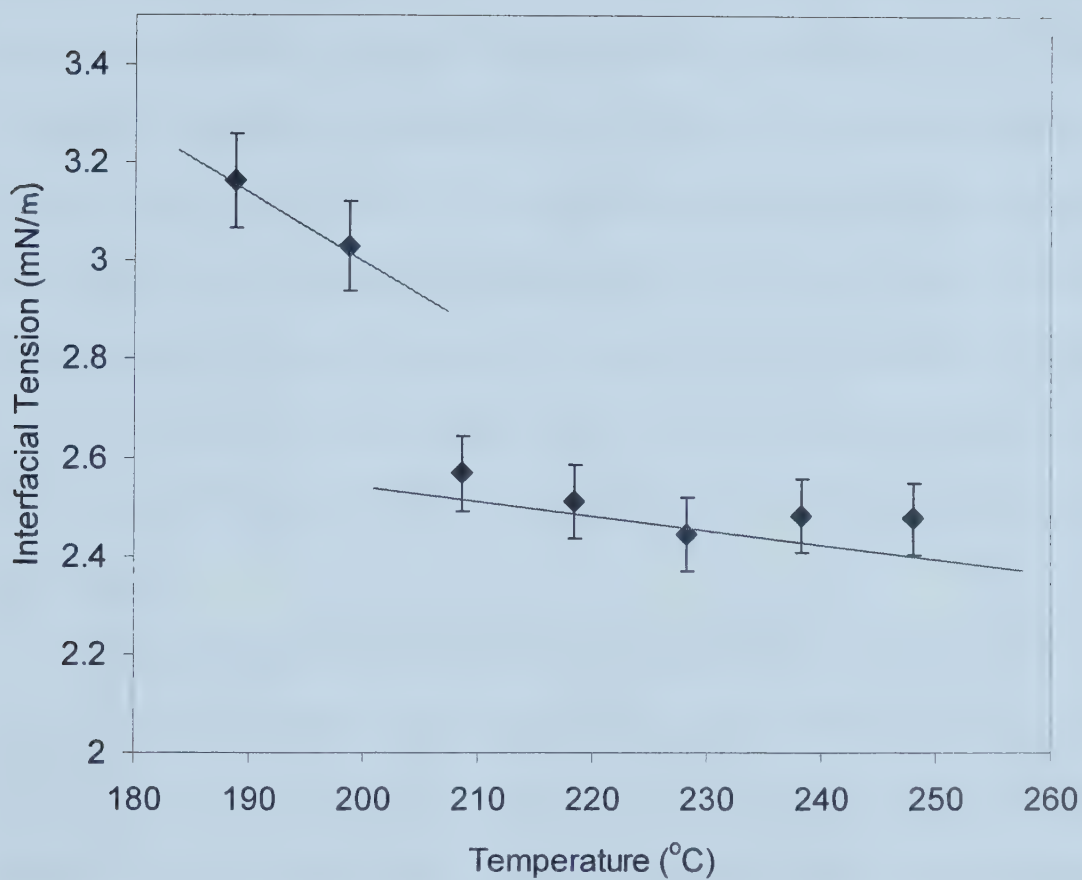


Figure 5.4b Run 2: The interfacial tension of the Exxon 6750 HDPE with the addition of 20,000 ppm anti-oxidant and silicone oil - B from 190 to 250 °C. A measurement was made every 10 °C.



### 5.5.3 Interfacial Tensions of LDPE Without Additional Anti-Oxidant

The interfacial tensions of “pure” LDPE resins (without additional anti-oxidants) and silicone oil-B were also measured in the temperature range of 190 to 250 °C. The branched structure of LDPE is commonly known to be more stable at high temperatures compared to its linear counterpart, such as the HDPE and LLDPE. Therefore, it was initially suspected that the LDPE may not undergo degradation as we saw with the HDPE samples. The original intention of conducting the interfacial tension experiments for the LDPE samples was to see if the same transition/peak in the interfacial tension can be observed for a sample that has not degraded. If indeed such observations can be found, then it may be concluded that the peak/thermal transitions seen in Figures 5.1 to 5.4 were not due to the degradation of the polymer sample itself.

The experimental methods for the LDPE samples were exactly the same as the ones described for HDPE without anti-oxidant. The LDPE experiment took approximately 1.5 hours, and at the end of the experiment, browning was again observed for the polymer sample. However, unlike the “pure” HDPE (with no additional anti-oxidants) drop which was rigid at the end of the experiment, the LDPE drop did not show signs of rigidity. Similar to the behavior of the PE drop observed in the 7,000 ppm, 10,000 ppm and 20,000 ppm experiments, the diameter of the drop changed easily when the rotation rate was changed. Degradation was not prevented in the LDPE experiments, even though the polymer was known to be more stable than the HDPE. However, the degree of degradation was probably less than the degree of degradation of the HDPE sample with no additional anti-oxidants.



The results for the interfacial tensions of LDPE and silicone oil-B is shown in Figure 5.5. The interfacial tensions for temperatures less than 200 °C were decreasing linear functions of temperature for all three runs. The temperature coefficients of all three sets of experiments at  $T < 200$  °C were almost similar at 0.06 mN/m °C. Discontinuities in the interfacial tension were observed for all three runs for  $T > 200$  °C. However, the discontinuity occurred at different temperatures for all three runs. For one of the experiments, the discontinuity in the interfacial tension was more obvious than the other two. Although the discontinuities in the interfacial tension are less pronounced than the ones observed in Figure 5.1 (for HDPE with no additional anti-oxidant), the observation that there is a difference in the transition temperature for the three separate runs was similar to the observations seen in Figure 5.1.

#### **5.5.4 Interfacial Tensions of LLDPE Without Additional Anti-Oxidant**

The interfacial tensions of LLDPE and silicone oil – B were measured between 190 and 250 °C. The interfacial tension of the LLDPE system was found to be monotonically decreasing with increasing temperature for both sets of experiments, as shown in Figure 5.6. Unlike the results seen in Figures 5.1 to 5.5, there was no peak/transition or discontinuity in the interfacial tension of the LLDPE (but the slopes of both curves changed over the range of 215 to 225 °C, which is not far from the HDPE regime of change). However, similar to the HDPE and LDPE samples, browning was observed on the LLDPE after the end of each experiment. The LLDPE



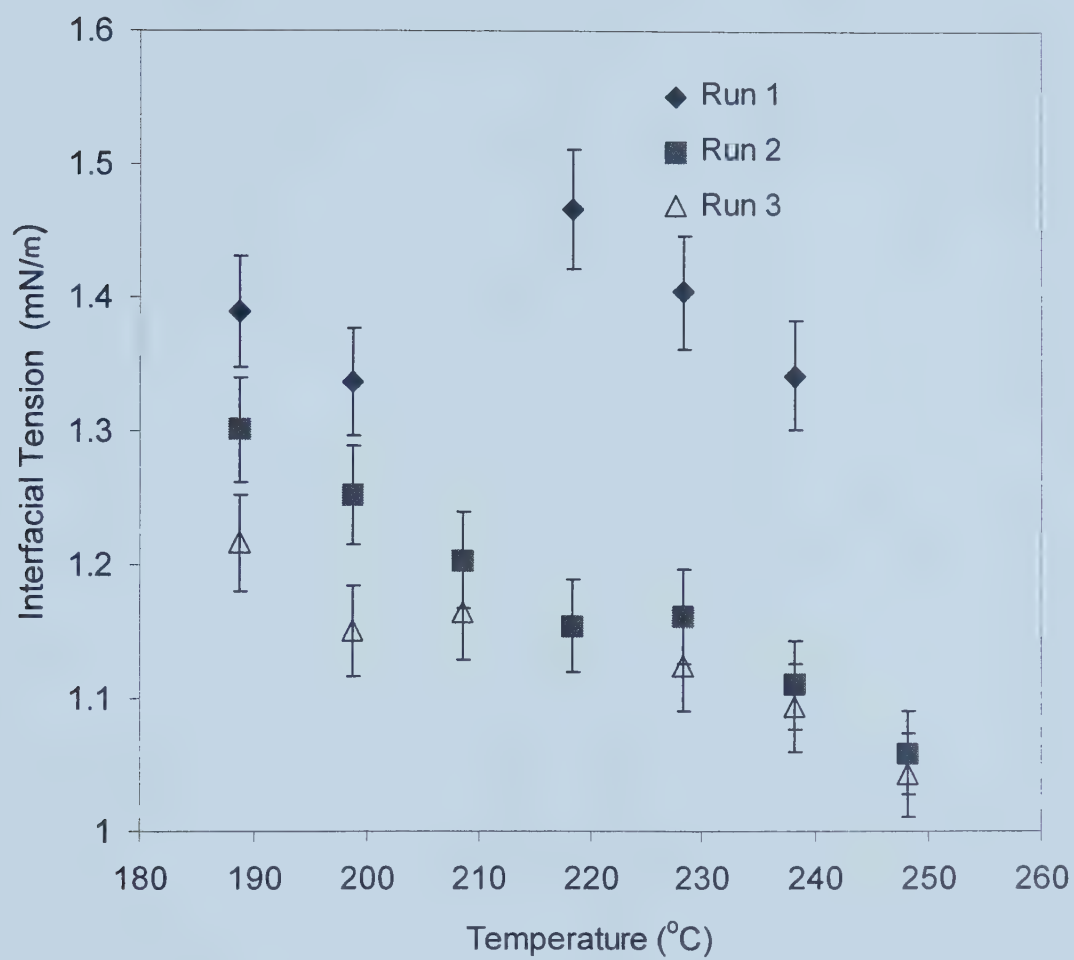


Figure 5.5 The interfacial tension of "pure" LDPE and silicone oil-B from 190 to 250 °C. A measurement was made every 10 °C.





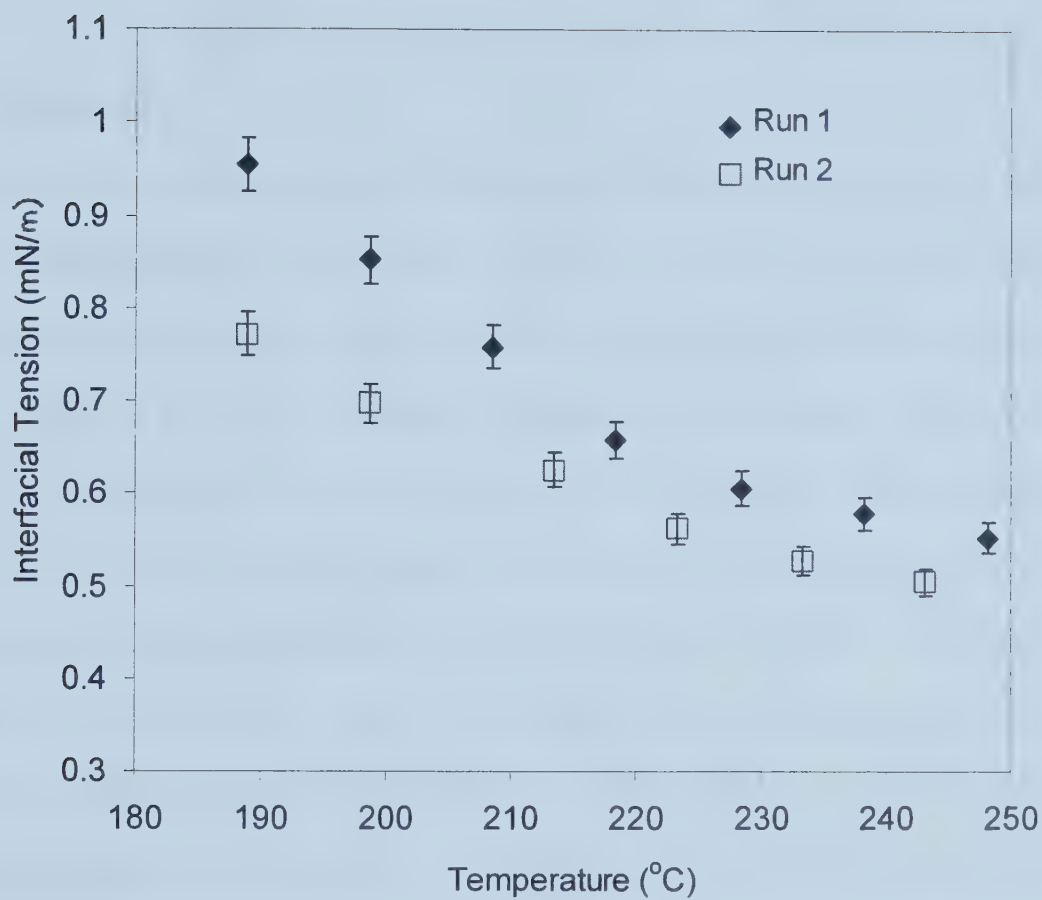


Figure 5.6 The interfacial tension of "pure" LLDPE and silicone oil-B from 190 to 250 °C. A measurement was made every 10 °C, and note that no transition in the interfacial tension is observed.



also showed signs of rigidity after the experiment, similar to the observations for the HDPE samples without additional anti-oxidant.

## 5.6 Discussion

Discontinuities in interfacial tension with respect to temperature were observed for all of the HDPE and LDPE experiments. For LLDPE, a possible discontinuity in  $d\gamma/dT$  was observed. The interfacial tensions of the PE before the transition temperature were found to be linearly decreasing with increasing temperature, which was the common observation for amorphous polymers by other workers. The temperature coefficients in this temperature range were on the order of  $0.01 \text{ mN/m } ^\circ\text{C}$ , which is in agreement with published data by Wu (1982). However, unlike most amorphous polymers, discontinuities or peaks in the interfacial tension were observed for all HDPE and LDPE samples. The temperature at which a peak was observed ( $\sim 220^\circ\text{C}$ ) in the interfacial tension was also in close proximity with interfacial tension results of Pham and Carriere (1997), Rao (1999) and Carriere (2000). Due to the limited number of data points collected, these authors did not provide an explanation of the observed peak, and rather they fitted a  $\gamma(T)$  linear regression line through the data points by assigning large standard deviation to the particular data point which obviously did not lie in the path of a linear function. From my work in this Chapter, the results shown in Figure 5.1 clearly show that in the transitional temperature range of 200 to  $230^\circ\text{C}$ , the interfacial tension of the HDPE was increasing with increasing temperature and once it reached a plateau, the interfacial tension was then decreasing with increasing temperature. This was consistently observed for all six runs and



supported by many data points in the transition temperature range. These sets of data are the most comprehensive study of the interfacial tension of PE melts to date, and we have shown that the transition/peak seen in Figures 5.1 to 5.5, and the results of Pham and Carriere (1997), Rao (1999) and Carriere (2000) are not due to experimental errors.

Degradation was observed for all of the PE (HDPE, LDPE and LLDPE) samples after the experiment, even with the addition of anti-oxidants with amounts as high as 20,000 ppm. Since the discontinuity in the interfacial tension curve was observed for the HDPE and LDPE samples, but not for the LLDPE samples, this suggests that the discontinuity or peak observed in Figures 5.1 to 5.5 may not be due to degradation of the polymer, but rather due to the intrinsic change in the physical properties of the PE at the transition temperatures. That is, the nature of LLDPE branching probably made liquid crystal-like ordering impossible.

The temperature range at which the discontinuities in the interfacial tension – temperature relationship were observed is consistent with the observations of Hussein and Williams (1998, 1999) who also saw a thermal transition in the rheological and thermal properties of the PE in the temperature range of 200 to 230 °C. This transition temperature is also consistent with the observed transition in the densities of the HDPE discussed in Chapter 4, even though the densities  $\rho(T)$  used in the calculations of interfacial tension in this chapter were taken as smoothed linear functions of temperature and thus, are not a mathematical cause of the  $\gamma(T)$  reported here.



Hussein and Williams (1998, 1999) suggested that the thermal transitions observed in the PE melts are analogous to the transition observed for liquid crystal polymers, and hence PE melts may exhibit structural order similar to that of liquid crystal polymers. The idea of structural order is also supported by the results published by Kruger (1980), Kamel and Charlesby (1981), and by Bremner and Rudin (1992). The results seen in Figures 5.1 to 5.5 also support the speculations of Hussein and Williams. The thermal transition in the interfacial tension resembled that of the transition from anisotropy to isotropy of liquid crystals. The interfacial tensions of liquid crystals (such as those with smectic or nematic structural order) undergo thermal transitions from an ordered anisotropic phase to a disordered isotropic phase once the transition temperature has been reached (George and Mohandas, 1992, 1992 and 1995; Salim and George, 1997). In the pre-transition state, interfacial tension increases with increasing temperature. Near the transition temperature, interfacial tension also increases with increasing temperature but with a much greater slope until a plateau is reached. After the transition temperature, interfacial tension then becomes a monotonically decreasing function of temperature. One or more peaks in the interfacial tension are sometimes observed for these liquid crystals.

In comparing the surface behavior of HDPE and LDPE to that of liquid crystals, the interfacial tension-temperature relationship in the pre-transitional temperature range seen in Figures 5.1 and 5.5 is different than that for the liquid crystals (Harthi and George, 1997); however, the behavior of the interfacial tension at the transition temperature is similar to that of liquid crystals. Kamel and Charlesby





(1981) and Bremner and Rudin (1992) found that three components exist in a PE melt: an ordered component, a disordered but entangled component, and an untangled segment. As such, the decrease in interfacial tension with increasing temperature at the pre-transitional state for the PE may be due to the contribution of the disordered components in the PE melt, while the sudden peak observed in the interfacial tension may be due to the transition of the ordered component in the PE melt to more of the disordered component.

For both HDPE and LDPE experiments, the temperature at which the transition was observed was different for each set of experiments, even though most of them lie in the range of 200 – 230 °C. Moreover, the transitions observed in the HDPE with additional anti-oxidant (Figures 5.2, 5.3 and 5.4) were less pronounced than the transitions observed for the HDPE with no additional anti-oxidants added. These observations may be due to difference in the thermal history of the samples which may have affected the transition behavior. Bremner and Rudin (1992) found evidence of ordered material in the PE melt, and the volume fractions of the ordered material largely depended on the particular polymer and its thermal history. The thermal history of the blended sample was different than the HDPE with no extra anti-oxidant: the HDPE with anti-oxidants added were initially heated up to 150 °C, blended at 50 rpm with the anti-oxidants for 10 minutes, and then quenched to room temperature before it was used for the interfacial tension experiment. The HDPE with no extra anti-oxidant, however, was not subjected to the mixing process.



## 5.7 Conclusions

- As a result of the experimental ease associated with the spinning drop technique used, more data points in a wide temperature range were obtained. Therefore, the results presented in this chapter are the most comprehensive study of the interfacial tension of PE melts to date.
- Thermal transitions in the interfacial tensions between 200 and 230 °C were observed for the HDPE (with and without extra anti-oxidants) and LDPE samples. This is consistent with the findings of Hussein and Williams (1998, 1999) and suggests the possible existence of an ordered state in the PE melt. No transition was observed for the LLDPE samples, which were decreasing monotonically with temperature, though with a gradual slope change in the “transition” region).
- The transition temperatures observed for the HDPE and LDPE samples were different. This may be due to a difference in the thermal history of the polymer as well as the difference in the structures of the polymer (HDPE vs. LDPE).
- The characteristics of the transition in interfacial tension for the HDPE and LDPE are analogous to those of liquid crystals.
- The addition of anti-oxidants (as high as 20,000 ppm) did not prevent degradation in the HDPE. However, the degree of degradation was reduced compared with the degradation of the HDPE with no anti-oxidant added.



- The LDPE and the LLDPE samples were somewhat degraded by the end of the experiments. The degree of degradation was more in the LLDPE sample than the LDPE sample.
- Since degradation occurred in the LLDPE, and no sharp transition or discontinuity was observed for the LLDPE, this implies that the transitions observed in HDPE and LDPE samples may not be due to the degradation of the polymer.



## CHAPTER 6

### CONCLUSIONS AND RECOMMENDATIONS FOR FUTURE WORK

---

#### 6.1 Conclusions

The objective of this thesis was to investigate anomalous surface behavior of HDPE, LDPE and LLDPE melts at high temperatures using the spinning drop tensiometer. In doing so, the temperature-volume relationship of the HDPE, and a detailed error analysis of the spinning drop apparatus were examined as well. The following are the conclusions from this work.

##### 6.1a. The Measurement of the Interfacial Tensions of PE/Silicone Oil and the High Temperature Anomalies

- The results presented in Chapter 5 are the most comprehensive study of the interfacial tension of PE melts to date.
- Thermal transitions in the interfacial tensions between 200 and 230 °C were observed for the HDPE (with and without extra anti-oxidants) and LDPE samples. This is consistent with the findings of Hussein and Williams (1998, 1999) and suggests the possible existence of an ordered state in the PE melt.
- No transition was observed for the LLDPE samples, which had an interfacial tension that decreased monotonically with temperature, though with a gradual slope change in the “transition” region).





- The transition temperatures observed for the HDPE and LDPE samples were different. This may be due to a difference in the thermal history of the polymer as well as the differences in the structures of the polymer (HDPE vs. LDPE).
- The characteristics of the transition in interfacial tension for the HDPE and LDPE are somewhat analogous to those of liquid crystals.
- The addition of anti-oxidants (as high as 20,000 ppm) did not prevent degradation in the HDPE. However, the degree of degradation was reduced compared with the degradation of the HDPE with no anti-oxidant added.
- The LDPE and the LLDPE samples were somewhat degraded by the end of the experiments. The degree of degradation was more in the LLDPE sample than the LDPE sample.
- The LLDPE is a similar molecule to the HDPE and the LDPE molecules. In this work, degradation was observed in the LLDPE samples but no transitions were observed. Therefore, the transitions seen in the HDPE and LDPE samples is not due to degradation alone.

#### 6.1b. The Measurement of the Density of HDPE and the High Temperature Anomalies

- A transition in the temperature range of 200-230 °C is observed in the densities of all five HDPE samples. This is consistent with Hussein's density measurements, and again suggests the possibility of melt order in the HDPE.



### 6.1c. The Error Analysis of the Spinning Drop Tensiometer

- The reading error associated with the operation of the spinning drop tensiometer was found to be 1% and 3% for water/air and silicone oil/air systems respectively.
- Rotation rate of the fluids was found to have a real effect on interfacial tension values measured. Increasing rotation rate appears to increase interfacial tension.
- Rotation rate affects interfacial tension when conditions investigated by Manning and Scriven (1977) for gyrostatic equilibrium were met, and when the droplet has the same rotation rate as the tube wall (Isaacs et al., 1988).
- Several possibilities were investigated and discarded as causing the effect of rotation rate on apparent interfacial tension value. These possibilities were: pressure effects, non-gyrostatic equilibrium, non-uniform temperature, different reticule placement method, calibration and parallax error in the spinning drop tensiometer software and non-rigid rotation. None of these possibilities could explain the effect of rotation rate on apparent interfacial tension values.
- The fluids in the spinning drop tensiometer may not be under gyrostatic equilibrium due to complicated multidimensional flow phenomena inside the tube under rotation which may cause the effect of rotation rate on apparent interfacial tension. The investigation of this possibility is beyond the scope of this project.
- In the experiments where the objective was to measure the interfacial tension of polymer systems at different temperatures, the rotation rate of the fluids was kept the same in each set of measurements so that the effect of rotation rate on interfacial tension did not need to be considered.



## **6.2 Recommendations for Future Work**

### **6.2a. Examination of the Molecular Order of PE Melts**

From the results obtained in this thesis, along with works by other authors (Kruger et al., 1980; Bremner and Rudin, 1992; Wang and Drda, 1997; Hussein and Williams, 1998), there is increasing evidence of molecular order in PE melts. As such, more work needs to be done to gain a better insight into the molecular order of PE melts up to 230 °C. The following are some possible studies to investigate further the types of molecular order present in PE melts:

- Study the molecular changes of liquid crystals during phase transitions and subsequently apply and compare the model to that of PE melts.
- Investigate the molecular structural changes of the PE melt during a transition using methods of optical spectroscopy such as X-ray diffraction.
- Examine the possible effects of polymer branch content, molecular weight and additives on the phase transition phenomena.

### **6.2b. Examination of the Spinning Drop Method**

- Examine the effects of different glass tube sizes and geometry on the error of the spinning drop tensiometer.
- Examine the effects of a different end plug geometry on the error of the apparatus.



# References

- Adamson, A.W., 1967, *Physical Chemistry of Surfaces*, 2<sup>nd</sup> ed., Wiley, New York, p60-61
- Arashiro, E.Y., Dermalquette, N.R., 1999, "Influence of Temperature, Molecular Weight, and Polydispersity of Polystyrene on Interfacial Tension between Low-Density Polyethylene and Polystyrene", *J. Appl. Polym. Sci.*, **74**, 2423-2431
- Bergmann, K., 1978, "Study of the Molecular Motions of Polyethylene by Line-Shape Analysis of Broad-Line Proton NMR Spectra", *J. Polym. Sci. Pol. Phys.*, **16**, 1611-1634
- Borchardt, J. K., Yates, C.W., 1993, "Design and Performance of a Dynamic Interfacial Tension Spinning Drop Tensiometer", *J. Am. Oil. Chem. Soc.*, **70**, 47-52
- Bremner, T., Rudin, A., 1990, "Persistence of Regions with High Segment Density in Polyethylene Melts", *J. Polym. Sc., Polym. Phys. Ed.*, **30**, 1247-1260
- Butts, A., 1954, *Copper. The Science and Technology of the Metal, Its Alloys and Compounds*, Reinhold Publishing Corporation, New York
- Capelle, A., 1981, "Measurement of Low Interfacial Tension Between Crude Oil and Formation Water with Dissolved Surfactants by the Spinning Drop Technique: Fact or Fiction", in *Surface Phenomena in Enhanced Oil Recovery* (D. O. Shah Ed.) Plenum, New York, 229-236
- Carriere, C.J., Biresaw, G., Sammler, R.L., 2000, "Temperature Dependence of the Interfacial Tension of PS/PMMA, PS, and PMMA/PE Blends", *Rheol. Acta*, **39**, 476-482
- Cayias, J.L, Schechter, R.S., Wade, W.H., 1975, in *Adsorption at Interfaces* (K.L. Mittal, Ed.), ACS Symposium Series No. 8, pp234-247. Washington, D.C.
- Chapleau, N., Favis, B.D., Carreau, P.J., 2000, "Measuring the Interfacial Tension of Polyamide/polyethylene and Polycarbonate/polypropylene Blends: Effect of Temperature", *Polymer*, **41**, 6695-6698
- Chappelear, D.C., 1964, "Interfacial Tension Between Molten Polymers", *Polym. Prepr.* **5**, 363-371
- Chemical and Engineering News, June 25<sup>th</sup>, 2001 "Facts and Figures for the Chemical Industry", American Chemical Society, Washington





Chen, C.C., White, J.L., 1993, "Compatibilizing Agents in Polymer Blends: Interfacial Tension, Phase Morphology, and Mechanical Properties", *Poly. Eng. Sci.*, **33**, 923-930

Chitwetelu, C.I., Hornorf, V., Neale, G.H., 1988, "The Measurement of Dynamic Interfacial Tension by Photo-micropendography", *J. Colloid Interface Sci.*, **125**, 586-601

Contreras, P., Olteanu, M., 2000, "Interfacial Tension Measurement by the Rotating Meniscus", *Colloids Surf.* **170**, 45-50

Cooke, D.L., Koyich, M., 1991, "LLDPE Resins for High Output Blown Film Extrusion", *Journal of Plastic Film and Sheeting*, **7**, 306-316

Correia, N.T., Ramos, J.J. M, Adao, M. H. C.V., Saramago, B. J. V., 1997, "Temperature Dependence of the Surface Behavior of a Side-Chain Liquid Crystalline Polymer Probed by Contact Angle Measurements", *Mol. Cryst. Liq. Cryst.*, **300**, 45-64

CRC Handbook of Chemistry and Physics, 2000-2001, 81<sup>st</sup> Edition, Editor in Chief: David R. Lide, CRC Press, Cleveland

Currie, P.K., Van Nieuwkoop, J., 1982, "Buoyancy Effects in the Spinning Drop Interfacial Tensiometer", *J. Colloid Interface Sci.*, **87**, 301-316

Elemans, P.H.M., Janssen, J.M.H., Meijer, H.E.H., 1990, *The Measurement of Interfacial Tension in Polymer/Polymer Systems: The Breaking Thread Method*. *J. Rheol.*, **34**, 1311-1325

Ellingston, P.C., Strand, D.A., Cohen, A.C., Sammler, R.L., Carriere, C.J., 1994, "Molecular Weight Dependence of Polystyrene/Poly(methylmethacrylates) Interfacial Tension Probed by Imbedded-Fiber Retraction", *Macromolecules*, **27**, 1643-1647

Elliott, J.A.W., Ward, C.A., Yee, D., 1996, "Bubble Shapes in Rotating Two-phase Fluid Systems: a Thermodynamic Approach", *J. Fluid Mech.*, **319**, 1-23

Elmendorp, J.J., DeVos, G., 1986, "Measurement of Interfacial Tensions of Molten Polymer Systems by Means of the Spinning Drop Method", *Polym. Eng. Sci.*, **26**, 415-417

*Encyclopedia of Polymer Science and Technology*, 1985, Editor-in-chief: Jacqueline I. Kroschwitz. , John Wiley and Sons, New York

Eriksson, J.C., 1962, "On the Thermodynamic Theory for the Effect of Pressure on Surface Tension", *Acta Chem. Scand.*, **16**, 2199-2211



Escudie, E., Graciaa, A., Lachaise, J., 1986, "Pendant Drop Measurements of the Polypropylene/Polystyrene Interfacial Tension between 220 °C and 270 °C", *Materials Chemistry and Physics*, **14**, 239-246

Flory, P.J., 1953, *Principles of Polymer Chemistry*, Cornell University Press, Ithaca, N.Y.

Garmabi, H., Demarquette, N.R., Kamal, M.R., 1998, "Effect of Temperature and Compatilizer on Interfacial Tension of PE/PA-6 and PP/EVOH", *Intern. Ploymer Processing XIII, J. Polym. Sci. Pol. Phys.*, **2**, 183-191

George, A.K., Mohandas, K.P., 1992, "Interfacial Tension of a Polymesomorphic Liquid Crystal Bounded by an Isotropic Liquid", *J. Phys.: Condens. Matter*, **4**, 7691-7698

George, A.K., Mohandas, K.P., 1995, "Pre-transitional Surface Ordering and Disorder at Liquid Crystal-Isotropic Liquid Interface", *Phys. Chem. Liq.*, 233-242

Greenspan, H.P., 1968, "The Theory of Rotating Fluids", Cambridge U.P., Cambridge.

Guido, S., Simeone, M., Villone, M., 1999, "Diffusion Effects on the Interfacial Tension of Immiscible Polymer Blends", *Rheol. Acta.*, **38**, 287-296

Harthi, S.A., George, A.K., 1997, "Anisotropic Surface Order in the Isotropic Phase of Nematic Liquid Crystals", *Cryst. Res. Technol.*, **32**, 519-523

Hu, H.H., Joseph, D.D., 1994, "Evolution of a Liquid Drop in a Spinning Drop Tensiometer", *J. Colloid Interface Sci*, **162**, 331-339

Hussein I.A., Williams M.C., 2000, "DSC evidence for microstructure and phase transitions in polyethylene melts at high temperatures", *Macromolecules*, **33**, 520-522

Hussein, I. A., Williams, M. C., 1998, "Anomalous Nonlinearities in Steady Shear of Polyethylene Melts", *J. Non-Newtonian Fluid Mech.*, **68**, 105-118

Hussein, I.A., 1998, *Ph.D. Thesis*, University of Alberta, Edmonton

Hussein, I.A., Ho, K., Goyal, S.K., Karbushewski, E., Williams, M.C., 2000, "Thermomechanical Degradation in the Preparation of Polyethylene Blends", *Polymer Degradation and Stability*, **68**, 381-392

Hussein, I.A., Williams, M.C., 1998, "Rheological Evidence for High-Temperature Phase Transitions in Melts of High-Density Polyethylene", *Macromol. Rapid Commun.*, **19**, 323-325



- Isaacs, E., Maunder, J.D., Li, J., 1988, "Interfacial Tension of Heavy Oil-Aqueous Systems at Elevated Temperatures" in *ACS Symposium Series 396*, **Chapter 17**, 324-344
- Joseph, D.D., Arney, M.S., Gillberg, G., Hu, H., Hultman, D., Verdier, C., Vinagre, T.M., 1992, "A Spinning Drop Tensioextensometer", *J. Rheol.*, **36**, 621-662
- Joseph, D.D., Preziosi, L., 1987, "Stability of Rigid Motions and Coating Films in Bicomponent Flows of Immiscible Liquids", *J. Fluid Mech.*, **186**, 323-351
- Kamal, M.R., Dermalquetter, N.R., Lai-Fook, R.A., Price, T.A., 1997, "Evaluation of Thermodynamic Theories to Predict Interfacial Tension Between Polystyrene and Polypropylene Melts", *Polym. Eng. Sci.*, **37**, 813-825
- Kamal, M.r., Lai-Fook, R., Dermalquette, N.R., 1994, "Interfacial Tension in Polymer Melts. Part II: Effects of Temperature and Molecular Weight on Interfacial Tension", *Polym. Eng. Sci.*, **34**, 1835-1839
- Kamel, I., Charlesby A., 1981, "NMR Spin-Spin Relaxations in Solid and Molten Polyethylene Structures", *J. Polym. Sci. Pol. Phys.*, **19**, 803-814
- Kell, G.S., 1975, "Density, Thermal Expansivity and Compressibility of Liquid from 0 °C to 150 °C: Correlations and Tables for Atmospheric Pressure and Saturation Reviewed and Expressed on 1968 Temperature Scale", *J. Chem. Eng. Data*, **20**, 97-105
- Kitamaru, R., Horii, F., Hyon, S.H., 1977, "Proton Magnetic Resonance Studies of the Phase Structure of Bulk-Crystallized Linear Polyethylene", *J. Polym. Sci. Pol. Phys.*, **15**, 821-836
- Kruger, J.K., Peetz, L., Wildner, W., 1980, "Evidence for Structural Transformations in Polymer Melts", *Polymer*, **21**, 620-626
- Lewis, G.N., Randall, M., 1923, *Thermodynamics and the Free Energy of Chemical Substances*, McGraw-Hill Book Company Inc., New York
- Manning, C.D., Scriven. L.E., 1977, "On Interfacial Tension Measurement with a Spinning Drop in Gyrostatic Equilibrium", *Rev. Sci. Instrum.*, **48**, 1699-1705
- Mekhilef, N., Carreau, P.J., Favis, B.D., Martin, P., Ouhlal, A., 2000, "Viscoelastic Properties and Interfacial Tension of Polystyrene-Polyethylene Blends", *Journal of Polymer Science: part B: Polymer Physics*, **38**, 1359-1368
- Menon, V.B., Nokolov, A.D., Wasan, D.T., 1988, "Interfacial Effects in Solid-Stabilized Emulsions: Measurements of Film Tension and Particle Interaction Energy", *J. Colloid Interface Sci.*, **124**, 317-327





Metals Handbook, Desk Edition, 1998, edited by J. R. Davis, ASM International, Ohio

Mohandas, K.P., George, A.K., 1992, "Thermal Variation of Surface Tension at Liquid Crystal-Isotropic liquid Interface", J. Chem. Phys., **96**, 4779-4781

Neale, G.H., Khulbe, K.C., Hornof, V., 1987, "Effects of Oil Phase Viscosity on Interfacial Tension Behavior of Oil/Alkaline Systems as Measured by the Spinning Drop Tensiometer", The Canadian Journal of Chemical Engineering, **65**, 700-703

Painter, P.C., Coleman, M.M., 1994, *Fundamentals of Polymer Science: An Introductory Text*, Techomic Publishing Company Inc., Pennsylvania

Peltonen, L. J., Yliruusi, J., 2000, "Surface Pressure, Hysteresis, Interfacial Tension, and CMC of Four Sorbitan Monoesters at Water-Air, Water-Hexane, and Hexane-Air Interfaces", J. Colloid Interface Sci, **227**, 1-6

Pham, H.T., Carriere, C. J., 1997, "The Effect of Temperature on the Interfacial Tension of Polycarbonate/Polyethylene Blends", Polym. Eng. Sci., **37**, 636-639

Princen, H.M., Zia, I.Y.Z., Mason, G., 1967, "Measurement of Interfacial Tension from the Shape of a Rotating Drop", J. Colloid Interface Sci, **23**, 99-107

Rao, N., 1999, *M.Sc. Thesis*, University of Alberta, Edmonton

Rodgers, P. A., 1993, "Pressure-Volume-Temperature Relationships for Polymeric Liquids: A Review of Equations of State and Their Characteristics Parameters for 56 Polymers", J. Appl. Polym. Sci., **48**, 1061-1080

Sanchez, I.C., Rodgers, P.A., 1990, "Solubility of Gases in Polymers", Pure & Appl. Chem., **11**, 2107-2114

Sasges, M.R., Ward, C.A., 1996, "Equilibrium Fluid Configurations in Low Gravity", J. Appl. Phys., **79**, 1996

Shah, V., 1984, *Handbook of Plastics Testing Technology*, Wiley-Interscience Publication, John Wiley & Sons

Slattery, J.C., Chen, J.D., 1980, "Spinning Drop Interfacial Viscometer", J. Colloid Interface Sci, **73**, 483-499

Stammer, A., Wolf, B.A., 1998, "Phase Behavior and Interfacial Tension of Polysiloxane Blends", Polymer, **10**, 2065-2067

Sullivan, D.E., Lipowsky, R., 1988, "On the Free Energy of Nematic Wetting Layers", Can. J. Chem., **66**, 553-556





Susnar, S.S., Hamza, H.A., Neuman, A.W., 1994, "Pressure Dependence of Interfacial Tension of Hydrocarbon-Water Systems Using Axisymmetric Drop Shape Analysis", *Colloids Surf.*, **89**, 169-180

Taylor, J.R., 1982, "An Introduction to Error Analysis: The Study of Uncertainties in Physical Measurements", University Science Books, California

Taylor, K.C., Schramm, L.L., 1990, "Measurement of Short-Term Low Dynamic Interfacial Tensions: Application to Surfactant Enhanced Alkaline Flooding in Enhanced Oil Recovery", *Colloids Surf.*, **47**, 245-253

Tjipto-Margo, B., Sen, A.K., Mederos, L., Sullivan, D.E., 1989, "The Liquid-Vapour Interface of Nematic Liquid Crystals", *Molecular Physics*, **67**, 601-614

Tjipto-Margo, B., Sullivan, D.E., 1988, "Molecular Interactions and Interface Properties of Nematic Liquid Crystals", *J. Chem. Phys.*, **88**, 6620-6630

Tomotika, S., 1935, "On the Instability of a Cylindrical Thread of a Viscous Liquid Surrounded by Another Viscous Fluid", *Proc. R. Soc. London*, **A150**, 322-337

Touhami, Y., Neale, G.H., Norhof, V., 1994, "Effects of Water-Soluble Polymers and Aqueous-Phase Viscosity on the Interfacial Tension Behavior of Reacting Oil-Alkaline Systems", *J. Appl. Polym. Sci.*, **53**, 309-316

Verdier, C., Vinagre, H.T.M., Piau, M., Joseph, D.D., 2000, "High Temperature Interfacial Tension Measurements of PA6/PP Interfaces Compatibilized with Copolymers using a Spinning Drop Tensiometer", *Polymer*, **41**, 6683-6689

Verma, S., Kumar, V.V., 1998, "Relationship between Oil-Water Interfacial Tension and Oily Soil Removal in Mixed Surfactant Systems", *J. Colloid Interface Sci.*, **207**, 1-10

Vinagre, H.T., Joseph, D.D., 1998, *Spinning Drop Tensiometer User's Manual*, SDT Ltd.

Visscher, E.J., Willemse, R.C., 1999, "Interfacial Tension of Polypropylene/Polystyrene: Degradation of Polypropylene", *Polym. Eng. Sci.*, **39**, 1251-1256

Vonnegut, B., 1942, "Rotating Bubble Method for the Determination of Surface and Interfacial Tensions", *Rev. Sci. Instrum.*, **13**, 6-9

Wang, S.Q., Drda, P.A., 1996, "Stick-Slip Transition in Capillary Flow of Polyethylene. 2. Molecular Weight Dependence and Low-Temperature Anomaly", *Macromolecules*, **29**, 4115-4119



Wang, S.Q., Drda, P.A., 1997, "Stick-slip Transition in Capillary Flow of Linear Polyethylene: 3. Surface Conditions", *Rheol. Acta*, **36**, 128-134

Wu, S., 1982, *Polymer Interface and Adhesion*, Marcel Dekker Inc., New York

Yan, Z.L., 1999, *M.Sc. Thesis*, University of Alberta, Edmonton

















University of Alberta Library



0 1620 1492 0563

**B45430**